VYSOKÉ UČENÍ TECHNICKÉ V BRNĚ
BRNO UNIVERSITY OF TECHNOLOGY

FAKULTA CHEMICKÁ
ÚSTAV CHEMIE MATERIÁLŮ

FACULTY OF CHEMISTRY
INSTITUTE OF MATERIALS SCIENCE

STUDY OF THIN-FILM SURFACES

DIZERTAČNÍ PRÁCE
DOCTORAL THESIS

AUTOR PRÁCE Ing. RUTUL RAJENDRA TRIVEDI
AUTHOR

BRNO 2010

VYSOKÉ UČENÍ TECHNICKÉ V BRNĚ
BRNO UNIVERSITY OF TECHNOLOGY

FAKULTA CHEMICKÁ
ÚSTAV CHEMIE MATERIÁLŮ

FACULTY OF CHEMISTRY
INSTITUTE OF MATERIALS SCIENCE

STUDY OF THIN-FILM SURFACES

STUDIUM POVRCHŮ TENKOVRSTVÝCH MATERIÁLŮ

DIZERTAČNÍ PRÁCE
DOCTORAL THESIS

AUTOR PRÁCE Ing. RUTUL RAJENDRA TRIVEDI
AUTHOR

VEDOUCÍ PRÁCE prof. RNDr. VLADIMÍR ČECH, Ph.D.
SUPERVISOR

BRNO 2010

Vysoké učení technické v Brně
Fakulta chemická
Purkyňova 464/118, 61200 Brno 12

Zadání dizertační práce

Číslo dizertační práce: **FCH-DIZ0029/2010** Akademický rok: **2010/2011**
Ústav: Ústav chemie materiálů
Student(ka): **Ing. Rutul Rajendra Trivedi**
Studijní program: Chemie, technologie a vlastnosti materiálů (P2820)
Studijní obor: Chemie, technologie a vlastnosti materiálů (2808V016)
Vedoucí práce **prof. RNDr. Vladimír Čech, Ph.D.**
Konzultanti:

Název dizertační práce:

Studium povrchů tenkovrstvých materiálů

Zadání dizertační práce:

Charakterizace morfologie a povrchových vlastností jednoduchých a vrstevnatých systémů
Studium hybridních vrstev
Charakterizace mechanických vlastností jednoduchých a vrstevnatých systémů

Termín odevzdání dizertační práce: 20.12.2010

Dizertační práce se odevzdává ve třech exemplářích na sekretariát ústavu a v elektronické formě vedoucímu dizertační práce. Toto zadání je přílohou dizertační práce.

\- -
Ing. Rutul Rajendra Trivedi
Student(ka)

\- -
prof. RNDr. Vladimír Čech, Ph.D.
Vedoucí práce

\- -
prof. RNDr. Josef Jančář, CSc.
Ředitel ústavu

V Brně, dne 1.9.2006

\- -
prof. Ing. Jaromír Havlica, DrSc.
Děkan fakulty

ABSTRACT

The doctoral thesis deals with the study of surface properties of single-layer and multilayer thin films deposited from of vinyltriethoxysilane and tetravinylsilane monomers. It also deals with adhesion characterization of single layer tetravinylsilane films.

The plasma polymerized thin films were prepared under steady-state deposition conditions on polished silicon wafers using plasma-enhanced chemical vapor deposition. The surface properties of the films were been characterized by different scanning probe microscopy methods and nanoindentation techniques such as conventional depth-sensing nanoindentation and load-partial-unload (cyclic) nanoindentation. While, the nanoscratch test was used to characterize the film adhesion properties.

Single layer films prepared at different deposition conditions were characterized with respect to surface morphology and mechanical properties (Young's modulus and hardness). The results of surface morphology, grain analysis, nanoindentation, finite elemental analysis and modulus mapping helped to know the hybrid nature of single layer films that were deposited at higher powers of RF-discharge. A novel approach was used in surface characterization of multilayer film by scanning probe microscopy and nanoindentation. The adhesion behavior of plasma polymer films of different mechanical properties and film thickness were analyzed by normal and lateral forces, friction coefficient, and scratch images obtained by atomic force microscopy.

ABSTRAKT

Disertační práce se zabývá studiem povrchových vlastností jedno a vícevrstvých filmů deponovaných z vinyltriethoxysilanových a tetravinylsilanových monomerů. Zabývá se také charakterizací adheze jednovrstvých filmů z tetravinylsilanu.

Plazmaticky polymerizované tenké vrstvy byly připraveny na leštěných křemíkových substrátech pomocí plazmové depozice z plynné fáze za ustálených podmínek. Povrchové vlastnosti vrstev byly charakterizovány pomocí různých metod rastrovací sondové mikroskopie a nanoindentačních technik jako je konvenční a cyklická nanoindentace. Vrypový test byl použit pro charakterizaci vlastností adheze vrstev.

Jednovrstvé filmy připravené za různých depozičních podmínek byly charakterizovány s ohledem na povrchové morfologie a mechanické vlastností (modul pružnosti, tvrdost). Výsledky morfologie povrchu, analýzy zrn, nanoindentace, analýzy konečných prvků a modulů mapování pomohly rozlišit hybridní charakter filmů, které byly deponovány při vyšších výkonech RF-výboje. Nový přístup byl použit v povrchové charakterizaci vícevrstvého filmu pomocí rastrovací sondové mikroskopie a nanoindentace. Adhezívní chování plazmaticky polymerizovaných vrstev různých mechanických vlastností a tloušťek bylo analyzováno pomocí normálních a laterálních sil, koeficientu tření, a snímků vrypů získaných pomocí mikroskopie atomárních sil.

KEYWORDS

plasma polymer, multilayer film, scanning probe microscopy, atomic force microscopy, conventional nanoindentation, cyclic nanoindentation, adhesion, scratch test

KLÍČOVÁ SLOVA

plazmový polymer, multivrstva, skenovací sondová mikroskopie, mikroskopie atomárních sil, konvenční nanoindentace, cyklická nanoindentace, adheze, vrypová zkouška

TRIVEDI, R; Study of thin-film surfaces, Brno, 2010, 116 p. Dissertation work at the institute of Materials Science, Faculty of Chemistry, Brno University of Technology. Supervisor prof. RNDr. Vladimír Čech, Ph.D.

STATEMENT

I state, that the doctoral thesis has been completed independently and all used references are quoted truly and exactly. The content of this doctoral thesis is a property of Faculty of Chemistry, Brno University of Technology and may be used for commercial purpose with permission of the doctoral thesis supervisor and the Dean of FCH VUT only.

....

Graduate signature

Thanks to:
My doctoral thesis Supervisor prof. RNDr. Vladimír Čech, PhD. and Dr. David Skoda, PhD. for help and guidance in NTegra Prima Scanning probe microscopy and Hysitron nanoindenter. Further, my thanks to Ing. Soňa Lichovníková and Ing. Lukáš Hoferek for deposition of plasma thin films.

Comment:
I have been working as a senior researcher and practical guide to Ing. Erik Pálesch on the topic “Adhesion study of organosilicon thin film on silicon substrate”. He has presented some of this work in his Diploma thesis.

INDEX

1 INTRODUCTION

Tailoring surfaces by plasma modification and polymerization has proven to be a powerful technology that has revolutionized surface modification and thin film formation. Plasma polymer films have been a key material in many areas, including electronics, magnetic recording media, optical devices, MEMS, protective coatings, etc. In such developments, a good understanding of the surface properties such as the surface morphology and mechanical properties is very important. Recently, scanning probe microscopy (SPM) and nanoindentation have become the most important methods to measure the surface properties of thin films and coatings.

The doctoral thesis is aimed at the application of Scanning Probe Microscopy (SPM) and nanoindentation method on the study of thin films surfaces. The thin films were been prepared by plasma polymerization technique from tetravinylsilane (TVS) and vinyltriethoxysilane (VTES) monomers at the Institute of Materials Chemistry, Brno University of Technology. The prepared films were been characterized by SPM (NT-MDT, Russia) and nanoindentation (Hysitron, USA). Important surface properties such as the surface roughness, surface analysis and mechanical properties were characterized.

In the chapter 2, the theoretical basics are introduced. The text deals with the basic information about plasma, plasma polymerization, Scanning probe microscopy and nanoindentation. Shortly we have discussed about the scanning probe microscopy construction, many methods developed under the SPM principle, nanoindentation equipments, theoretical background of nanoindentation method, and nanoscratch test. Chapter 3 deals with the experimental sets-up of plasma deposition chambers and process, NT-DMT NTegra Prima Scanning Probe Microscopy and Hysitron Triboscope. The obtained results are presented in detail in chapter 4.

2 THEORETICAL BACKGROUND

2.1 Plasma polymer films

2.1.1 Introduction

Plasma

Generally, there are three states of matter, i.e., solid, liquid or gas. The plasma is considered as being a fourth state of materials, and it is more highly activated than other three states. Plasma is a mixture of electrons, negatively charged particles, positively charged particles, neutral atoms and molecules. To achieve a plasma state, a temperature more than a few thousand centigrade is applied which brings the collision to the level of ionization of atoms. Thus, the plasma state is in an extremely high energy level compared with solid, liquid and gas state.

The processes whereby an atom or a molecule gains energy are mainly particle collision and photon energy absorption. Both are essential for ionization. The magnitude of the energy required for ionization is equivalent to that of carrying away an electron in an atomic nucleus towards an infinite distance. The energy for the ionization must be input into atoms and the molecules from an external energy source. Normally the electric energy is a convenient source of energy, which helps to bring the ionization of atoms and molecules. For that purpose, a pair of electrodes working in a capacitive coupling manner or inductive coupling manner is placed in the reaction chamber to supply the electric energy in reaction chamber.

The controlled plasma state is very helpful to carry out the plasma polymerization reaction of gaseous monomer or surface treatment. There are three essential terms for plasma generation for plasma polymerization: (1) an energy source for the ionization, (2) a vacuum system for maintaining a plasma state, and (3) a reaction chamber. Further history and discussion about plasma polymerization is mentioned in next chapter 1.1.2.

Low-temperature plasma

Plasmas are, generally divided into two groups according to the temperature of the plasma species [1],
(a) High temperature plasmas (HPT) are having the temperature in the range of 10^6 – 10^8 K. These kinds of plasmas are mostly present in stars or thermonuclear reactors.
(b) Low temperature plasmas (LTP), which are present in temperature range below than 10^6. Low temperature plasmas are further divided into two types: (1) thermal plasmas and (2) non-thermal plasma.

The thermal plasma is characterized by the same temperature of the plasma particles, $T_e \approx T_i \approx T \leq 2 \times 10^4$ K and mostly present in arc discharge at the atmospheric pressure. The non-thermal plasma of electric gas discharge is weakly ionized and is characterized by a significant nonequilibrium state. In which, the electron temperature is much higher than the ion and neutral gas temperature, i.e. $T_i \approx T \approx 300$ K << $T_e \leq 10^5$ K. The non-thermal plasma is also known as cold plasma. They are mostly present in various glow discharges at low pressures. Here, the power supplies that can be used to ignite and sustain the plasma are direct current (DC), radio frequency (RF) or microwave (MW). The power may be delivered by means of an electric field (using electrodes) or electromagnetic (using a coil or MW). The electrodes may be placed either within plasma vessel (direct coupling) or within external to it (indirect coupling). This cold plasma technique that is having low temperature and low-pressure deposition conditions are widely used for commercially plasma deposition techniques such as PECVD etc. The detail description about PECVD is mentioned in next chapter 1.1.2.

2.1.2 Plasma polymerization

In the early 19th century, some researcher observed the formation of oily or polymer like products at the surface of electrodes and at the wall of glass tubes because of electric discharge process. During that time, they considered it as the by the products or unwanted product of the experiment [2]. In the beginning of 1960s, some researchers drew attention to it. They understood that electric discharge could initiate the monomer's polymerization and gives the polymer product in the form of pinhole-free thin films which is chemically & thermally stable as well as insoluble in organic solvents [2]. For them, it was a question what is the mechanism behind this kind of polymerization. With time, some of typical mechanisms were proposed (1) ionic mechanism (2) radical mechanism and (3) atomic polymerization. However, ionic mechanism and radical mechanism were not able to explain the whole concept behind this kind polymerization.

Yasuda [3] gave the new aspect of atomic polymerization from his experience to explain the mechanism. According to Yasuda, in presence of plasma, the monomer molecules gain high energy from electrons, ions and radicals and are fragmented into activated small fragments, in some cases into atoms, These activated fragments are recombined, sometimes carried out rearrangement, and the molecules grow to large-molecular weight ones in a gas phase or at the surface of substrates. The repetition of activation, fragmentation, and recombination (or rearrangement) leads to polymer formation. The schematic of plasma polymerization reaction is mentioned in Fig. 1. Many researchers believe that atomic polymerization is a reasonable concept to explain the mechanism of plasma polymerization and the chemical and physical properties of the formed polymers. This concept is quite different from the polymerization mechanism of conventional polymers.

Yasuda [3] concept explains if the same monomer was used for plasma polymerization, then also it is not possible to predict the chemical structure of formed polymers. This is due to the fragmentation and rearrangement of the monomer taking place during the polymerization. In some cases, hydrogen, nitrogen, oxygen or some other particles present in reaction chamber can also become activated and are incorporated into the formed polymers.

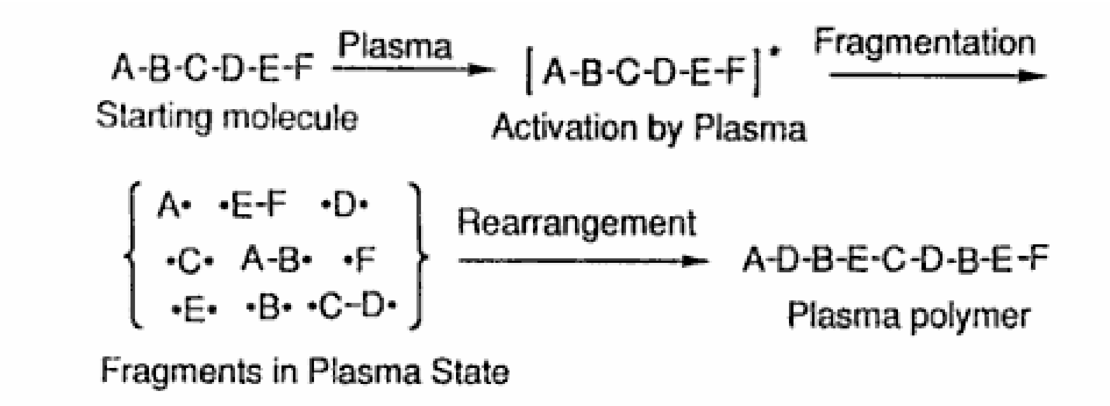

Fig. 1 Schematic presentation of plasma polymerization [13]

By this way, the era of plasma polymerization and its products thin films was started. In simple word, plasma polymerization is a thin film forming process on a substrate without any fabrication. In this process, the thin film formation is carried out from low molecular weight molecules (monomers) with assistance of the plasma energy, which involves activated electrons, ions, and radicals.

Plasma-Enhanced Chemical Vapor Deposition (PECVD)

In terms of reaction, the PECVD is a kind of chemical vapor deposition (CVD) technique. The chemical vapor deposition (CVD) is a chemical reaction process, which takes place between the gaseous monomer inside a chamber to form solid films. The energy required to drive the chemical reactions can be supplied in a number of different forms such as heat, electrical discharge (also known as plasma enhanced or activated CVD), photons and even sound.

In PECVD, the plasma polymerization takes place at low temperature and low-pressure plasma conditions. It uses the electrical energy to generate a glow discharge (plasma) in which the energy is transferred into a gas mixture. This transforms the gas mixture into reactive radicals, ions, neutral atoms and molecules, and other highly excited species. Either these atomic and molecular fragments interact with a substrate and, depending on the nature of these interactions, etching or deposition processes occur at the substrate. Since the formation of the reactive and energetic species in the gas phase occurs by collision in the gas phase, the substrate can be maintained at a low temperature. Hence, film formation can occur on substrates at a lower temperature than is possible in the conventional CVD process, which is a major advantage of PECVD.

As mentioned previously, the two most common methods for coupling the electrical energy into a gas discharge in PECVD are capacitive coupling plasma (CCP) or induction as is done with inductively coupled plasma (ICP). Inherently different plasma conditions are created with CCP and ICP discharges and the choice of ICP or CCP discharge depends on the application. The design of PECVD chamber is based on type of energy supply is used. For example, capacitive coupling type of PECVD reactors is mentioned in Fig. 2.

Figure 2 shows a schematic diagram of a parallel plate PECVD reactor [4], which is using capacitive coupling system for supply electrical energy to the gas mixture in reaction chamber. It is a cold wall parallel-plate reactor inside a cylindrical aluminum chamber. The chamber is maintained at low pressure using vacuum pumps, except when loading and unloading wafers. The top plate or electrode is a showerhead through which gases are injected. The wafers are being placed on the bottom of electrode plate. The high side of the RF power supply is connected to the top electrode. The bottom electrode is grounded.

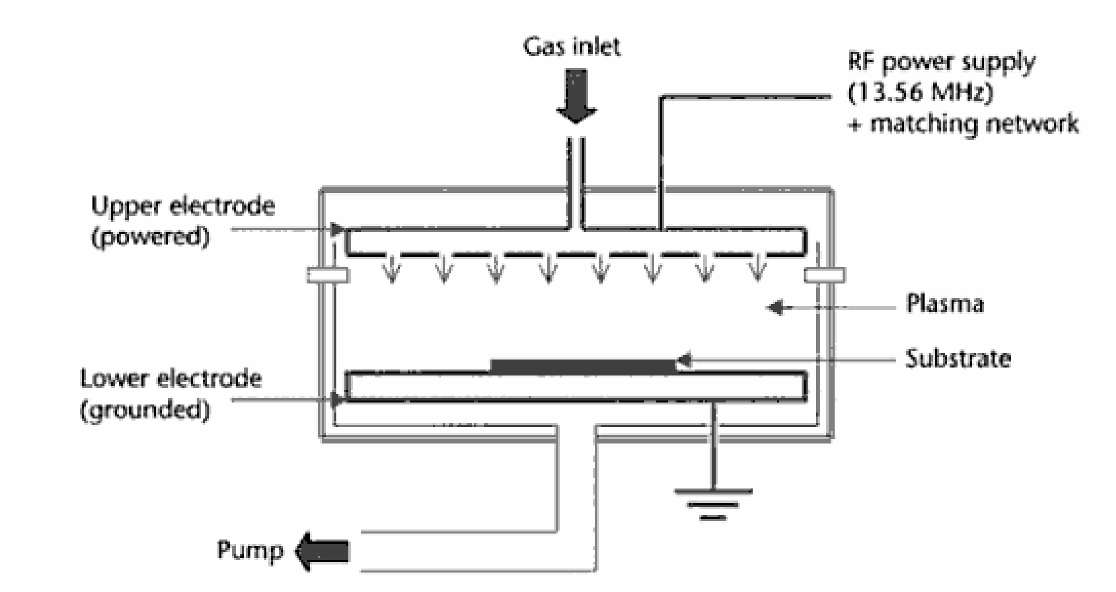

Fig. 2 Schematic diagram of a parallel-plate PECVD reactor [4]

The plasma polymerization in PECVD mostly depends on monomer flow rates, system pressure and discharge power. Some of the desirable properties of PECVD films are having good adhesion, low pinhole density, good step coverage, and uniformity.

2.1.3 Organosilicon monomer

Organosilicon monomers are molecules consisting of at least a single atom of silicon and organic groups where one can find the atoms of carbon, oxygen, nitrogen and hydrogen. This class of materials possesses a special characteristic, which distinguishes it from other plasma polymers – the ability to vary and control the degree of this organic/inorganic choice of fabrication variables [5]. This allows one to control many physicochemical properties over wide ranges, resulting in an extraordinary potential for useful applications, which are only now beginning to be tapped. The organosilicon plasma polymers are widely recognized for their potential in optical, mechanical, and electric applications. Most used monomers in this family of compounds include tetramethylsilane, vinyltriethoxysilane, vinyltrimethylsilane, HMDSO and hexamethyldisilazane containing Si, H, C, O or N atoms [6].

The field of research covered by organosilicon chemistry is very broad from biochemical aspects to electronic going through out all the aspects of chemistry. Some organosilicones are used as monomers in low pressure plasma deposition of silicone-like and silicon oxide thin films, due to their availability, liquid state, volatility at room temperature, safe handling, and low cost. By choosing a suitable monomer and/or by changing the feed oxygen content, a wide range of materials can be obtained, which matches performances required in different technological arenas. The chemistry of the deposits can be, in fact, tuned from silicone like, where the organic moiety (C, H content) of the film is of relevance, to SiO_2-like inorganic coatings of completely different chemistry and properties. Many potential applications exist for these films in microelectronics (dielectric layers), optics (hard transparent coatings), food packaging and fuel transport (gas, vapor, and liquid diffusion barrier films), biomedical engineering (inert coatings, low-energy surfaces), and corrosion-weathering protection (passivating layers) [7].

HMDSO is a choice of industries because it is a non-toxic material and no harmful materials are produced during processing. It can be used in production environment without any special safety considerations. While, vinyltriethoxysilane (VTES) monomer is one of the organofunctional silane coupling agent recommended for surface modification of glass fibers used as reinforcement as unsaturated polymer resin [8].

2.1.4 Factor affecting the plasma polymerization

There are some important factors, which are needed to be kept in consideration because it affects the way of plasma polymerization reaction. Such as

- The hydrodynamic factor [2] has influences on plasma polymerization reaction and is very important for plasma polymerization of thin film coatings. The hydrodynamic factor can be determined with the help of a description of the shape and scale of the reaction chamber and the relative position of the plasma zone, the monomer inlet and the plasma polymer collecting location. By using same monomer and same experimental conditions, the two plasma polymers formed in two reaction chambers are never identical because of the difference in hydrodynamic factor. Hence, the plasma polymerization is a reactor dependence process
- Yasuda [3] proposed a controlling parameter W/FM, where W is RF power in Joules/second, F is the monomer flow rate in moles/sec, and M is the molecular weight of the monomer in kg/mole. This parameter describes the input energy per unit monomer molecule in J/Kg. It is proportional to the concentration of activated species in the plasma and is very useful for understanding the plasma polymerization phenomenon. Fig. 3 shows the deposition-rate dependence on W/FM parameter.

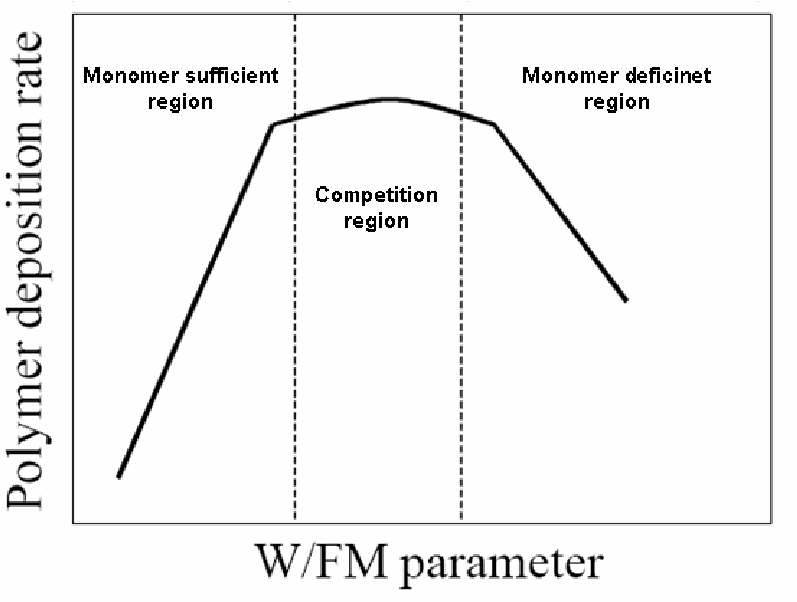

Fig. 3 The domain of plasma polymer deposition

The rate of polymer deposition increases at low W/FM parameter, reaches a maximum value, and then decreases at high W/FM value. This trend is explains nicely by the competitive process that exists in the reactor at these different power levels. It should be pointed out that in monomer sufficient region, monomers subjected to less fragmentation and polymerize with less rearrangement. In the monomer deficient regions, monomer molecules are subjected to heavy fragmentation and plasma polymerization takes place with great rearrangements.

- The magnitude of RF-power has a strong influence on chemical composition as well as on physical properties of plasma polymerized thin films [9].
- Plasma polymerization is also influenced by monomer flow rate, system pressure and discharge power among other variable parameters such as the reactivity of the starting monomer, the frequency of the excitation signal and the temperature of the substrate.

2.1.5 Multilayer film

There has been a worldwide intensive research in past years in the development of nanostructured multilayer in which the dimensions of the individual layers are in the range of few nanometers. They represent a new class of engineering materials. By using the different types of control chemical vapor deposition (CVD) system, it is possible to produce the multilayer thin films. They are mostly used to changed surface characteristic compared to the bulk materials.

Multilayer structures have been used for many years in the coating technology for improving the performance of hard coating for various machining application [10,11]. Due to the complex requirements for the materials used as protective coatings such as high hardness, good adhesion at the substrate, low reactivity and friction with the materials in contact, an optimum solution seems to be a multilayer coating. An ideal coating structure consists of an inner layer with a good adhesion, one or more intermediate layers having high hardness, strength and toughness and an outer layer with a low reactivity and friction coefficient [12]. In recent years, some multilayer show attractive features for wear-corrosion properties of materials are TiN/AlN, TiN/NbN, TiN/VN, TiN/CrN etc.

Some optical multilayer thin-film coatings such as band-pass filter, edge filter, anti reflective coating are key components of consumer electronics products [13]. Some dielectric multilayer of SiO_x depositions at low frequency PECVD are used as barrier films for lithium micro batteries [14]. These multilayer are exhibiting very low permeation rates for water vapor and oxygen to protect the lithium micro batteries from degradation.

To improve the adhesion between the fibers and polymer matrix in Fiber-Reinforced Plastics (FRP), the complex multilayered structures of controlled properties are able to fulfill the demesnes of chemical composition and structure together with mechanical and interfacial properties [15]. These multilayer films are having a wide range of other industrial and engineering applications, such as high-strength/high-conductivity materials, dielectric barrier in semiconductor devices, tribological coatings for aeronautical applications [16], protective coating against wear, corrosion and oxidation, cutting tools and micro-electromechanical systems [17] etc. Thus one can say that, multilayer films are new prospects of surface engineering technology.

2.1.6 Application of plasma thin films

Various applications [6] of plasma polymer films include anticorrosive surfaces, humidity sensors, electrical resistors, scratch resistance coatings, optical filters, protective coatings, chemical barrier coatings, etc. Metalized surfaces of synthetic materials can be protected against corrosion with a thin polymer layer deposited by plasma polymerization. The processes can be customized to produce hydrophobic or hydrophilic (antifogging effect) coatings. Scratch resistant coatings have been successfully applied on optical lenses but three-dimensional objects, such as reflectors for the motor car and lighting industries are complicated by the fact that power input may not be uniform over the entire substrate surface during the polymerization process [18].

2.2 Scanning Probe Microscopy

2.2.1 Introduction

Many crucial material properties like adhesion, friction, lubrication, biocompatibility, hydrophobicity etc. are governed by the molecular state of their topmost surface [19]. Tailoring the surface by the use of plasma modification and polymerization is proved to be a powerful technology that has revolutionized surface modification and thin film formation. Many important applications are developed by this technology. Some of the classic microscopy techniques such as optical microscopy, Scanning Electron Microscopy (SEM) have been used for the characterization of the film from long time but they have some limitations.

The revolution in surface analysis was carried out when the scanning tunneling microscope (STM) technique was invented by Dr. Gerd Binning and his colleagues in 1981 at the IBM Zurich Research Laboratory, Switzerland. It was the first instrument capable of direct obtaining three-dimensional (3-D) images of solid surfaces with atomic resolution [20]. Further, Dr. Binning and his team received a Noble Prize in Physics for their extraordinary invention in 1986. However, STM technique got some limitations like those that it can be used only for analysis of eclectically conducting surfaces. This limitation of STM, further in 1985 motivated Dr. Binning et al. to develop the Atomic force microscope (AFM) to measure ultra small forces (less than 1 nN) present between the AFM tip surface and sample surface [21]. It was a major breakthrough in the developments of Scanning probe microscopy (SPM) methods, which has given a new vision to the world for studying the surface topographies and normal forces on the micro to nanoscale [22]. With further developments, AFMs have been used for measurements of friction, scratching, wear and adhesion properties [22, 23, 24] and also for the measurement of the elastic/plastic mechanical properties [22, 25 - 27].

These methods are used at extreme magnifications ranging from 10^3 to 10^9 in x, y and z directions for imaging micro to atomic dimensions with high resolution and for spectroscopy. These instruments can be used for analysis of samples in any environment such as ambient air [21], various gases [23], liquid [28, 29], vacuum [20, 30], low temperatures (lower than about 100 K) [31] and high temperatures [32, 33].

The STMs and AFMs belong to the Scanning Probe Microscopes (SPMs) family. There are many more methods developed with time under SPMs family for various applications of scientific and industrial interest. This includes – Friction Force Microscopy (FFM) (or Lateral Force Microscopy (LFM)) [34], Scanning Forces Acoustic Microscopy (SFAM) (or Atomic Force Acoustic Microscopy (AFAM)) [35], Scanning Magnetic Force Microscopy (SMM) (or Magnetic Force Microscopy (MFM)) [36], Scanning Near Field Optical Microscopy (SNOM) [37], Scanning Thermal Microscopy (SThM) [38], Scanning Kelvin Probe microscopy (SKPM) [39] and many more.

Commercial production of SPMs started with STM in 1987 and the AFM in 1989 by Digital Instruments Inc [21]. With time, there are many other companies such as Veeco Instruments Inc., NT-MDT Inc., etc have introduced the SPM instruments. It is clear that research and industrial applications of SPMs are rapidly increasing.

2.2.2 Basic concept of Scanning Probe Microscope

In Scanning Probe Microscope (SPM), research of a surface structure and its local properties is performed by measuring highly localized tip-sample interactions. The characteristic distance between a tip and a surface of samples in probe microscopes makes about 0.1 – 10 nanometer [40]. Various kinds of tip-sample interactions are laid in the basis of probe microscopy work. Some of them are, Scanning Tunneling Microscopy (STM), which measures an electronic tunneling current between a metallic tip and conductive surface; Atomic Force Microscopy, which measures the force interaction between tip-sample surfaces; and near field Scanning Optical Microscopy (NSOM), which measures local optical properties by exploiting near-field effects [41].

Another important parameter in SPM construction is feedback system (FS). The Feedback system is supervising the distance between a tip and a sample. The feedback systems try to keep the constant interactions force between a tip and the sample hence it can approach the tip to the surface or retracting it to keep a constant interaction force. In existing probe microscopes, the accuracy of keeping the tip-surface distance reaches the value of ~ 0.01 Å [40].

2.2.3 Atomic Force Microscopy

The Atomic Force Microscopy (AFM) is also known as the Scanning Force Microscopy (SFM). The AFM is the most widely used technique of SPM families because of its experimental flexibility and broad applicability. The AFM can produce very high resolution, 3 D images of sample surfaces. The main working principle in AFM is the measurement of ultrasmall forces (less than 1 nN) present between an AFM tip and a sample surface. AFMs are capable of investigating the surfaces of both conductive and insulating sample at an atomic scale.

On the base of construction, there are two different kind of AFMs are available commercially – (1) small sample AFMs and (2) large sample AFMs. In the case of small sample AFMs, during analysis of sample surface, the sample is generally scanned instead of the tip (i.e. tip is remains in stationary position and sample is moving under the tip) because the AFM measures the relative displacement between the AFM tip surface and reference surface and any cantilever movement would add vibrations [21]. Hence, it can be produce very high-resolution surface images. While in the case of measurement of large samples, AFMs are available, where the tip is scanner (moving) and the sample is stationary. Because of vibrations added by tip movement, lateral resolutions are poor compare to the previous case.

In our present research work, the analyses of small samples were carried out. Hence, we have the AFMs system for small sample. The principle of operation of commercially small sample AFM is shown in Fig. 4. The sample is generally smaller than 10 mm x 10 mm. It is mounted on a PZT tube scanner, which controls the movement of sample in *x*-*y* plane in a raster pattern and to move the sample in *z* direction. A sharp tip at the free end of the cantilever is brought in contact with the sample. The features on the sample surface cause the tip and its cantilever to deflect vertical and lateral directions as the sample is scanned under the tip. A laser beam from a diode is focused on the backside of the cantilever at an angle of 10°. Hence, the reflected beam is captured by the photo diode. The photo diode is connected with the feedback systems. According to the twist and movement of tip cantilever captured by photodiode, the feedback system is used to modulate the voltage applied to the PZT scanner to adjust the height of PZT.

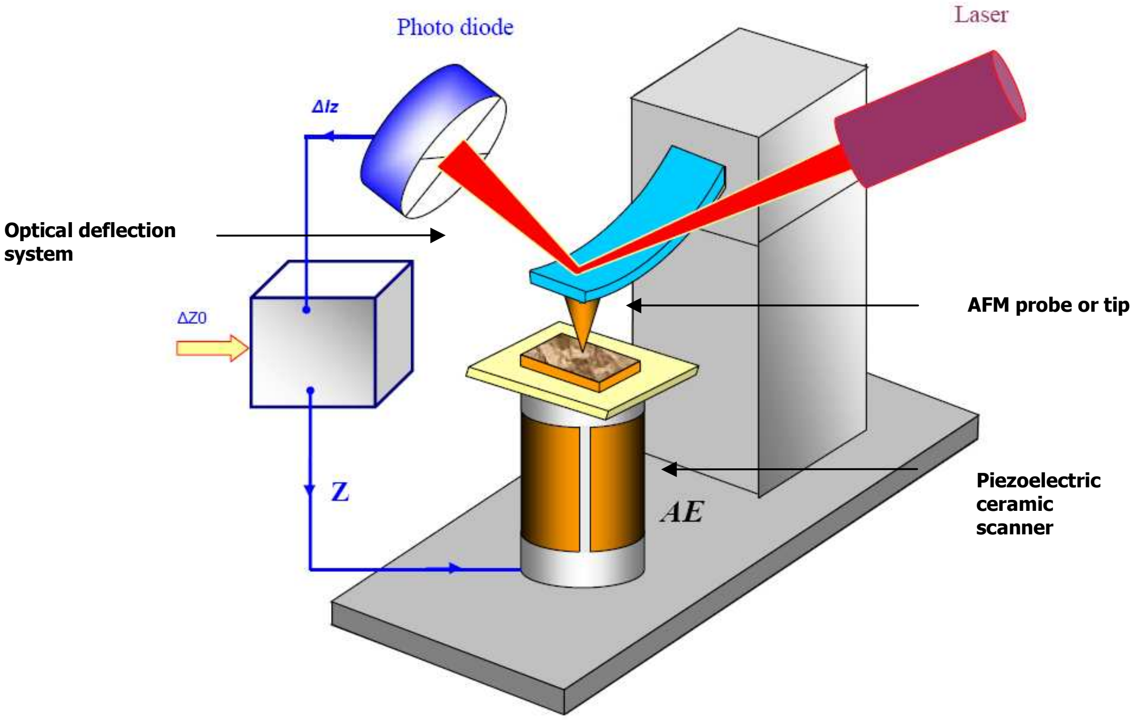

Fig. 4 Schematic diagram of an atomic force microscope

In the AFM microscope construction, there are three main parts:
(a) AFM probe or tip,
(b) Sample stage and piezoelectric ceramic scanner, and
(c) Optical deflection system consisting of a laser diode and photo detector (or photo diode).

AFM probe or tip

In AFMs, the images are generated by tip-sample interactions during the raster scanning of a sharp probe over a sample. A well-characterized tip is the key element in AFMs for good data interpretation and it is typically the limiting factor.

Commercially available AFM probes are made from silicon and silicon nitride. They are microfabricated by lithographic and anisotropic etching techniques. The qualities of newly produced AFM probes can be characterized by imaging the nanometer scale standard materials of know geometry and dimensions. For AFM tips, the scan image resolution roughly corresponds to the radius of curvature of the tip, the tip aspect ratio and the sample height. The schematic image of AFM probe and its electron microscope image is mention in Fig. 5.

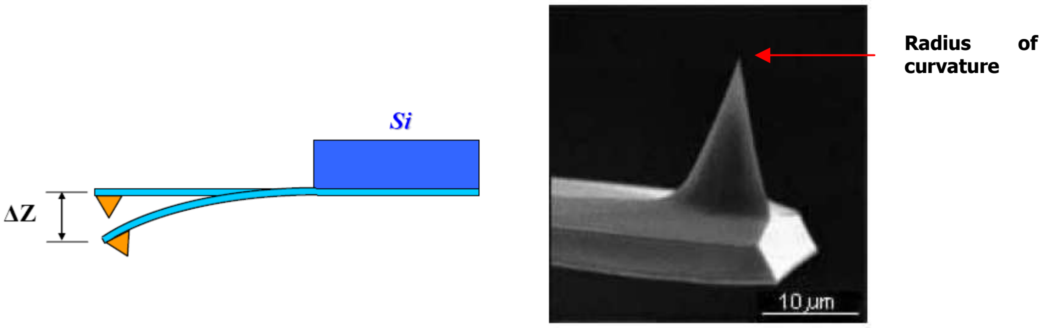

(a) **(b)**

Fig. 5 AFM probe – (a) Schematic image of the AFM probe and (b) Electron microscope image of AFM tip

Commercially available silicon and silicon nitride tips are micro-scale in dimensions, having spring constants range from 0.01 to 100 N/m, and resonant frequencies ranging from 5 kHz to over 300 kHz [40]. These AFM probes are having somewhat larger radius of curvature (Fig 2.2), low aspect ratio and limited lifetime due to wear or friction but still they are most widely used for AFM analysis because of their broad availability.

Some newly developed and advanced AFM probes are also available in market. They are made entirely of diamonds – both the tip and the cantilever in a monolithic process. This kind of diamonds probes are having smaller radius of curvature, better resolution and longer durability compared to the silicon and silicon nitride probes. Major drawback of this kind of probes is very high price compared to normal AFM probes.

Several strategies have been developed to improve AFM tip performance such as oxide sharpening, focused ion beam (FIB) milling and electron beam deposition (EDB). By using these methods, it is possible to improve the tip sharpness, tip asperities, high aspect ratio. However, they have also limitation with high cost and difficulties of process. Finally, carbon nanotubes have also been employed as AFM tips because of their nanometer-scale diameter, long length, high stiffness and elastic buckling properties. Nanotubes can manually attach to silicon or silicon nitride AFM probes or grown on to the tips by chemical vapor deposition (CVD) methods, which should soon make them widely available.

Piezoelectric ceramic scanner

A high-resolution surface image is obtained by SPM method, by monitoring the tip-sample distance with high accuracy (at a level of Angstrom fractions). The position between tip-sample distances is monitor by scanners. The scanning elements of probe microscopy are made of piezoelectric materials – the materials having piezoelectric properties (i.e. materials change their sizes in external electric field). The scanner moves the sample relatives to the cantilever in three dimensions.

There are many different kinds of scanner designs available. In which, the piezo tripod is one way to achieved three-dimensional movement of a tip attached to its center. However, the tripod needs large area (~ 50 mm) for its construction. Hence, its large size and asymmetric shape makes it susceptible to thermal drift error. The Scanners made based on one tubular element are most widely used in the scanning probe microscopy. Theses scanner prove ample scanning range with small size. Control electronics systems for AFMs can use either analog or digital feedback. It is suitable for ultra low noise operation. The general view of a tubular scanner and arrangement of electrodes are presented on Fig. 6.

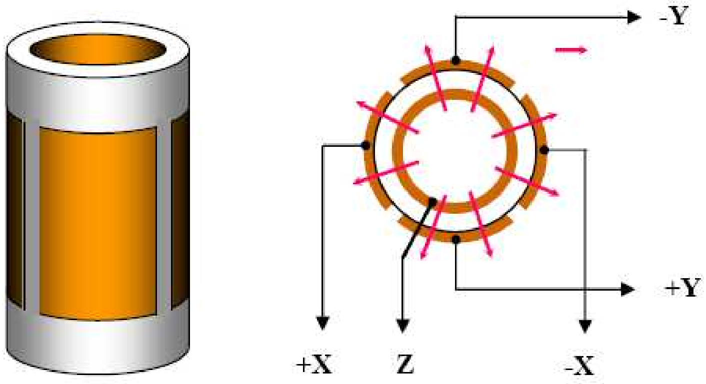

Fig. 6 Tubular piezo-scanner

Optical deflection system

The key component in AFM design is the sensor for measuring the tip movement because of the tip – sample interactions. The force on the tip due to its interaction is sensed by detecting the deflection of the complaint lever with a known spring constant. There are number methods used to measure the cantilever deflection. Compare to other methods, the optical techniques are believed to be more sensitive, reliable and easily implemented than others [41, 42]. The optical beam deflection method (Fig. 7) has the largest working distance and capable of measuring angular changes (because of friction forces). Hence, it is the most commonly used in the commercial AFMs (i.e. SPMs).

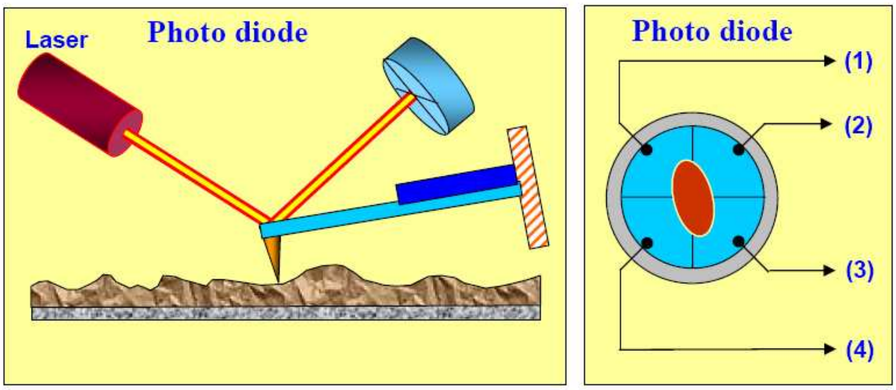

Fig. 7 Schematics of optical deflection system used in SPM

The schematic diagram of optical system used to measure a probe deflection is described in Fig 4. The laser diode stage is a tilt stage used to adjust the position of a laser beam on the backside of the cantilever. It consists of the laser diode, collimator, focusing lens, photodiode. The laser beam is reflected off the backside of the cantilever. A four quadrant photodetector gives the opportunity to measure both normal bending (1-2) and torsion (2-3) of the cantilever, corresponding to normal and lateral forces.

AFM modes

The AFM can be used either in static or dynamic mode. In the static mode, also referred to repulsive mode or contact mode [21], the tip at the free end of the cantilever is brought in contact with the sample surface. During initial contact, the atoms at the end of tips experience a very weak repulsive force due to the electronic orbital overlap with the atoms of the sample surface, as mentioned in Fig 8. The force acting on the tip causes the cantilever deflection, which is detected by the optical deflection system. The up and down motion of the sample is therefore a record of the sample topography. The dragging motion of the tip, however, combined with adhesive and lateral forces, can cause substantial damage to both the tip and sample.

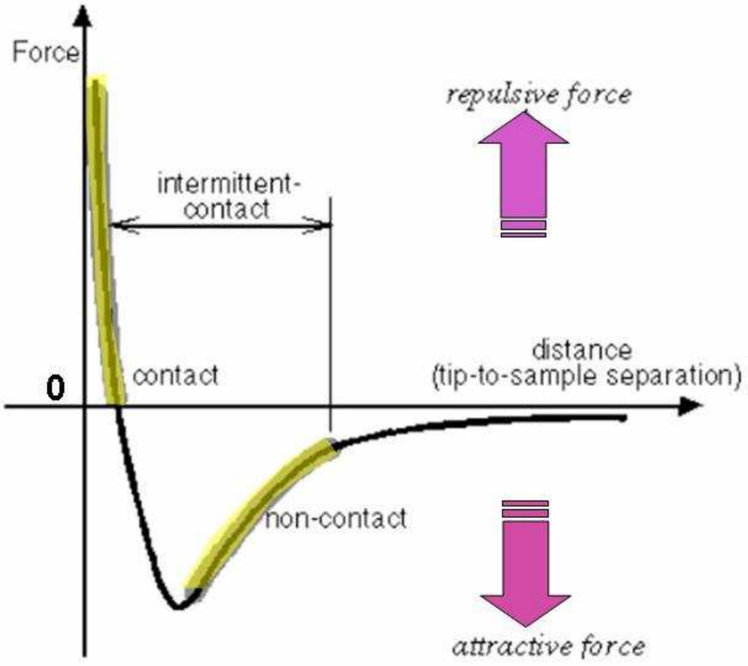

Fig. 8 The diagram of tip-sample interaction

To alleviate this problem, the dynamic mode operation of the AFM, also referred as tapping or intermittent contact mode (Fig 8). In this mode, the cantilever is oscillating at or near its resonant frequency using a piezoelectric actuator. The oscillation amplitude of the cantilever in air can be greater than 20 nm when tip is out of the contact of the sample. When tip is approaching the sample, and when it begins to lightly touch or tap the sample surface. The oscillation amplitude of the tips is reduced. This reduction in oscillation amplitude is now becomes the feedback control signal which can be used to produce the surface topography. Here, the oscillating amplitude is kept large enough so that the tip does not stick to the sample. The mode is used in topography measurements to minimize effect of friction and other lateral forces to measure the topography of soft surfaces.

2.2.4 Scanning tunneling microscopy

Giaever [21] proposed the principle of electron tunneling. Further, it was used to develop scanning tunneling microscopy technique. Scanning Tunneling Microscopy is the first invented microscopy method of SPM family. The working principle of scanning tunneling microscopy is electrons tunneling thorough a narrow potential barrier between a metal tip and a conducting surface in an external electric field. STM can produce the highest resolution images, routinely achieving atomic resolution [43] on flat, conductive surfaces. The schematic of STM is mentioned in Fig. 9.

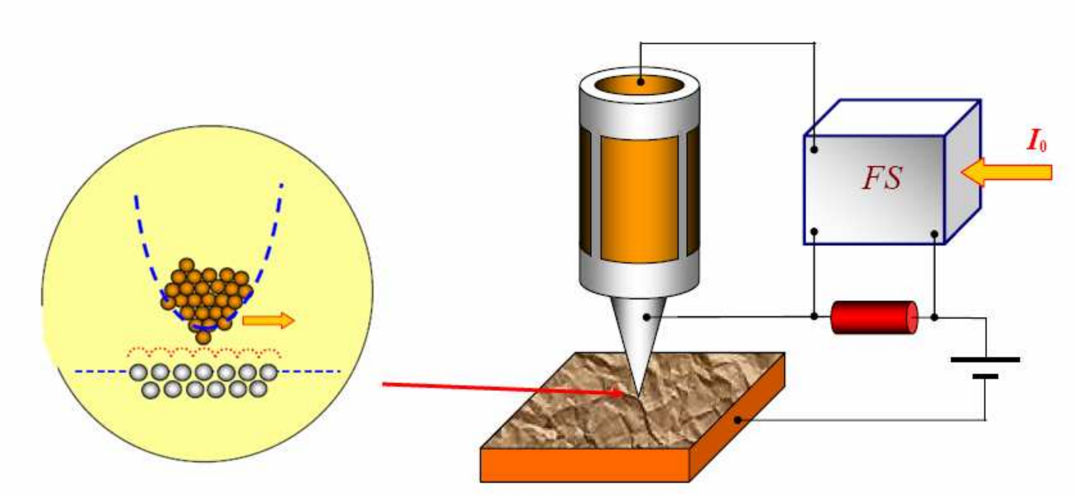

Fig. 9 Schematic diagram of scanning tunnel microscope

In STM, the sample is positioned on sample holder. The STM tip consists of sharpened metal wire that is held 0.3 to 1 nm away from the sample. The PZT tube scanner is attached with tip to maintain *x*, *y* and *z* movement of it. A potential difference of 0.1 V to 1 V between the tip and the sample leads the tunneling currents ranging from 0.1 to 1 nA. The tip, which is mounted on tube scanner, moves in raster fashion above the sample. The feedback system (FS) calculates the desired separation of the tip from the sample by sensing the tunneling current flowing between the sample and the tip. The FS is adjusting the z-position of the sample under tip to maintain tunneling current constant. The Z – position data represents the topography of the sample surface. The tip properties and its structure is the important parameter for resolution of the image.

It is very difficult to prepare a tip with a known atomic structure. STM tips are fabricated by simple mechanical procedures such as grinding or cutting the metal wires. Tungsten is a common tip material because of its high hardness and resistant to damage but its application is limited to ultrahigh vacuum conditions since it readily oxidized. For ambient conditions experiment, an inert tip material such as platinum and gold is preferred. Platinum is typically alloyed with iridium to increase its stiffness.

2.2.5 Lateral Force (LF) measurement

The Lateral Force (LF) Microscopy is a standard contact mode Atomic Force Microscopy (AFM) method that identifies and maps relative differences in surface frictional characteristics. In LF measurement, the probe is scanned over the surface (or the sample is scanned under the probe) in an x-y raster pattern as mention in Fig. 10. A laser beam is focused on the cantilever and reflects onto a segmented photodiode detector to monitor the deflection of the cantilever during raster-scanning. A feedback loop maintains a constant force on the sample by adjusting the height of the cantilever to compensate for topographical features of the surface resulting in a three-dimensional map of the sample. The torsion, or twisting, of the cantilever supporting the probe will increase or decrease depending on the frictional characteristics of the surface (greater torsion results from increased friction). The laser quadrant has four diodes, it can simultaneously measure and record topographic data and lateral force data.

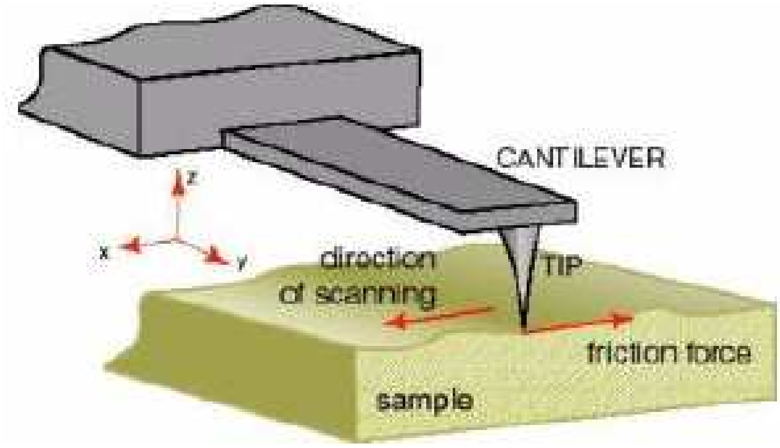

Fig. 10 Principle of Lateral force microscopy

2.2.6 Atomic Force Acoustic Measurement (AFAM)

Atomic Force Acoustic Microscopy is a new SPM measuring mode developed at the Fraunhofer Institute of Nanodestructive Testing, Saarbruecken, Germany [35, 44]. This technique, licensed to NT-MDT, allows measuring the qualitative and quantitative local properties of different materials. AFAM is a non-destructive technique, which enables to measure elastic properties of thin films and structure that cannot be measured with the help of other techniques.

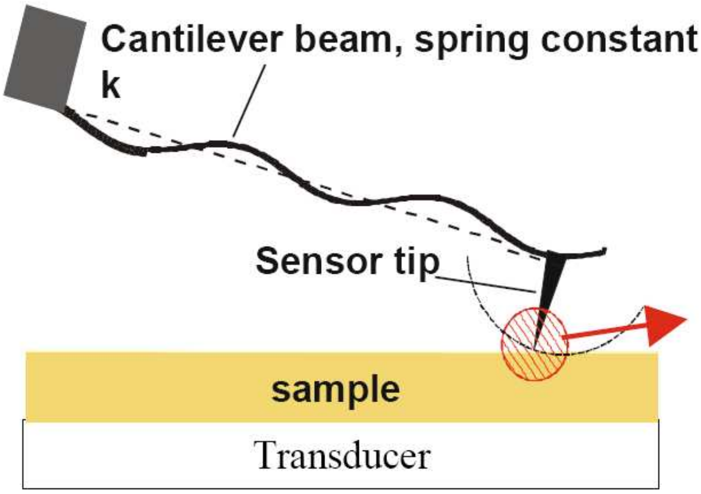

Fig. 11 working principle of AFAM method

In the AFAM setup, the sample is coupled to a piezoelectric transducer as mentioned in Fig. 11. It emits longitudinal acoustic waves into the sample, which cause out-of-plane vibrations of the sample surface. The surface vibrations are transmitted into the cantilever via the sensor tip. The cantilever vibrations are measured by a 4-sectioned photo-diode and evaluated by a lock-in amplifier. This setup can be used either to acquire cantilever vibration spectra or to take acoustic images. The latter are maps of the resonant frequency of the tip-sample system. The varying frequency keeps the resonance of the system in each point. This is established by the constant phase shit of the vibrations. The contact-mode topography image is acquired simultaneously with the acoustic one. The frequency range employed covers the flexural modes of the cantilever from 10 kHz up to 2 MHz.

2.2.7 Electric force microscopy

Improved understanding of the surface properties of conducting polymers as well as the factor affecting the morphology and electric properties of thin films kind of materials may be achieved by Scanning Probe Microscopy (SPM) instrument using the Electric force microscopy method. [45]. Electric Force Microscopy (EFM) is an efficient technique for imaging of electric fields and electric charge distributions on the sample surface with sub-micron resolution [40]. Images obtained by means of this technique are interpreted as spatial distribution of the Z-component of the electric filed gradient on the sample surface. The technique has been found to be especially useful for study of semiconductor devices [46, 47]. EFM is basically two-pass technique. Surface topography of the scanning line is determined in first pass in the semicontact mode of operation. During the second pass, the cantilever is piezodrived at resonant frequency and cantilever is grounded or biased by dc voltage V, which is mentioned in Fig. 12.

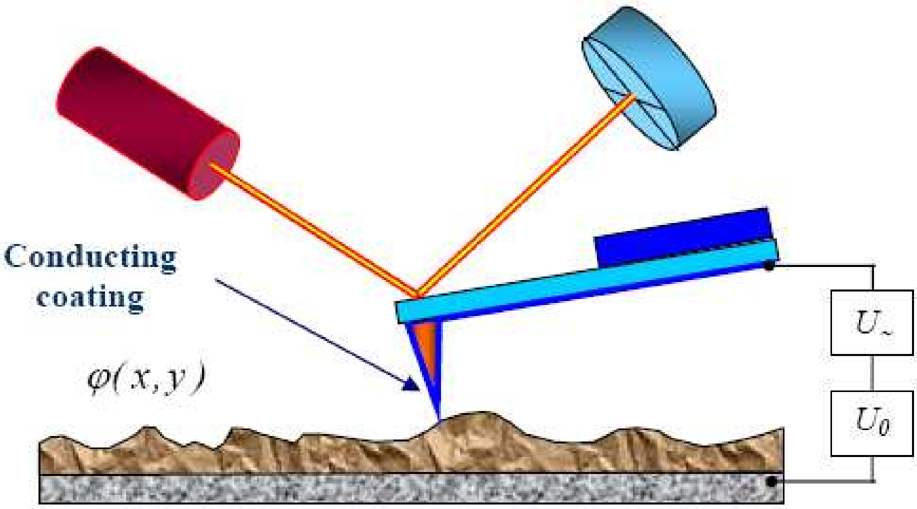

Fig. 12 Electric Force Microscopy

Capacitive tip-sample electric force leads to resonance frequency shift. Accordingly, amplitude of the cantilever oscillation decreases and phase of oscillation changes [48]. Both amplitude and (or) phase of oscillation deviations can be measured and electric potential distribution over the sample surface can be imaged.

2.2.8 Other SPM methods

Magnetic Force Microscopy (MFM) is a technique for imaging of magnetic field spatial distributions on the sample surface. MFM is used for the study of magnetic data storage devices properties, magnetic structure of magnetic with sub-micron resolution etc. This method is also used in two-pass measurement scheme. For MFM, the tip is coated with a ferromagnetic thin film. The system operates in non-contact mode, detecting changes in the resonant frequency of the cantilever induced by the magnetic field's dependence on tip-to-sample separation. MFM can be used to image naturally occurring and deliberately written domain structures in magnetic materials.

Scanning Thermal Microscopy (SThM) is a type of scanning probe microscopy that maps the local temperature and thermal conductivity of an interface. The probe in a scanning thermal microscope is sensitive to local temperatures - providing a nanoscale thermometer. Thermal measurements at the nanometer scale are of both scientific and industrial interest.

The *Scanning Near-Field Optical Microscope* allows optical imaging of samples with a resolution below the diffraction limit. This is achieved by scanning the sample surface with an aluminum-coated fiber tip having a sub-wavelength aperture at its end. Instead of measuring the tunneling current, a shear force detection is coupled to the STM electronics. With its small size of only about 4 cm the scanner is almost unaffected by external mechanical vibrations. Samples under examination at the Institute include ferromagnetic thin films with perpendicular magnetization. Utilizing the Faraday effect, the local magnetization of samples can be measured with high resolution at the Nanometer scale.

Kelvin Probe Force Microscopy (*KPFM*), also known as surface potential microscopy, is a noncontact variant of atomic force microscopy (AFM) that was invented in 1991. With KPFM, the work function of surfaces can be observed at atomic or molecular scales. KPFM is a scanning probe method where the potential offset between a probe tip and a surface can be measured using the same principle as a macroscopic Kelvin probe.

2.2.9 Applications

These techniques have the ability to operate on a scale from microns down to nanometers and can image clusters of individual atoms and molecules. STM relies on the electrical conductivity of the sample, so at least some features on the sample surface must be electrically conductive to some degree. AFM is used for studies of non-conductors and is the technique more commonly used for studies of macromolecules and biological specimens. AFM has been used for measurements on a wide variety of sample types, including surfaces of metals, polymers, ceramics, natural surface topography, surface chemistry, silicon wafers and data storage media. It is also used to study the nanostructures of carbon nanotubes, diffraction gratings, integrated circuits etc.

They have very wide applications in biological materials. They are widely used to study the muscle proteins, DNA, plant cell walls, bacterial flagella, cell and membrane surfaces etc.

2.2.10 Limitation of scanning probe microscopy

- The detailed shape of the scanning tip is sometimes difficult to determine. Its effect on the resulting data is particularly noticeable if the specimen varies greatly in height over lateral distances of 10 nm or less.
- The scanning techniques are generally slower in acquiring images, due to the scanning process. As a result, efforts are being made to greatly improve the scanning rate. Like all scanning techniques, the embedding of spatial information into a time sequence opens the door to uncertainties in metrology, say of lateral spacing and angles, which arise due to time-domain effects like specimen drift, feedback loop oscillation, and mechanical vibration.
- The maximum image size is generally smaller.
- Scanning probe microscopy is often not useful for examining buried solid-solid or liquid-liquid interfaces.

2.3 Nanoindentation

2.3.1 Importance of nanoindentation

Tailoring surfaces by plasma modification and polymerization has proven to be a powerful technology that has revolutionized surface modification and thin film formation. Plasma polymer films have been a key material in many areas, including electronics, magnetic recording media, optical devices, MEMS, and chemical and mechanical protection of engineering components [49].

In such developments, a good understanding of the mechanical properties of thin film is essential. It is, however, not a simple undertaking to evaluate the mechanical properties of a thin structure unit at submicron level using conventional testing methods. However, recent years, several techniques have been developed to study the nanomechanical properties of thin films. Among these, nanoindentation is a widely used technique for evaluating nanomechanical properties such as elastic modulus, hardness, and stiffness [50]. Although nanoindentation is an excellent tool, good interpretation of the indentation data is important in order to achieve reliable and repeatable results regarding the mechanical behavior of the thin films.

2.3.2 Equipment for nanoindentation

The goal of majority nanoindentation tests is to extract elastic modulus and hardness of the specimen material from load-displacement measurements. The idea of nanoindentation test came from the traditional indentation test (macro or micro indentation), which is an excellent way to measure mechanical properties of thick coatings. The traditional indentation test involves the measurement of the size of a residual plastic impression in the specimen as a function of the indentation load, which provides a measure of the contact area for that particular indenter load.

The same concept is applied for the nanoindentation test but the problem is determining the indentation contact area, which is very small. It can be difficult to see without a powerful microscope. To solve this problem depth sensing indentation methods were developed. In this method, the load and displacement of the indenter is recorded during the indentation process and these data are analyzed to obtain the contact area, and thereby mechanical properties, without having to see the indentations.

In simple word, nanoindentation refers to a depth-sensing testing in the submicrometer range. It has been made possible by the development of (1) machines that can make such tiny indentations while recording load and displacement with very high accuracy and precision, and (2) analysis models by which the load displacement data can be interpreted to obtain hardness, modulus, and other mechanical properties.

From early 1980s to till date, because of a special interest in nanoindentation has spawned a number of nanoindentation instruments manufacturer. These instruments are very interesting for universities, private and government research organizations, and quality control laboratories. They have shown a particular interest within the semiconductor industry that is concerned with the mechanical properties of a wide range of thin films. The instruments typically measure depth of penetration using either a changing inductance or capacitance displacement sensor. A typical nanoindentation test instrument has a depth resolution of less than a tenth of a nanometer and a force resolution of less than a nanonewton. The load can be applied by the expansion of the piezoelectric element, the movement of a coil in a magnetic field, or electro statically. Maximum loads are usually limited to the millinewton range. Detail description about some of the widely used instruments is given below.

(1) “Nano Indenter®”, MTS systems Corporation

The Nano Indenter indentation instrument is widely used in this field and has a development history dating back to about 1981 [51]. This instrument applied a load via a calibrated electromagnetic coil and displacement of the indenter is measured using a capacitive plate transducer. The load and displacement resolutions are reported to be 50nN and 0.04 nm respectively [52]. The patented [53] continuous stiffness measurement (CSM) option is of particular interest in this instrument. Further detail regarding CSM is given in chapter 3.8.

(2) “NanoTest®,” Micro Materials Ltd.

The Micro Materials NanoTest® platform has been designer to support three modules: (a) nanoindentation, (b) scanning for scratch testing, and (c) impact (for thin film adhesion failure, erosive wear and contact fatigue). In this instrument, the load is applied by means of a coil and a magnet is located at the top of the pendulum. The pendulum is supported by a frictionless spring flexure. The resultant displacement of the probe into the surface is monitored with a sensitive capacitive transducer and displayed in real time as a function of load.

(3) “TriboIndenter®,” Hysitron Inc.

The Hysitron TriboIndenter® is a low load indentation system designed for measuring the hardness and elastic modulus of thin films, coatings, and bulk materials. The TriboIndenter® provides quantitative testing capabilities with both normal and lateral force (nanoscratch) loading configurations. It can operate in static or dynamic lading modes. The patented transducer technology [54-55] used within the instrument uses a capacitive displacement measurement technique combined with electrostatic force generation. The transducer and the indenter tip are both fixed to a piezoelectric scanner the TriboIndenter® is capable of in situ SPM (scanning probe microscopy) imaging.

Nanoindentation Tip (Nano indenter)

To run a successful nanoindentation test, a well-defined geometrical indenter tip is very important. There are numerous geometries available for the nano indenter such as three sided pyramids, four sided pyramids, wedges, cones, cylinders or spheres. The tip end of the indenter can be made sharp or flat or rounded to a cylindrical or spherical shape.

The nano indenter is mostly made up from diamond and sapphire materials. In some cases, other hard materials can also be used to make a nanoindenter such as quartz, silicone, tungsten, steel, tungsten carbide and almost any other hard metal or ceramic. Some widely used nano indenters are known as Berkovich, cube corner, Vickers, conospherical, knoop etc. Nano indenters are mounted on holders, which could be the standard design from a manufacturer of nano indenting equipment, or a custom design. The holder material can be steel, titanium, ceramic or other suitable material.

The Berkovich tip is the standard nanoindentation tip, which is widely used for the nanoindentation experiments of thin films. The geometry of a Berkovich tip can be described as a three-sided pyramidal tip with a total included angle of 142.35 degrees and a half-angle of 65.35 degrees mentioned in Fig. 13. The standard Berkovich tip is available with radius of curvature of 150 nm while the sharper ones are with a radius of curvature of 50 nm. Such pyramidal tips are commonly used in nanoindentation of ceramics, glass, metals, hard polymers, hard & smoothed biomaterial and thin films.

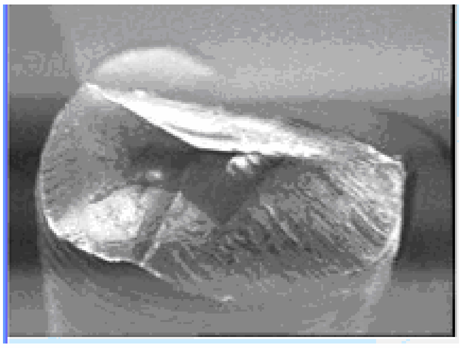

Fig. 13 Optical microscopy image of Berkovich diamond probe

Cube corner tips are also three-sided pyramidal tip. The total included angle of the cube corner tip is 90^0. The tip is available with radius of curvature less than 30 nm. The main advantage of this tip is the sharpness. It is widely used for indentation study of rough samples. Vickers tip is a four-sided pyramidal tip. It has depth to area ratio and area function is same as Berkovich tip. It has a radius of curvature larger than 500 nm. This kind of tip is used for special purpose like to find scale connectivity between the nanoindentation and microindentation worlds.

However, with longer usage, it is expected to change the shape of tips because of wear and deformation. Therefore, regally tip area calibration is a very important procedure for correct nanoindentation measurements of thin films and coatings. The detailed description about tip area calibration is given in chapter 2.3.5.

2.3.3 Theoretical analysis

Oliver-Pharr method

The two mechanical properties are measured most frequently using load and depth sensing indentation techniques are the elastic modulus, E, and the hardness, H. The data are obtained from one complete cycle of loading and unloading of commonly used indentation method [56].

The analysis performed in nanoindentation relies heavily on the pioneering work in elastic contact theory performed by Boussinesq, Hertz and Sneddon [50]. Boussinesq developed a theory based on computing the stresses and displacement in an elastic body loaded by a rigid, axisymmetric indenter. This theory was successfully applicable for indenter geometries such as cylindrical and conical indenter. Hertz generalized this theory by considering an elastic contact between two spherical surfaces. Sneddon made further, major contribution in this work, which considered elastic indenter of different geometries and suggested the load-displacement relationships for many simple punch geometries can be written as

$$P = \alpha h^m \quad (1)$$

Where P is the indentation load, h is the elastic displacement of the indenter, and α and m are constant.

This pioneer work was further developed by many other researchers and used by Oliver-Pharr also [50] to suggest a simple method to measure the mechanical properties of thin films using the indentation technique. From indentation experiment, a typical load vs. displacement curve obtained is mention in Fig. 14. The curve can be expressed in three parts: a loading portion during which the load is increased monotonically to its maximum value; a constant load portion during which the load is remained unchanged also known as hold time or dwell time; and the unloading portion during which the indenter is gradually withdrawn from the specimen. During unloading process, the behavior of upper portion of unloading part is due to the elastic recovery of sample. While the final value of the unloading displacement is due to the residual imprint of the indent that is created in the specimen. The three key parameters obtained from the load vs. displacement curve are the Peak load (P_{max}), the maximum indentation depth (h_{max}), and the initial unloading contact stiffness (S).

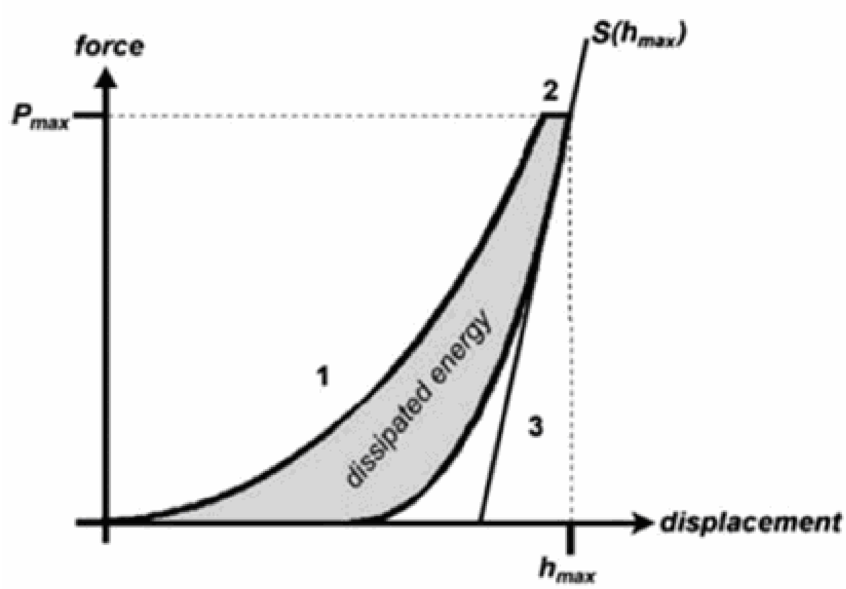

Fig. 14 a typical load vs. displacement curve

In load vs. displacement curve, the upper portion of unloading curve is analyzed by applying the power law relation. Hence, the value of constant stiffness obtained from the slope of unloading curve. It is described as,

$$S = \frac{dp}{dh} \tag{2}$$

The area of contact A at the maximum load is determined by geometry of the indenter and depth of contact, h_c. We are using the Berkovich indenter tip of known geometry. So we can described the projected contact area at maximum load as the function of contact depth,

$$A = F\,(h_c) \qquad (3)$$

The obtained value of contact stiffness S and projected contact area $A\,(h_c)$ are helpful to calculate the reduced modulus of sample by the help of a equation described by Sneddon. The expression related to the contact stiffness and reduced modulus was used by Bulychev et al. in early 1970's to determined the modulus is rewritten by Oliver-Pharr [50] as

$$\mathrm{E_r} = \frac{\sqrt{\pi}}{2\sqrt{A(h_c)}}S \qquad (4)$$

where, S = contact stiffness, and,
$A\,(h_c)$ = projected contact area.

The reduced modulus is itself a function of the Young's modulus, E, and Poisson's ratio, υ, of both the test specimen and the diamond indenter. This relationship is given as

$$\frac{1}{E_r} = \frac{1-\upsilon_s{}^2}{E_s} + \frac{1-\upsilon_i{}^2}{E_i} \qquad (5)$$

where, E_S and υ_s are the Young's modulus and Poisson's ratio of the sample, and,
E_i and υ_i are the Young's modulus and Poisson's ratio of the indenter.

Therefore, by selecting an indenter with known properties, and estimating the Poisson's ratio of the specimen, it is possible to obtain the value of the Young's modulus of the specimen from nanoindentation load-displacement curves.

In addition to Young's modulus, the hardness, H, of the specimen can also be obtained from nanoindentation load-displacement curves. This quantity is given simply by:

$$H = \frac{P_{\max}}{A(h_c)} \qquad (6)$$

Equations (1) to (6) form the basic framework for analysis of nanoindentation response. This framework was developed over several years with contributions from numerous researchers, and was formalized in landmark papers by Oliver and Pharr in 1992 [50]. Therefore, this method of analyzing nanoindentation results is now, commonly called the **Oliver-Pharr method**.

However, this method is widely used and accepted but it has some limitations. First, the specimen is assumed to be an isotropic, homogeneous, monolithic and elastic in nature. Second, this method is not applicable for creep study or where they samples show the pile-up phenomena [57, 58]. Therefore, this method must be refined and extended to solve its limitations.

<u>Field and Swain method</u>

The Field and Swain [59] method of analysis feature a single partial unload rather than a series of unload data points from maximum load. The advantage of this is speed and convenience. By using the curve fitting, multiple data points obtained from partial unloaded. However, the degree of partial unload must be chosen so that the unloading is elastic and no reverse plasticity is involved. In this method, there is more possibility of errors which introduced by thermal drift.

Both the Field and Swain and the Oliver and the Pharr methods have their own foundation. These both methods are using the Hertz's theory about elastic contact as their pioneer. The main difference between the two methods is that the Field and Swain methods fits a single pair of data points (maximum load and some percentage unload) to the Hertz equation, while the Oliver and Pharr method is using a series of data points and fits the slope of the initial unloading to the derivative of Hertz equation. The Oliver-Pharr method is time consuming and long but there is very less possibility of errors in that data. While, the Field-Swain method is appropriate where the experiment is running under undesirable mechanical and thermal influences.

2.3.4 The Rule of Thumb (The 10 % rule)

The 10 % rule was first recommended by buckle [60], for microindentation of thicker films. Further, it was used as the extension of Oliver – Pharr (o-p) method for thin films. According to the rule, the substrate will not influence the nanoindentation experimental data as long as the total indentation depth is less than 10 % of the film thickness.

However, in films of nanometer scale thickness, limiting the indent depth to 10 % of the films results in data reduction errors, as the indenter's geometrical features are comparable in size to the indent depth [60]. Thus, a more precise and universal methods were sought to better determine the true film mechanical properties.

2.3.5 Tip area calibration

The ideal geometry of Berkovich tip can be explained by the following equation

$$A = 24.5\, h^2 \tag{7}$$

Where, A = projected contact area
h = indentation depth

Because of longer usage or indentation of very hard materials, the ideal geometry of the Berkovich is expected to deviate because of the finite radius of curvature of the indenter tip. The radius of curvature is increased or changed due to the wear and contact damage during usage. Therefore, very often the tip area calibration is necessary to get the correct contact area between the film and tip.

For the tip area calibration, install the standard sample fused quartz, which was provided with the instrument. The known hardness (9.25 GPa) and reduced modulus (69.6 GPa) values of standard fused silica were used as a reference. Several indents are performed in the standard fused quartz materials. Typically, indentation loads were varied from 100 µN to 10000 µN for a set of 20 to 40 indents. The area function of the indenter is then determined by comparing the indentation depths with the respective projected area. The standard practice in nanoindentation is to fit the area function to a fifth order polynomial of the form:

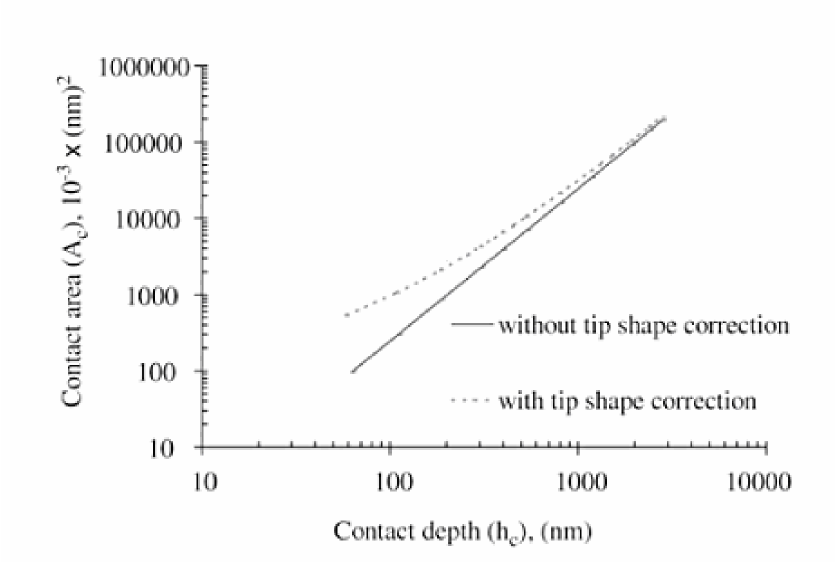

Fig. 15 Contact area vs. contact depth curve representing the tip area calibrations

$A = C_0h^2 + C_1h + C_2h^{1/2} + C_3h^{1/4} + C_4h^{1/8} + C_5h^{1/16}$, (8)
Where, C_k, K = 0, 1, 2, 3, 4, 5 are the constants of the empirical fit.

Fig. 15 shows a representative example in which the projected contact area is plotted as a function of the indentation depth. The constants obtained from the polynomial fit of this data using the Hysitron software are:

$C_0 = 24.5$,
$C_1 = 9.5197 \times 10^3$,
$C_2 = -3.9692 \times 10^5$,
$C_3 = 3.1290 \times 10^6$,
$C_4 = -6.9240 \times 10^6$, and,
$C_5 = 4.1874 \times 10^6$.

2.3.6 Drift

Drift can be due to the vibration or thermal heating (which referred as thermal drift). Thermal drift is caused by the different thermal expansion in the machine or heat generation in the electronic device. Drift can also be referred as the unintentional and unwanted motion to the specimen relative to the indenter, and any unwanted changes in control electronics, during measurement. Drift is especially important while studying time varying phenomenon like creep property of material. Further explanation to creep is given in next paragraph 2.3.7.

Two types of drift behavior might be observed in nanoindentation testing [61]. First, one is observed during the holding phase, where the indentation depth is decreased with time, suggesting that the specimen is expelling the indenter. This kind of response has not been known for the mechanical behavior of that particular sample. It can lead to large errors in estimating mechanical properties of specimen. Another kind of behavior is, during hold phase, here the displacement or depth reading increases as the indenter sinks into the specimen. This might be due to the thermal expansion or contraction of the apparatus.

We have the Hysitron Triboscope instrument with open loop function (i.e. loading without any feedback control) [62], hence, there are more possibilities of introducing the drift errors in indentation experiments. Therefore, it is very important to remove or minimize the drift effect in real indentation experiment. Hence, before every indentation experiment, the drift was monitored and analyzed for preset time (*s*). This measured drift rate is used to correct the load-displacement data.

To correct the thermal drift errors during indentation experiments by Hysitron Triboscope, many scans of the same place before indentation experiments were, carried out. Hence, the tip remains more time in contact with the sample. In addition, acoustic covers to avoid the external vibrations and temperature changes covered the instrument.

2.3.7 Creep experiment

Plastic deformation in all materials is time and temperature dependent which is due to creep effect. The Creep is the tendency of a solid material to slowly move or deform permanently under the influence of stresses. The mechanical properties of nanocrystalline materials, which exhibit essential strain rate sensitive, have been reported recently [63, 64]. Several time-dependent deformation studies were carried out during indentation testing of Zr-based metallic glass coatings [65], Pd-based metallic glasses [66], polycrystalline thin films [67], and polycarbonate polymer films [68].

For bulk materials, the creep study mostly carried out by the help of tensile testing or compression testing. However, Nanoindentation can be also used to obtain creep data in cases where there in not enough material available to machine tensile or compression creep specimens or in case where the creep properties of small amounts of materials need to be locally assessed.

Creep behavior has a remarkable influence on mechanical properties such as the modulus and hardness of the thin films. The Creep study of thin films was carried out by nanoindentation technique under following experimental conditions.

(a) different loading/unloading rate
(b) different dwell time or hold time at highest load
(c) constant strain rate

2.3.8 Continuous Stiffness Measurement (CSM)

A newly developed technique, continuous stiffness measurement (CSM), offers a significant improvement in nanoindentation testing. The CSM techniques provided in nanoindenter XP instrument. The CSM is accomplished by imposing a small, sinusoidally varying signal on top of a DC signal that drives the motion of the indenter [69, 70]. By analyzing the response of the system by means of a frequency specific amplifier data are obtained. This allows the measurements of contact stiffness at any point along the loading curve and not just at the point of unloading as in the conventional measurements. This technique makes the continuous measurement of mechanical properties of materials possible in one sample experiment without the need for discrete unloading cycles, and with a time constant that is at least three orders of magnitude smaller than the time constant of the more conventional method of determining stiffness from the slope of an unlading curve. The measurements can be made at exceedingly small penetration depths.

2.3.9 Scratch test

The scratch resistant of thin films and protective coatings is usually expressed in terms of their ability to withstand abrasion with fracturing [61]. The scratch test is helpful to study the surface mechanical properties of thin films and coatings such as adhesion, fracture and deformation. The scratch tester's ability to characterize the film-substrate system and to quantify parameters such as friction and adhesive strength, using a variety of complementary methods, makes it an invaluable tool for research, development and quality control.

Although the scratch test has been widely used as an indicator of film adhesion strength [71], until recently it was difficult to perform such a test on films less than 1 µm thickness. However, the development of nanoindentation technique makes it possible to perform such a scratch test on films less than 1 µm thickness. In order to perform a successful scratch test in sub-micron films the scratching apparatus has to satisfy two requirements: to apply controlled very low loads (nN) to the tip, and the precise movement of the tip relative to the film at controlled loads [72]. Another important requirement is the use of a procedure, which can offer in situ monitoring of the induced scratch damage. The schematic of nanoindentation scratch test is shown in Fig. 16. In this mode of operation, a normal force F_N is applied to the indenter, while at the same time, the specimen is moved sideways. In some instruments, an optional force transducer can be used to measure the friction, or tangential force F_T. In some case, a lateral force F_L, normal to F_T can also be applied.

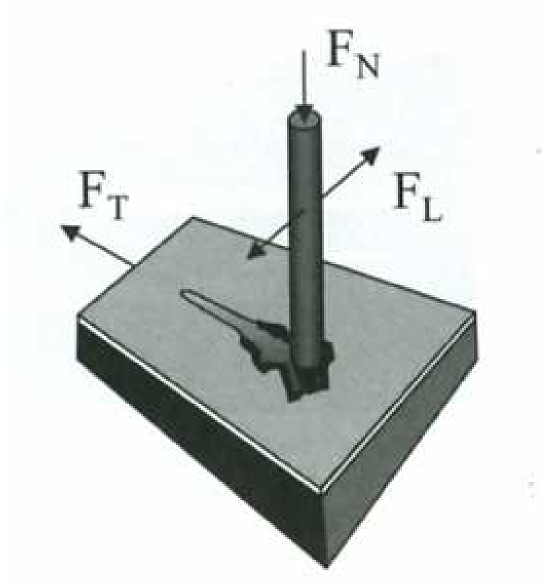

Fig. 16 Configuration of indentation scratch test

This technique involves generating a controlled scratch with a sharp tip on a selected area. The tip is commonly made up of diamond or hard metal (WC) materials. There are two types of tip with different geometry are widely used for scratch test.

(1) Three-sided pyramidal tips
Bekovich is mostly widely used three-sided pyramidal tip for nanoindentation purpose. It can also be used for scratch and wear testing. Another type of three-sided pyramidal tip, which is used for scratch test, is conospherical tip. The conospherical tips are not short enough to provide the sensitivity needed of thinner films. However, the Berkovich tip, which is available with radius of curvature from 50-150 nm, is better to use for scratch testing of thinner film than conospherical ones.

(2) 90 degree (cube corner) tips
Cube corner tip can be used for similar scratch and wear applications as the Berkovich. The cube corner tips are sharper than other tips, so they are best for testing scratch resistance of ultra thin films and coating (typically less than 20 nm). It can produce the images of the scratches will more resolution than other tips. The major drawback of this kind of tip is they can easily blunted or damaged.

3 Experiment

3.1 Plasma polymer film

The plasma polymer films used for analyses in this dissertation were deposited from organosilicon monomer with the help of plasma enhanced chemical vapor deposition (PECVD) method. This part of the chapter introduces the organosilicon monomers, thin film deposition systems and plasma polymerization.

3.1.1 Organosilicon monomer

There were two types of organosilicon monomers used for plasma-polymerized thin film. The monomers are (1) tetravinylsilane (TVS) and (2) vinlytriethoxysilane (VTES).

(1) Tetravinylsilane
The chemical structure of tetravinyl silane is : $Si – (CH = CH_2)_4$. Sigma Aldrich supplied it with purity of 97%.
(2) Vinyltriethoxysilane
The chemical structure of Vinyltriethoxysilane is $CH_2 – CH – Si (– O – CH_2 – CH_3)_3$. Fluka supplied it with purity ≥ 98%.

The VTES is one of the organofunctional silane coupling agents recommended for surface modification of glass fibers. This monomer molecule is a multifunction one, which reacts at one end with the glass surface and at the other end with the polymer matrix.

3.1.2 Thin film deposition systems

There are two types of thin film deposition systems in Brno University of Technology.

(1) Parallel plate (capacitive coupling) deposition system and
(2) Helical (capacitive coupling) deposition system.

Parallel plate (capacitive coupling) deposition system

It is a novel plasma reactor, that has been developed as a part of the joint Czech-Japan project (2002 – 2004) supported by the Czech and Japan Ministry of Education under the guidance of Prof. Vladimír Čech. The plasma system is mentioned in Fig. 17, which is used in preparation of functionally nanostructured thin films of high reproducibility. The deposition system is a new creative design equipped with many non-standard components. It mainly consists of deposition chamber, using plan-paralleled electrodes [73]. It was derived from a typical capacitive coupling system. The bottom rotary electrode enabled to stick in/out samples from the chamber under vacuum hence without reactor contamination. It can be heated or cooled ranging from -100 to 300 °C. The upper electrode is made up with shower-type facility and it can be positioned in a distance of 20 – 60 mm from the bottom one. An RF-generator was connected to the system using an automatic matching network. With apparatus, it is possible to achieve a range of effective power density from 1 x 10^{-4} to 4 x 10^{0} W cm^{-3} (1 x 10^{-3} to 4 x 10^{0} W cm^{-3}) using pulsed (continuous) plasma regime.

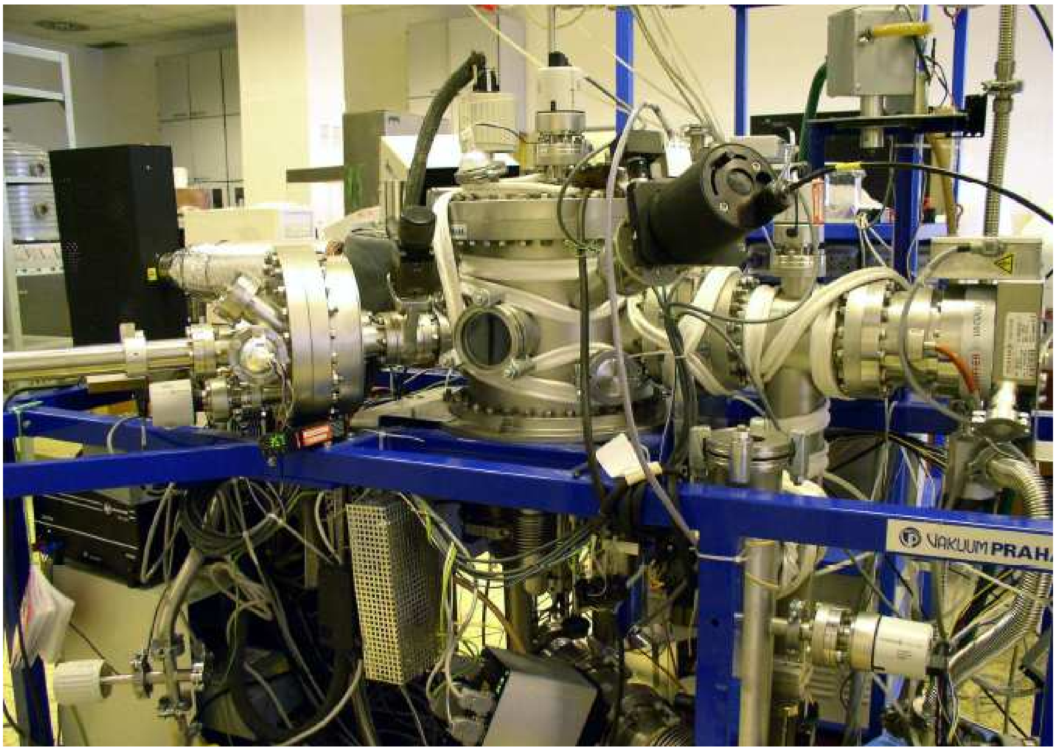

Fig. 17 Schematic diagram of film deposition apparatus

This apparatus is equipped with mass spectrometer, in-situ spectroscopic ellipsometer (UVISEL, Jobin-Yvon), and optical emission spectrometer to monitor the plasma process and film growth.

<u>Helical (capacitive coupling) deposition system</u>

The plasma chamber is made up from Pyrex-glass tube, which is 400 mm long, and its inner diameter is 40 nm. The inductive coil wrapped around the outside of the Pyrex tube (plasma chamber) is connected to a RF generator, operating at a frequency of 13.56 MHz, through the matching network. The system is able to work with power up to 500 W. The system enables a thin film deposition on planar substrate, single filament and continuously rewound bundle of fibers. Schematic diagram of the deposition system is shown below in Fig 18. The details of the apparatus for the same were described by Prikryl et al. [74].

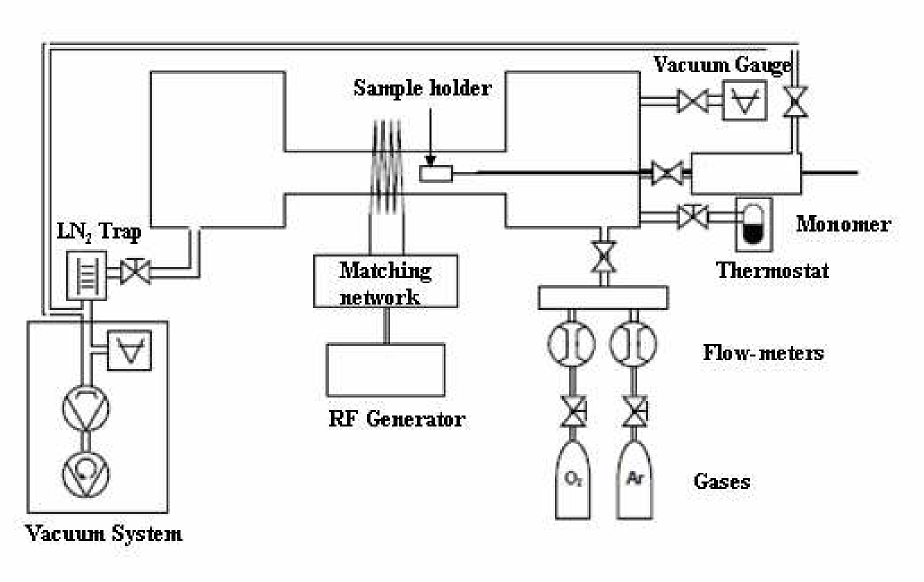

Fig. 18 Schematic diagram of film deposition apparatus

3.1.3 Plasma Polymerization

The plasma polymerized thin films were deposited on polished silicon (100) wafers (Terosil) by PECVD using an RF (13.56 MHz) capacitive coupling plasma system working in the pulse mode or continuous mode with the help of deposition apparatus. The main variable parameters in deposition method are the effective power (W_{eff}), basic pressure (P), monomer flow rate (F) and deposition time. The effective power (W_{eff}) of pulsed plasma was controlled by changing the ratio of the time when plasma was switched on (t_{on}) to the time when plasma was switched off (t_{off}), $W_{eff} = t_{on} / T \times W_{\mathrm{total}}$, in which the period was defined as $T = t_{on} + t_{off}$ and $W_{\mathrm{total}} = 50$ W [75].

The general procedure steps for plasma thin film preparation by Helical coupling system are mentioned below:

I. First, load the sample inside the reaction chamber.
II. Then, reactor chamber is evacuated to the basic pressure.
III. The silicon wafer is pre-treated with O_2 plasma for few min and then stored in a load lock separately. Put the Ar plasma with the same effective power and time like O_2 plasma to clean the chamber.
IV. Desired monomer flow rate is set and after the pressure is stabilize, the plasma is igniting.
V. Employing a mechanical manipulator, the pre-treated silicon wafer is placed into the plasma zone after the plasma has reached a steady state characterized by a constant pressure. The films were deposited of desired thickness by varying the deposition time or deposition effective power.
VI. Switch off plasma and switch off monomer.

VII. Finally, the deposited sample is stored in the load lock, flushed with argon gas for one hour, and then flushed with air up to atmospheric pressure. The sample was removed from the load lock and stored in desiccators until the next measurements.

The general procedure steps for plasma thin film preparation by Parallel plate (capacitive coupling) system are mentioned below:

I. Load the sample into the bottom electrode in the reaction chamber with the help of load-lock chamber.

II. The reactor chamber is evacuated to the basic pressure. Adjust the pumping flow rate by butterfly valve.

III. The silicon wafer is pre-treated with argon plasma at 5 W for 10 min. Thus, the silicon surface is activated by argon plasma.

IV. After pre-treatment, the reactor is evacuating for maximum time of 10 minutes. For that purpose, glow discharge is switched off, argon flow rate is stopped, reactor is evacuated to the basic pressure.

V. Set up the monomer flow rate at 3.8 sccm.

VI. For plasma polymer deposition, set the required generator power and generator regime: continual or pulse (in this regime also pulse duty cycle). Switch on the plasma glow discharge for required deposition time. The films were deposited of desired thickness by varying the deposition time or effective power.

VII. The plasma is monitored by mass spectroscopy and characterized by a constant pressure.

VIII. After plasma deposition, 10 sccm of argon gas is let in to reactor for 1 hour. After an hour, the argon gas is switched off, the reactor chamber is evacuated and samples are measured by spectroscopic ellipsometry to obtain their optical properties and thickness after deposition. Samples are kept in the reactor to the next day to get rid of free radicals. Finally, the samples are taken out from the reactor for further analysis.

3.2 The Scanning Probe Microscope

All the scanning probe microscopy experiments discussed in this dissertation were done in a NT-MDT NTegra Prima scanning probe microscope with optical viewing system (Optical microscope). This part of the chapter introduces the basic design of NT-MDT scanning microscope, microscope head, scanner, specification of NTegra Prima instrument and SPM probe. Finally, the characterization steps and Nova software of NTegra Prima Scanning Probe Microscope is discussed.

3.2.1 Scanning Probe Microscope basic setup

The NTegra Prima Scanning Probe Microscope comprises the following basic systems and set up :

- Base unit, which supports the completely scanning probe microscope operating system.
- Measuring module, which is made up of measuring head, exchangeable mount, scanner and heating stages, liquid cells etc.
- Protective hood – to protect the scanning probe microscope from external vibration.
- Optical viewing system, and
- Vibration isolation system, which is manufactured by Table stable Ltd., Switzerland under brand name of TS-150. It is a vibration damping system, which is protecting the SPM system from vibration coming through ground.

The schematic illustration of basic modes of the NTegra Prima SPM is mentioned in Fig. 19 (a) and the NT-MDT SPM mentioned in Fig. 19 (b). By making changes in measuring modules, it is possible to operate different scanning probe microscopy methods such as Atomic Force Microscopy, Scanning Tunneling Microscopy, Lateral Force Microscopy, Atomic Force Acoustic Microscopy, Magnetic Force Microscopy, Electrical Force Microscopy, Kelvin Probe Microscopy, Lithography etc. The detail discussion about some of the main method is mentioned in the following part the chapter.

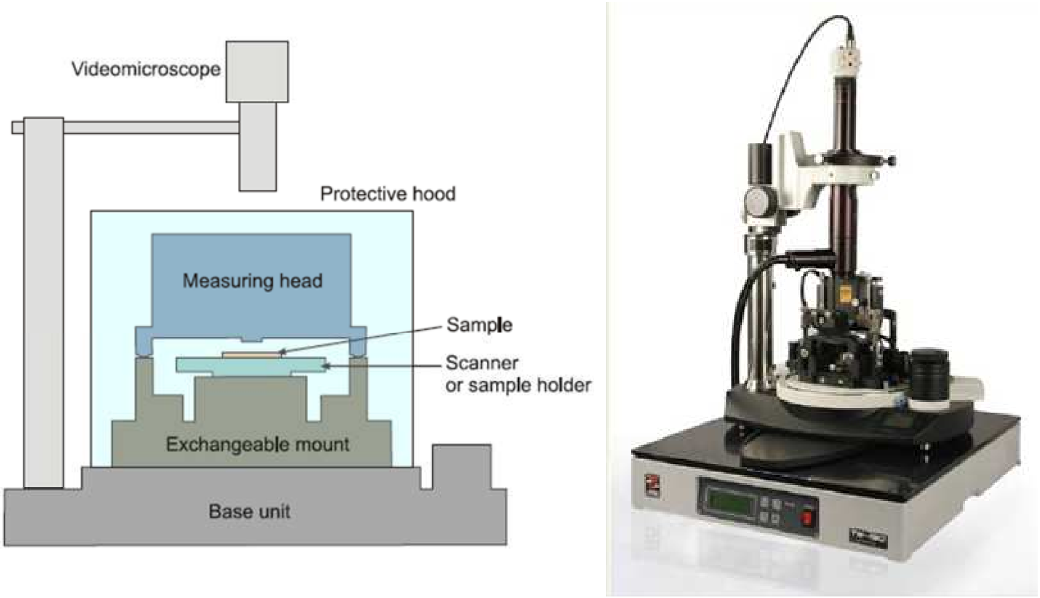

Fig. 19 NT-MDT NTEGRA Prima scanning probe microscope: (a) Schematic illustration of basic modes of the system, (b) photo of SPM system.

SPM Measuring heads

There are three types of measuring head available with Ntegra Prima system (a) Universal measuring head, (b) Scanning measuring head and (c) STM head.

(a) Universal measuring head

The universal measuring head can be used to realize almost all SPM techniques both in air and in liquid. A broad range of measurement techniques is realized by using a set of adjustment units, which are specially designed for particular techniques and for measurements of certain parameters. An overview of the universal measuring head with the adjustment unit connected to it is presented in Fig. 20.

The universal measuring head is widely used in small smaple AFM analysis. It consists of diode laser & lens, mirrored prism, mirror and a quad photodetector. (Split photodetector with four quadrants). By the help of adjustment screw, one can set the laser beam at the back side of the cantilever and also the reflected beam from the back side of cantilever strikes to the center of the photodiode. The adjustment unit accomodates the probe holder.

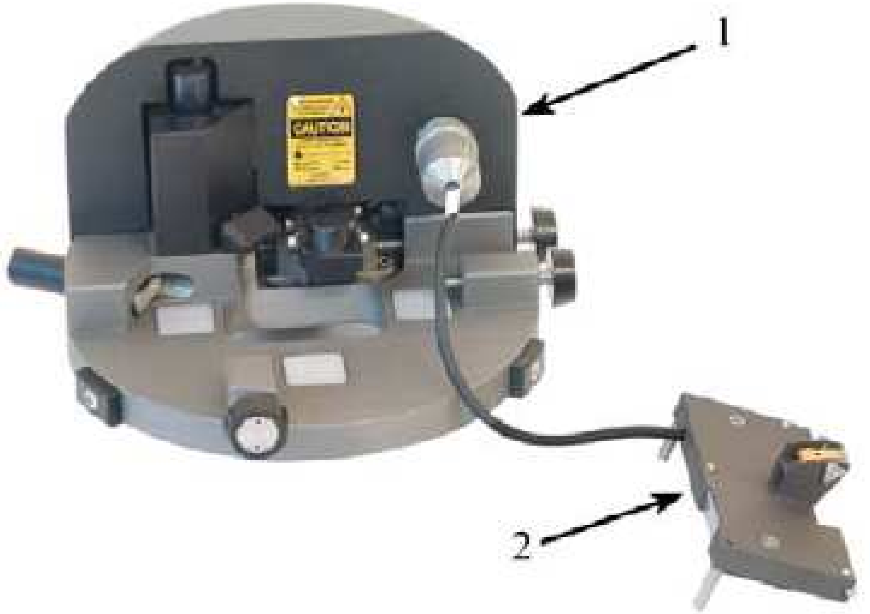

Fig. 20 SPM measuring head (1) Universal measuring head; (2) adjustment unit.

(b) Scanning measuring head

It is also called as the large sample AFM head. It is consist of both force sensors using optical deflection system (laser diode, mirroed prism, mirror and quad photodetector) and scanning unit. Because of the vibration added by cantilever movement, the lateral resolution of this design is some what poorer than the univeral measuring head. It is also used for AFAM measurement, where sample is mounted on piezoelectric transducer.

(c) STM head

This head is specially used for Scanning Tunneling Microscopy (STM) measurement. The head consists of probe holder part which can hold sharped part of a PtIr or W wire of 8 – 10 mm length and of 0.25 – 0.5 mm diameter. This wire is used as an STM probe.

<u>Scanners</u>

The piezo-electric tube (PZT) scanner is widely used for SPM method. It is consists of separated electrodes to scan precisely the sample in the x – y plane in a raster pattern and to move the sample in the vertical (z) direction. There are two types of scanners are available with NTEGRA Prima instrument.

1. Scanner without capacitance sensors. This scanner is connected to the base unit through the connected Scanner.
2. Scanner with capacitance sensors. This scanner is connected to the base unit through the connector Scan+Sensor.

A piezo ceramic tube, which is enclosed within a metal housing (Fig. 21) is the basic component of the exchangeable scanner. Carriage mentioned as 2 in Fig 21 is fastened to the housing.

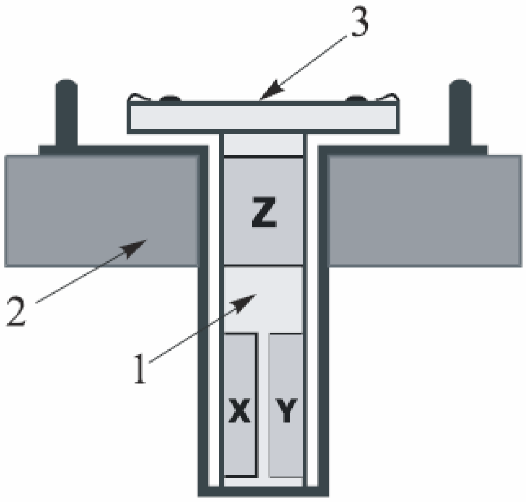

Fig. 21 PZT scanner design and arrangement for NTegra Prima SPM instrument 1 – piezo ceramic tube for the scanner; 2 – carriage; 3 – sample stage

3.2.2 NTEGRA Prima specification

The NTegra Prima SPM instrument is able to operate AFM (contact + semi-contact + non-contact), Lateral Force Microscopy (LFM), Phase imaging, force modulation, adhesion force imaging and lithography (AFM force) techniques in air and also in liquid medium. While, some other methods such as STM, Magnetic Force Microscopy, Electrostatic Force Microscopy, Scanning Capacitance Microscopy, Kelvin Probe Microscopy, spreading resistance imaging, AFAM, lithography (AFM current) are only possible to operate in air. The specification of NTEGRA Prima is mentioned in the following table 1.

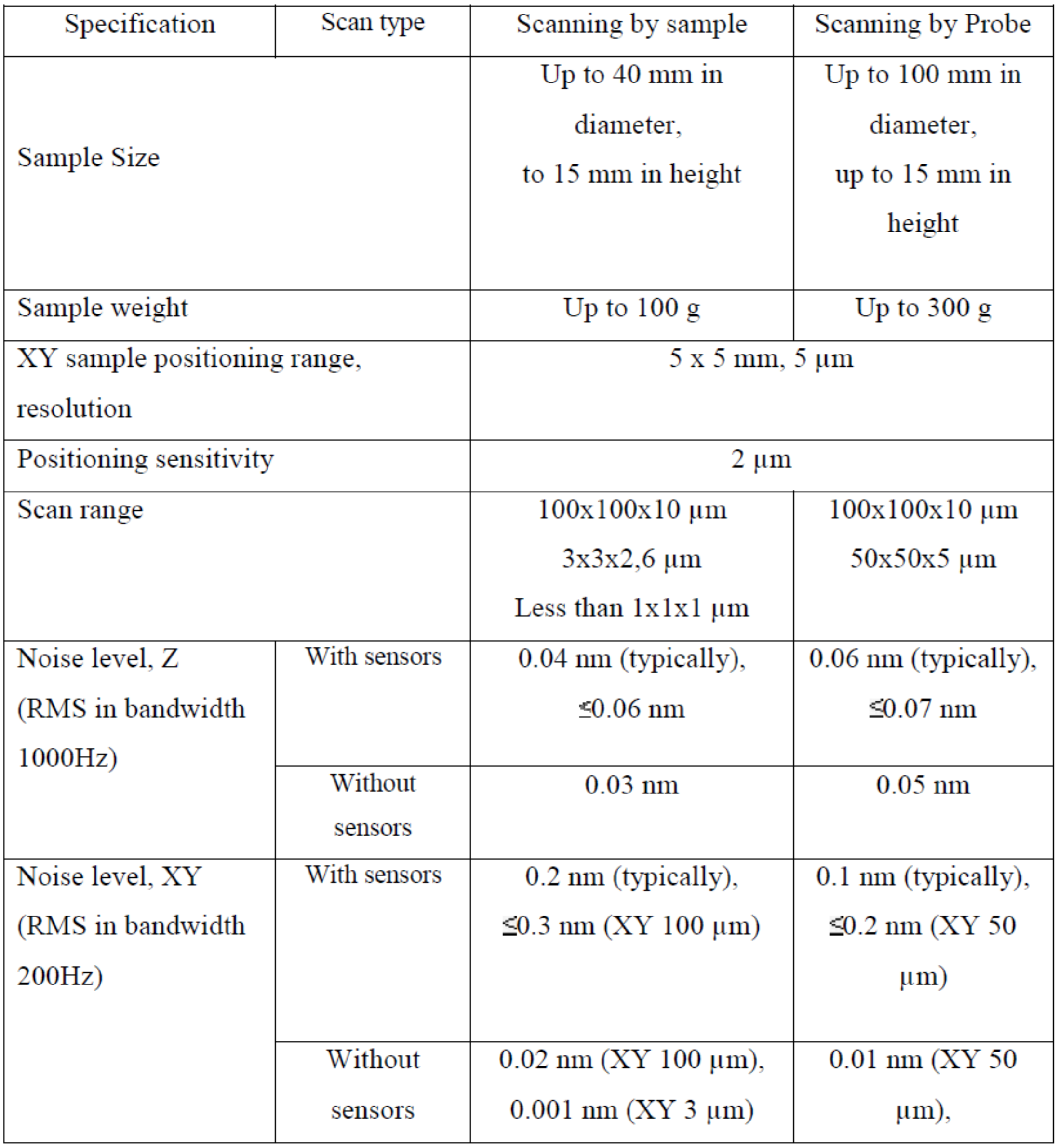

Specification	Scan type	Scanning by sample	Scanning by Probe
Sample Size		Up to 40 mm in diameter, to 15 mm in height	Up to 100 mm in diameter, up to 15 mm in height
Sample weight		Up to 100 g	Up to 300 g
XY sample positioning range, resolution		5 x 5 mm, 5 μm	
Positioning sensitivity		2 μm	
Scan range		100x100x10 μm 3x3x2,6 μm Less than 1x1x1 μm	100x100x10 μm 50x50x5 μm
Noise level, Z (RMS in bandwidth 1000Hz)	With sensors	0.04 nm (typically), ≤0.06 nm	0.06 nm (typically), ≤0.07 nm
	Without sensors	0.03 nm	0.05 nm
Noise level, XY (RMS in bandwidth 200Hz)	With sensors	0.2 nm (typically), ≤0.3 nm (XY 100 μm)	0.1 nm (typically), ≤0.2 nm (XY 50 μm)
	Without sensors	0.02 nm (XY 100 μm), 0.001 nm (XY 3 μm)	0.01 nm (XY 50 μm),

Table 1 NTEGRA Prima Specification

3.2.3 SPM probes

In scanning probe microscopy analysis, the tip-sample intercation is the most important parameter to produce the images. For that purpose, a well-characterized tip is the key element in data interpretation. The schematic diagram of a rectaguar cantilever is mentioned in Fig. 22. The probe has the form of an elastic girder called “cantilever” (mentioned as 2, in Fig 22), which is fixed to the silicon base, called chip, of the probe. The probe tip which is in the form of a sharp pin, is located on the free end of the cantilever.

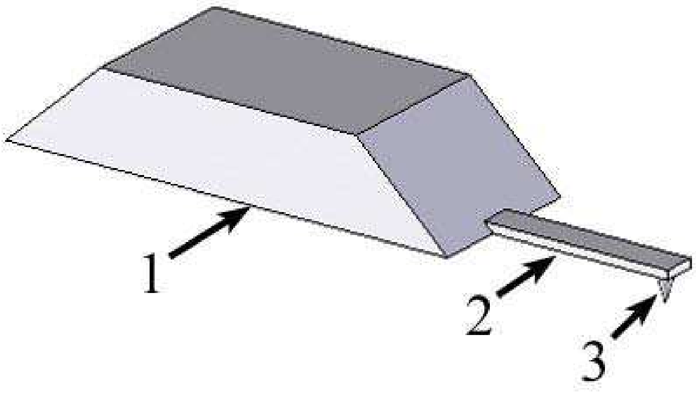

Fig. 22 Probe design for SPM measurements 1 – chip; 2 – cantilever; 3 – probe tip

The probes used for SPM analysis are from NT-MDT company. The detailed description about the cantilever’s shape, size and their properties are mentioned in table 2.

Cantilever	Properties					Applications
	Cantilever Length, L±5 μm	Cantilever width, W±5 μm	Cantilever Thickness, μm	Resonant Frequency, kHz	Force Constant, N/m	
NSG10/Au	100	35	1.7 – 2.3	190 – 325	5.5 – 22.5	AFM (non-contact)
NSG10/W2C						SKM, SCM
NSG03/Au	100	35	0.9 – 1.5	62 – 123	0.4 – 2.7	AFM (non-contact)
NSG03/Co						MFM
CSG10/Au	250	35	0.7 – 1.3	14 – 28	0.03 – 0.2	AFM Contact mdoe, LFM, AFAM,
CSG10/Pt						SRI

Table 2 Scanning porbe microscope Probes

Characteristics of NT-MDT probes are:

- have Au (Silver) high reflectivity coating on backside of the cantilerver (reflectivity property is increased by 3 times in comparison with uncoated cantilevers);
- tip side of the conductive chip NSG10/W2C series is coated by W2C (tungsten Carbide), CSG10/Pt is coated by Pt (pletinum), thickness of W2C/Pt film is 20-30 nm;
- tip NSG03/Co series is coated by Co (Cobalt) for Magnetic force microscopy (MFM).
- high aspect ratio conical tips (cone angle is is less than 22°);
- typical curvaure radious of the uncoated tip is 10 nm, of the coated tip is 35 nm

3.2.4 Nova software and chatacterisation steps for Ntegra Prima SPM

Ntegra Prima SPM insturment is operated by Nova.exe software. It is a very friendly user and informative software. The general steps for the preparation of scanning probe microscope analysis are:

(1) Installing the probe i.e. install the probe to the adjustment unit (mentioned as 2, in Fig 20).
(2) Adjusting the systems for detecting the cantilever deflections i.e. adjust the laser beam to the reflective back side of the probe tip (mentioned as 3, in Fig 22).
(3) Centering the scanner i.e. put the scanner in the center of the exchangeable mount unit (mentioned in Fig 19 (a)).
(4) Preparing and mounting the sample. For SPM, the sample is stick on sapphire plate or on still ring with the help of scotch tape (adhesive in nature on the both side of tape). After preparing the sample, put it on the sample stage of the scanner (mentioned as 3, in Fig 21).
(5) Installing the measuing head on exchangeable mount as mentioned in Fig 19 (a).
(6) Initial approach. Manually approach the sample near to the probe with the help of height adjustment screw.
(7) Installing of a protective hood as mentioned in Fig 19 (a).
(8) Final approach. Final approach of sample to the probe is applied with the help of nova.exe software. Hence, the sample comes in contact with the probe for analysis.
(9) Set the scanning parameter in the nova.exe software and run the scan for anlaysis.

There are many different methods developed under scanning probe microscopy for different purpose. Every method is developing the surface image with the help of some singals. The details about methods, their purposes and useful singals are mentioned in table 3.

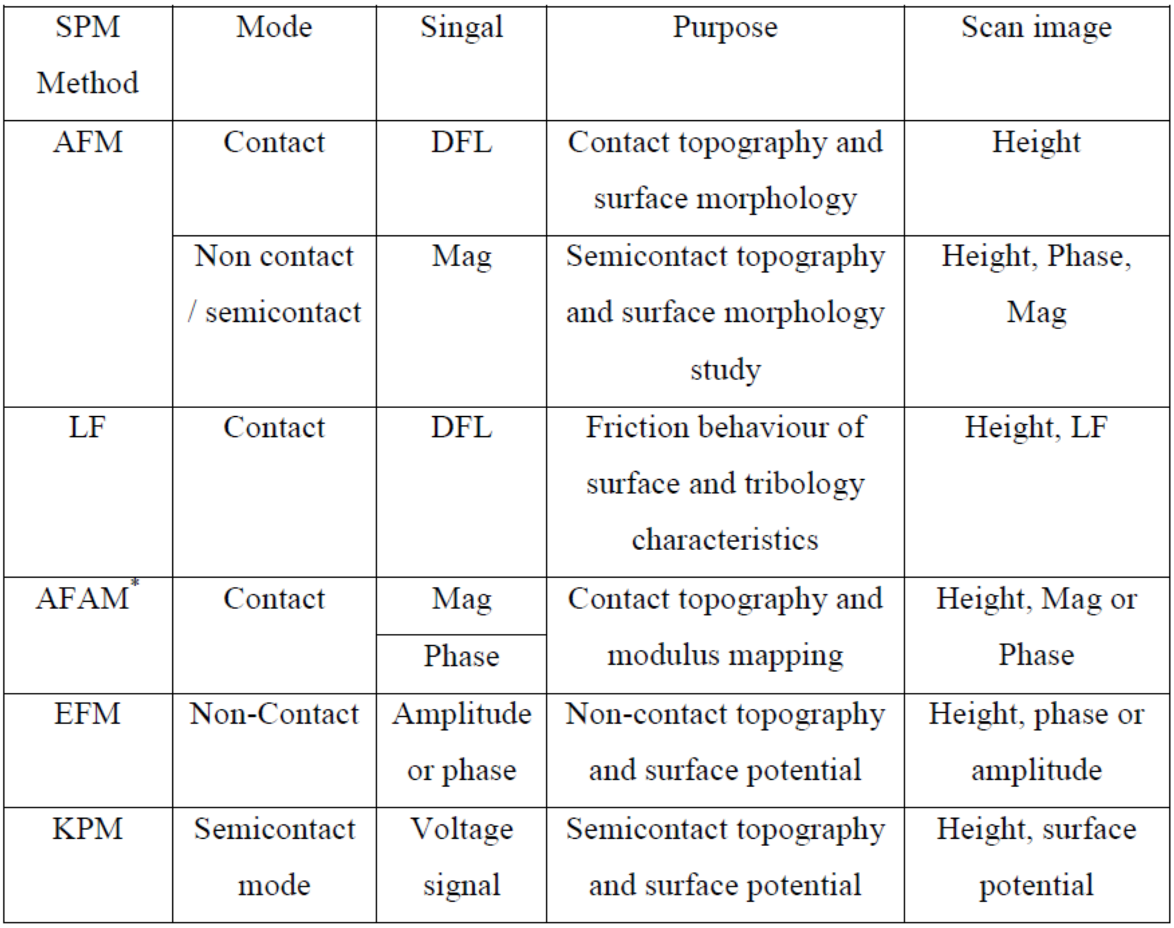

SPM Method	Mode	Singal	Purpose	Scan image
AFM	Contact	DFL	Contact topography and surface morphology	Height
	Non contact / semicontact	Mag	Semicontact topography and surface morphology study	Height, Phase, Mag
LF	Contact	DFL	Friction behaviour of surface and tribology characteristics	Height, LF
AFAM*	Contact	Mag	Contact topography and modulus mapping	Height, Mag or Phase
		Phase		
EFM	Non-Contact	Amplitude or phase	Non-contact topography and surface potential	Height, phase or amplitude
KPM	Semicontact mode	Voltage signal	Semicontact topography and surface potential	Height, surface potential

Table 3 Scanning probe microscopy methods

3.3 Nanoindentation Techniques

The nanoindentation experiment discussed in this dissertation was carried out on Triboscope system from Hysitron, Minneapolis, USA. This instrument can be attached to any commercially available Scanning Probe Microscopy system to produce the qualitative depth-sensing nanoindentation experiment with in-situ imaging. This part of the chapter introduces the design of Hysitron Triboscope equipment, different nanoindentation methods and scratch testing.

3.3.1 Introduction of Hysitron equipment

We have the 2D Triboscope (Hysitron) system attached to an NTegra Prima Scanning Probe Microscope (NM-MDT, Russia). The displacement and load resolutions of the Triboscope (Hysitron) instrument are 0.0004 nm and <1 nN, respectively. While, the noise floor for displacement and load are 0.2 nm and 100nN, respectively.

The detailed description about Hysitron Triboscope system is mentioned in diagram Fig. 23. The Triboscope nanoindenter is attached to NTegra Prima SPM via a cord, which could be seen in Fig 23 (a). The complete system is placed on the vibration isolation system (table Stable Ltd, Switzerland) which can act as vibration dumping system during the experiment and protects the instrument and experiment from error. The close up look of Triboscope head is mentioned in Fig. 23 (b), which is consists of a three-plate capacitive force/displacement transducer. It maintains the movement of tip. The detailed description of Triboscope transducer is discussed in next part of the chapter. To protect the whole system and experiment from external acoustic noise, a protective hood as described in Fig. 23 (c) covers the instrument.

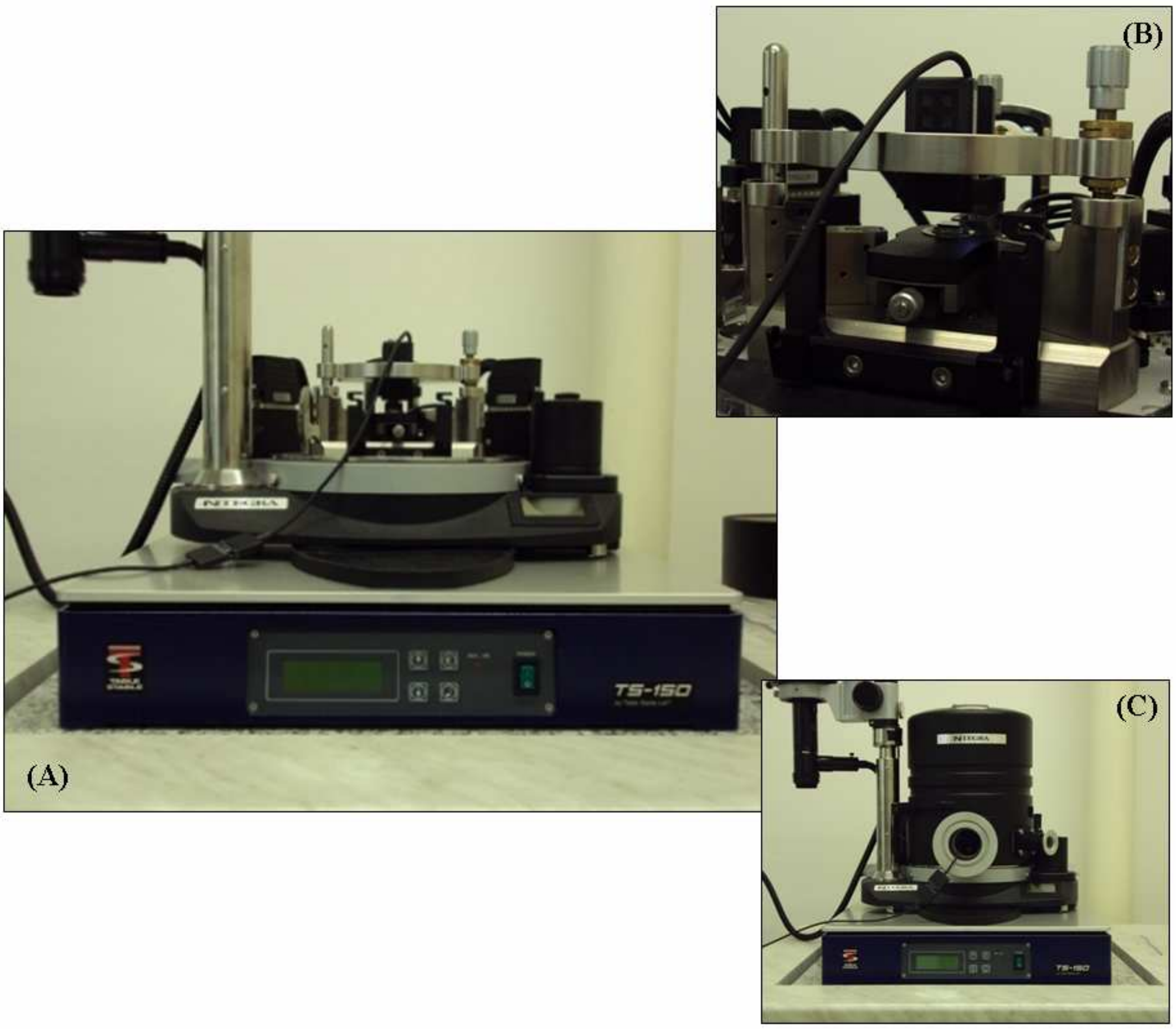

Fig. 23 Hysitron Triboscope system:
(a) Triboscope arrangement with the NT-MDT SPM system; (b) close up look of triboscope head; (c) protective hood

Triboscope transducer

The three-plate capacitive force/displacement transducer could be referred as the heart of the testing instrument. It is a pattern technology from Hysitron Company, USA. This transducer provides high sensitivity, large dynamic range, and a linear force or displacement output signal [76]. The schematic of Triboscope transducer is mentioned in Fig. 24. The center plate of the transducer has a lower mass (200 mg) which facilitates to minimize the instrument's sensitivity to external vibrations and also allows light load (less than 25 µN) indentations to be made.

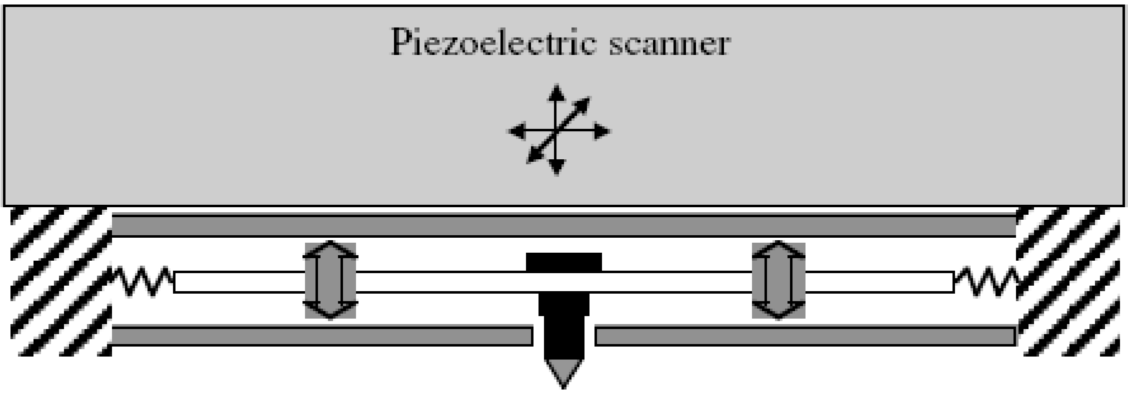

Fig. 24 Schematic diagram of Triboscope Transducer

The sensor also consists of two fixed outer electrodes (drive plates). They are driven by AC signal 180^0 out of phase with each other. At any instance the signals applied to drive plates are equal in magnitude but with different polarity. The input impedance of the synchronous demodulator is larger than the output impedance, thus the pickup electrode will assume the same potential present at its position between the drive plates.

A large DC charge is applied to the lower plate of the transducer, which thereby applies force to the tip. Varying the amount of charge will vary the applied force. According, to the Hysitron manual maximum load force available from a standard transducer is approximately 10 mN, while it would be increased to 30 mN with an optional extended force transducer.

Berkovich tip

Berkovich tip is a three-sided pyramidal tip with a total included angle of 142.35° and a half-angle of 65.35°. Some details and an optical microscope image (Fig. 13) of it are mentioned in theoretical background chapter. In our nanoindentation study, the Berkovich tip with a radius of curvature of about 150 nm or50 nm were used for the analysis of thin films, multilayer films, gradient films and for scratch study of thin films on silicon substrate. The Berkovich tip with known tip area function is important for correct indentation and scratch experiment. Hence, at proper interval of time, the tip area calibration is carried out. The procedure of tip area calibration is mentioned in theoretical background chapter.

Sample preparation

The sample preparation is necessary to be carried out with care. For nanoindentation and scratch test, special cyanoacrylate adhesive glue (Loctite 495) is used to stick the sample on steel ring sample holder or sapphire plate sample holder. In most of the cases, the steel ring sample holder is used because it is cheaper.

3.3.2 Nanoindentation measurements

Two types of nanoindentation experiments were carried out with this instrument:

(a) Conventional nanoindentation test,
(b) Cyclic nanoindentation test.

The drift measurement is very important parameter in indentation test. The drift measurement is performed immediately before the testing. The displacement versus time of linear character was measured at 40 (default) or 120 (suggested) s and the drift rate was evaluated using the linear regression for last 20 (default) or 100 (suggested) s, respectively. The drift rate was used to correct the acquired data from the real indentation testing. The drift rate was maintained in a range of 0.05 nm/s to 0.5 nm/s during indentation experiment.

Conventional Nanoindentation test

Conventional indentation test consist of three segments (1) loading, (2) dwell time or hold time and (3) unloading. Here, the loading segment is followed by a dwell time at maximum load, and followed by an unloading segment. The graphical presentation of conventional nanoindentation test is mentioned in Fig. 25.

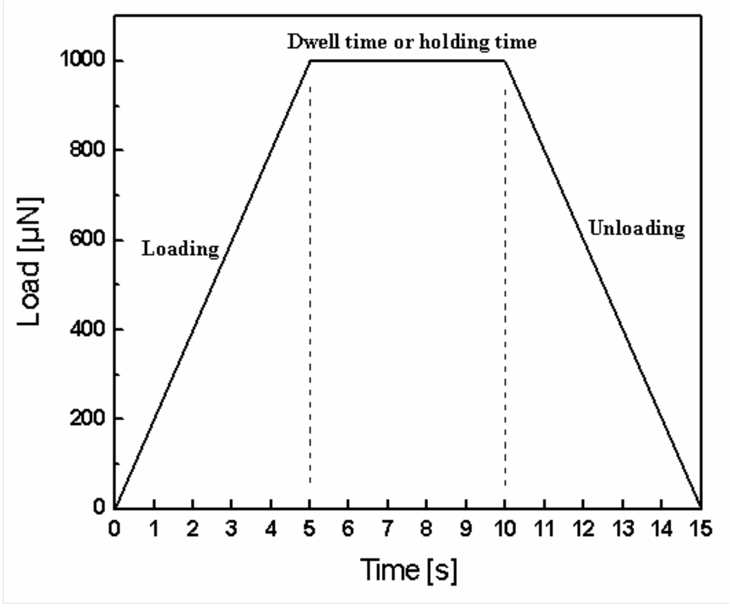

Fig. 25 Graphical presentation of conventional nanoindentation test

The main variable parameters for conventional test are the different loads (µN) and measurement time (s) of experiment. One can change the load, from 1 µN to 10 mN and also experiment time from minimum 3 sec to minutes. The load/unload vs. displacement curve (Fig. 26) is obtained by indentation experiment. In general, the loading causes both elastic and plastic deformation under the indenter, while unloading is dominated by recovery of elastic deformation. The upper portion of the unloading curve can be used to calculate the mechanical properties at a given contact depth of the indenter according to the Oliver-Pharr method [50]. The detailed description of Oliver-Pharr method is mentioned in previous chapter. A conventional indentation experiment gives only a single value of mechanical properties at a particular load at a time. Hence, one needs to do many conventional indentation experiments at different loads to produce a depth profile of mechanical properties.

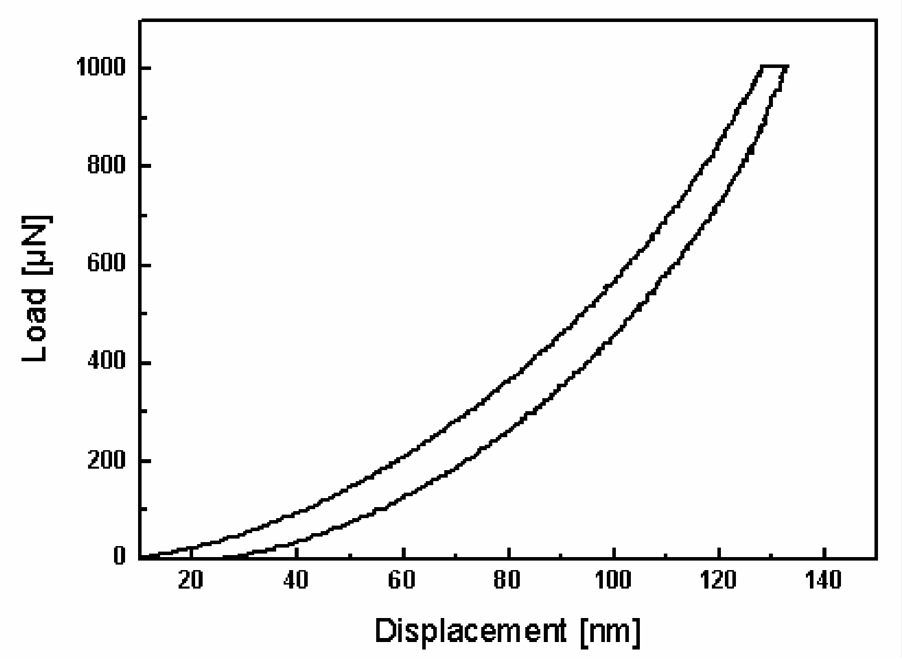

Fig.26 load/unload vs. displacement curves obtained by conventional indentation test

For creep behavior or strain sensitivity experiment, dwell time is the important parameter. The variation of dwell time from few second to minutes helps to study the creep behavior or strain sensitivity of materials.

Cyclic Nanoindentation test

A new variation of the conventional test is the cyclic nanoindentation test, where the sample is reloaded immediately to higher loads/depths than pervious loading cycle. The important variable parameters in cyclic test are number of cycles, maximum load, displacement exponent, unloading fraction and segments (loading/hold/unloading) time. The number of cycles can vary from 2 to 650. Here, the maximum load can change from 1 µN to 10 mN. One can change the rest parameters like displacement exponent, unloading fraction and segments time to create the desired experiment conditions. For better understanding, the graphical presentation of seven-cycle indentation test is mentioned in Fig. 27 (a).

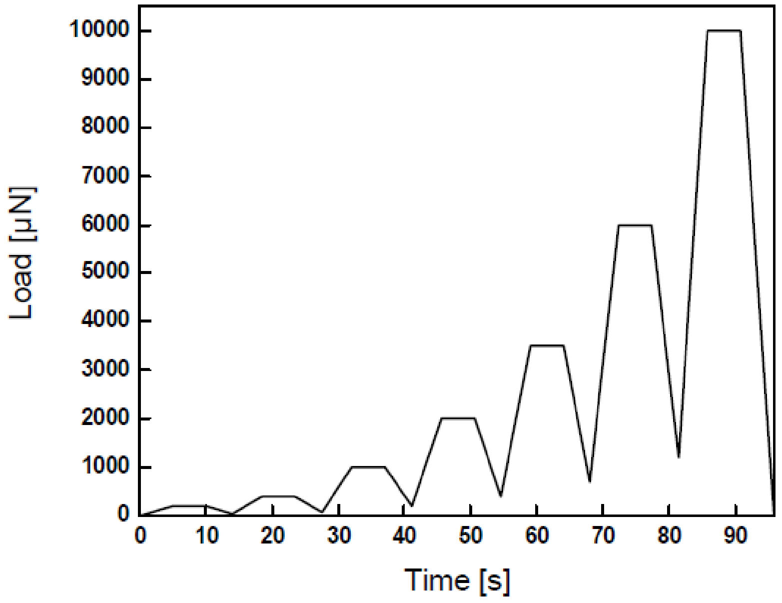

(a)

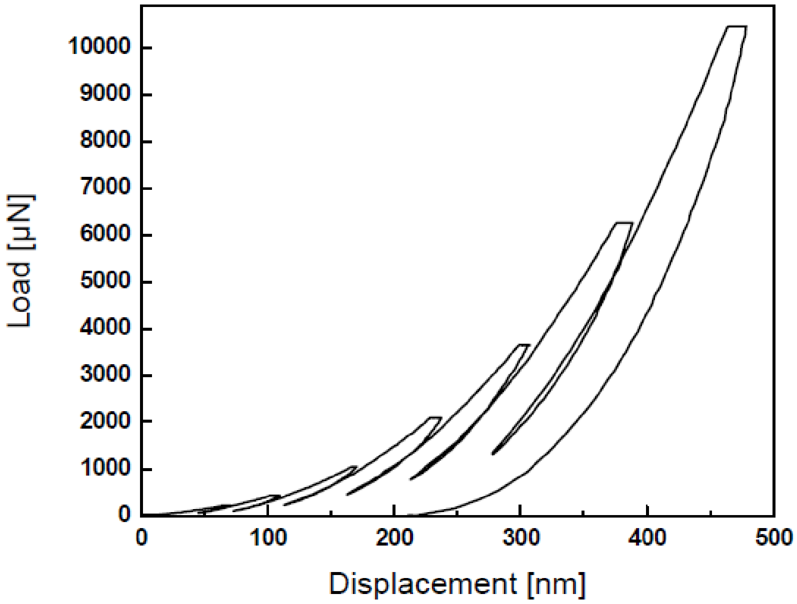

(b)

Fig. 27 Graphical presentation of seven-cycle indentation: (a) indentation cycle, (b) load/unload vs. displacement curves obtained by indentation.

The multiple load/unload vs. displacement curve is obtained by cyclic indentation experiment, mentioned in Fig. 27 (b). The Oliver-Pharr method is used in a similar way like conventional method to calculate the mechanical parameters from load/unload vs. displacement curve.

3.3.3 Scratch test

The scratch test was used to study the adhesion failures of thin films on silicon substrate. The Berkovich tip with radius of curvature of 150 nm was used for all the scratch testing. The proper tip area calibration was carried out before the experiment and obtained calibrated curve was used to correct the experimental data. The drift rate was measured immediately before every experiment like mentioned in indentation experiment and resulted drift rate (nm/s) was used to correct the experimental data. The X-axis and Z axis calibration was also carried out for Triboscope transducer calibration.

For scratch testing, the ramp force scratch positive direction experimental condition was used, as mentioned in Fig 28. The variable parameters in ramp force experiment are the peak force (µN), time (s) of experiment, segment time (s), displacement (µm) and lateral displacement (µm). The Fig. 28 shows that the plots of normal force (µN) vs. time (s) and x displacement (µm) vs. time (s) are used for scratch test.

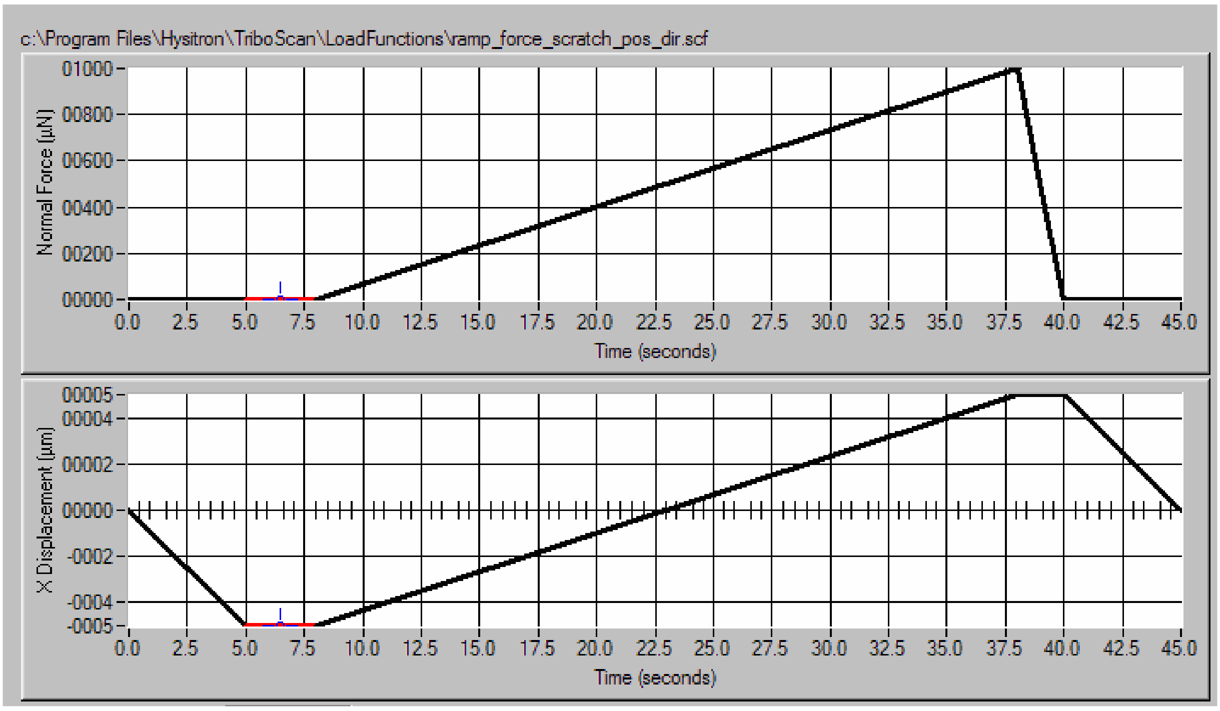

Fig. 28 Ramp Force scratch test in positive direction

The data obtained from scratch experiment was in terms of plots of normal force (µN) vs. time (s), normal displacement (nm) vs. time (s), lateral force(µN) vs. time (s) and lateral displacement (µm) vs. time (s) as shown in Fig. 29. It gives information about the adhesion failure of thin films on substrate. The friction coefficient information was available from friction coefficient vs. time plot.

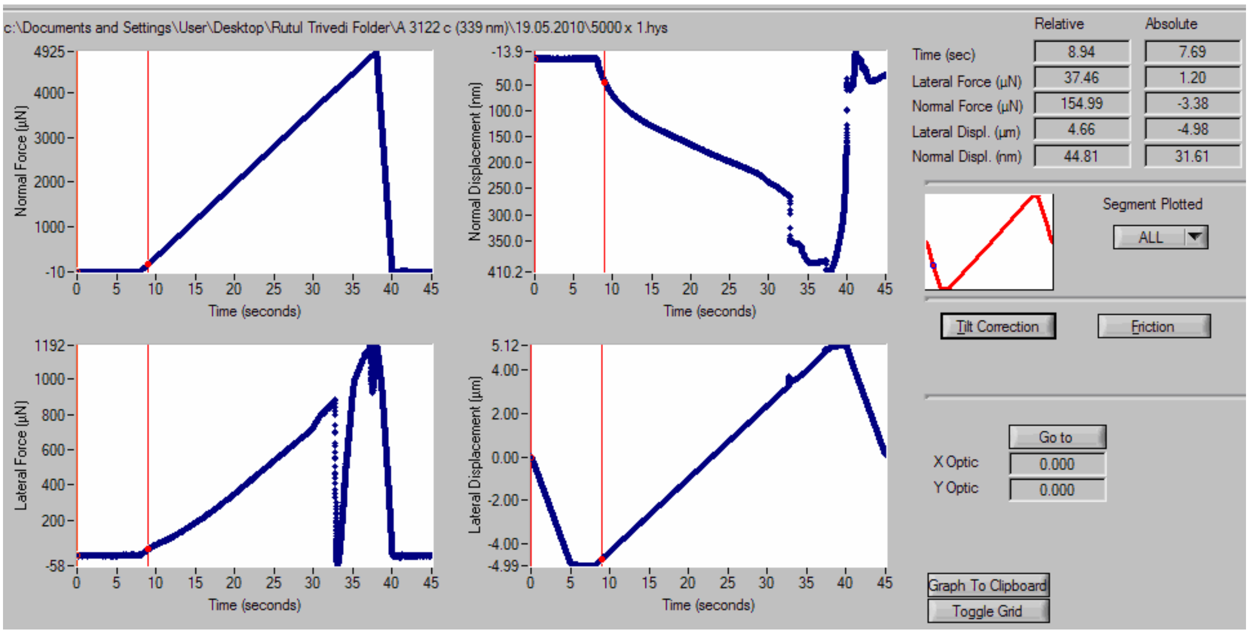

c:\Documents and Settings\User\Desktop\Rutul Trivedi Folder\A 3122 c (339 nm)\19.05.2010\5000 x 1.hys

	Relative	Absolute
Time (sec)	8.94	7.69
Lateral Force (µN)	37.46	1.20
Normal Force (µN)	154.99	-3.38
Lateral Displ. (µm)	4.66	-4.98
Normal Displ. (nm)	44.81	31.61

Segment Plotted: ALL

X Optic: 0.000

Y Optic: 0.000

Fig 29 Scratch test analysis data

4 RESULTS AND DISCUSSIONS

4.1 Single layer film

In this part of the chapter, the Atomic Force Microscopy (AFM) and nanoindentation (NI) was used for the analysis of plasma polymer thin films. The various deposition conditions have some effect on the surface morphology and mechanical properties of plasma thin films, which were confirmed by AFM and NI analysis.

4.1.1 Surface analysis by AFM

The films were prepared for this analysis from two different types of monomer under following deposition conditions.

Thin film preparation

The plasma-polymerized vinyltriethoxysilane (pp-VTES) films were prepared on polished silicon wafers by PECVD using an RF (13.56 MHz) helical coupling plasma [75] system working in the pulse mode. The deposition chamber was evacuated to the basic pressure of 1 x 10^{-3} Pa and the pretreatment of silicon wafers was carried out by pulse plasma (1:1 ms) in the presence of Argon plasma (10 sccm, 10 Pa, 25 W) for 10 min. The monomer flow rate was set at 0.45 sccm and the pressure maintain in the deposition chamber was around 1.5 Pa. The film deposition was operated at pulsed plasma ($t_{on}/t_{off} =$1 ms : 9 ms) and 5 W by applying plasma discharge. Single films were deposited during deposition times ranging from 5 to 4800 s, which corresponded to film thickness varying from 13 nm to 8.6 μm. A phase-modulated spectroscopic ellipsometry UVISEL (Jobin-Yvon) was used to determine the film thickness.

As well as, a series of plasma-polymerized tetravinylsilane (pp-TVS) films were also prepared on polished silicon wafer by PECVD employing RF (13.56 MHz) working in continuous plasma mode. The vaccum system was evacuated to a basic pressure of 1 x 10^{-5} Pa. The substrates were pretreated with argon plasma (10 sccm, 5.0 Pa, 5 W) for 10 min. The mass flow rate of TVS monomer is 29 sccm. The set of samples was prepared with the film thickness of about 100 nm at different rf power of 10, 25, 50 and 70 W.

The surface morphology of pp-VTES and pp-TVS films were observed by Atomic Force Microscopy, NTegra Prima/Aura (NT-MDT, Russia), and the RMS roughness was determined from scanned area.

4.1.2 Surface analysis results

The single layer pp-VTES films with thickness ranging from 13 nm to 8.6 μm were prepared at constant deposition conditions mentioned in the experimental details. The film thickness increased [77] as the deposition time increased as given in Fig. 30. The mean deposition rate was determined from the ratio of the film thickness to deposition time. The mean deposition rate decreased slowly from 250 to 100 nm min^{-1} with the increase in deposition time as shown in Fig. 30. It means that the growth kinetics varied during deposition and dominated the film properties [75].

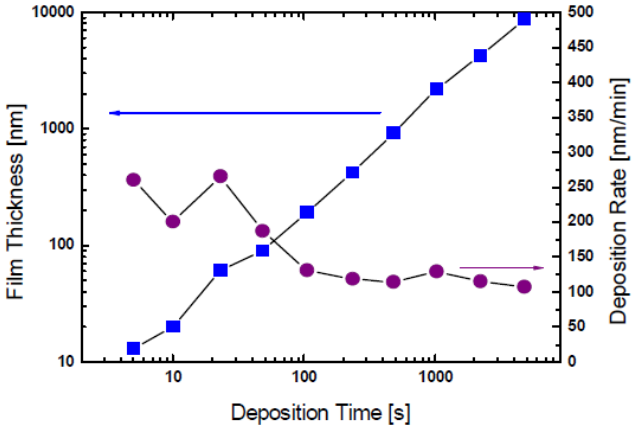

Fig. 30 Film thickness of pp-VTES film and mean deposition rate as a function of deposition time

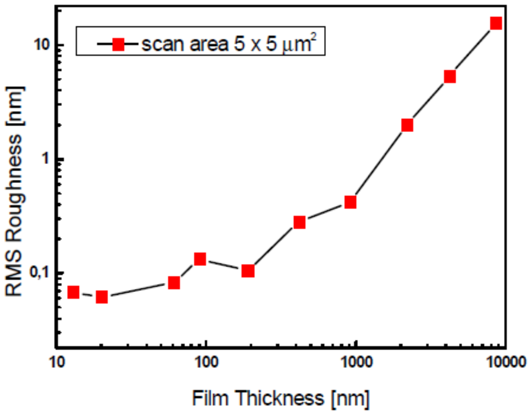

Fig. 31 Evolution of RMS roughness vs. film thickness for pp-VTES films

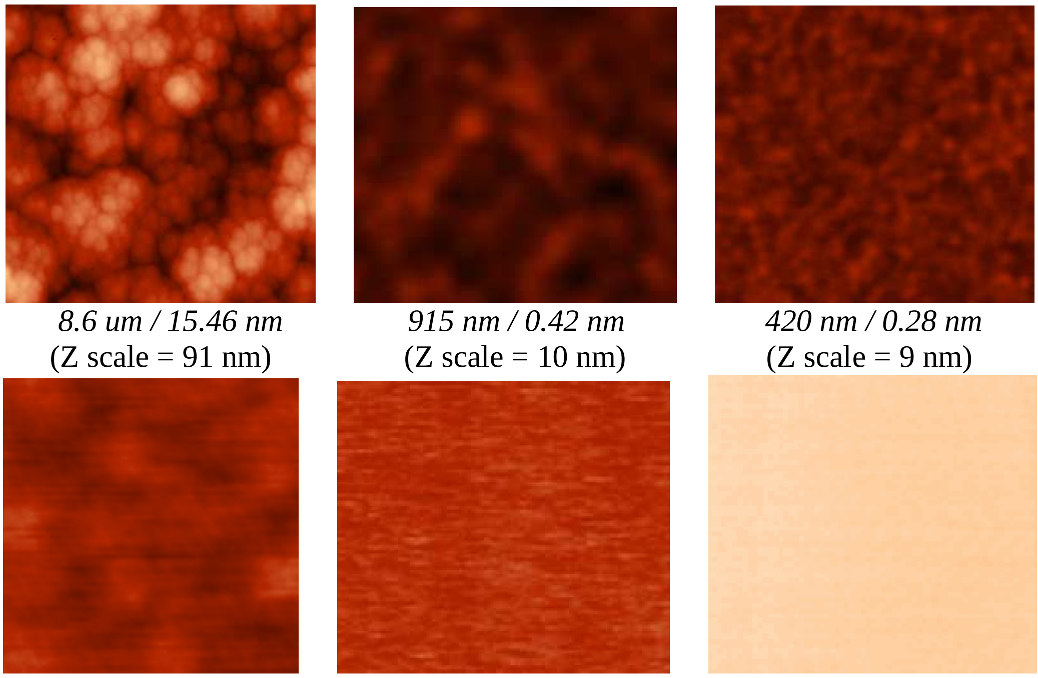

8.6 um / 15.46 nm
(Z scale = 91 nm)

915 nm / 0.42 nm
(Z scale = 10 nm)

420 nm / 0.28 nm
(Z scale = 9 nm)

190 nm / 0.105 nm
(Z scale = 1.2 nm)

90 nm / 0.132 nm
(Z scale = 2.0 nm)

61 nm / 0.083 nm
(Z scale = 0.3 nm)

Fig. 32 Surface morphology of pp-VTES film observed by AFM (scan area: 5 µm x 5 µm); film thickness/RMS roughness is indicated.

The information about the surface morphology and the surface roughness for pp-VTES films were obtained from AFM analysis. The scan area 5x5 µm^2 was used for this purpose. The RMS roughness increased from 0.041 nm to 15.46 nm with the increase of film thickness as shown in Fig. 31. The surface morphology of pp-VTES films also changed as film thickness decreases from 8.6 µm to 15 nm and it is evident from the images in Fig. 32. The film thickness and RMS roughness were indicated for each image, in Fig 32. A cauliflower structure on the film surface is apparent for films with thickness ≥ 2 µm.

In another experiment, the RMS roughness of pp-TVS films were increased with increasing RF power, as mentioned in Fig. 33. It could be explained by the slight ablation of the film surface in the glow discharge. It may disrupt the overlayer of the material and increase roughness [75].

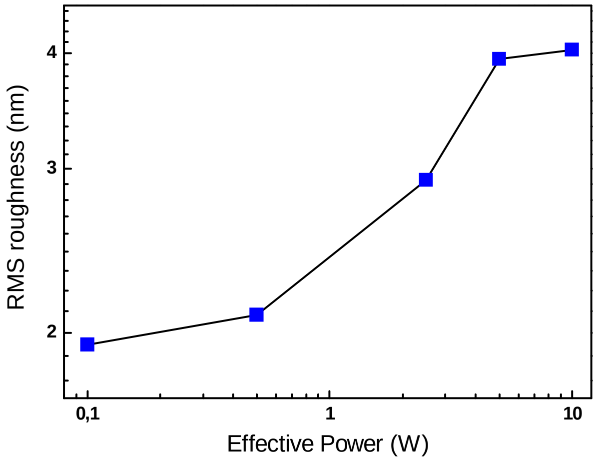

Fig. 33 Comparison of RMS roughness with different RF power used for deposition of pp-TVS films

4.1.3 Mechanical Properties

The mechanical properties of single layer films were determined by nanoindentation technique. The Hysitron Triboscope nanoindenter allows the mechanical properties analysis by conventional indentation as well as by cyclic indentation technique. The controlled drift correction and proper tip area calibration are important procedure to obtained correct mechanical properties of thin films or coatings. This part of the chapter includes the information about thin film preparation, effect of controlled drift, mechanical properties at a shallow depth and a limited applicability of the 10 % rule.

Thin film preparation

Plasma-polymerized films of tetravinylsilane were prepared by plasma-enhanced chemical vapor deposition (PECVD) method by employing RF (13.56 MHz) helical coupling plasma system working in the pulsed mode. The film was deposited on double-side polished silicon wafer, which was pretreated with oxygen plasma (5 sccm, 4 Pa, 25 W) for 10 min. The deposition chamber was cleaned by Ar plasma (10 sccm, 10 Pa) for 10 min to remove remaining oxygen.

The effective power (W_{eff}) of the pulsed plasma was controlled by changing the ratio of the time when the plasma was switched on (t_{on}) to the time when it was switched off (t_{off}), $W_{\mathrm{eff}} = t_{\mathrm{on}} / T \times W_{\mathrm{total}}$, in which the period was defined as $T = t_{\mathrm{on}} + t_{\mathrm{off}}$ and $W_{\mathrm{total}} = 50$ W. The pp-TVS film was deposited at a flow rate of 0.50 sccm and a corresponding pressure of 1.3 Pa using TVS plasma under selected effective power. The deposited film was held for 1 hour in argon gas (10 sccm, 10 Pa) and then moved to the load lock and flushed with air to atmospheric pressure. Hence, the plasma polymer films were deposited by PECVD method from tetravinylsilane monomer at different effective power of 0.1, 2.5, and 10 W to influence polymer cross-linking.

Thin film nature

The film thickness was measured by spectroscopic ellipsometry and it was 1268 nm (0.1 W), 1035nm (2.5 W), and 960 nm (10 W). All the pp-TVS films were deposited under steady-state plasma conditions, which were monitored by mass spectroscopy. The ellipsometric spectra and their analysis as well as the elemental composition analysis of the films by X-ray photoelectron spectroscopy (XPS) and Rutherford backscattering spectrometry (RBS) confirmed that the deposited films were homogeneous in nature and isotropic materials, with an invariable depth profile [78]. Therefore, we expect that the mechanical properties of pp-TVS film are also depth-independent. The nanoindentation measurement of the pp-TVS films were carried out at room temperature. The experiments carried out in 2 sets.

4.1.4 Mechanical Properties Results

The mechanical properties measurement of pp-TVS films were carried out at two different experimental conditions (a) drift rate ≤ 0.5 nm/s and (b) drift rate ≤ 0.05 nm/s. The main purpose of this experiments to check the influence of different drift rate on mechanical properties measurement of pp-TVS film.

Set 1 (drift rate ≤ 0.5 nm/s)

Set 1 Experiment

The mechanical properties of pp-TVS film deposited at 10 W were evaluated in set 1 experiment. A Berkovich tip with a radius of curvature of about 150 nm was used. The drift rate was measured for 40 s and evaluated from the last 20 s. The drift rate was ≤ 0.5 nm/s. Two types of indentation tests were conducted: (i) conventional indentation and (ii) cyclic indentation.

(i) Conventional indentation

Conventional indentation of the pp-TVS film was carried out at 200, 400, 1000, 2000, 3500, 6000 and 10,000 µN loads. The loading, unloading and dwell time were kept constant at 5 s for all the measurements. The experiment for each load was repeated ten times.

Variation in dwell time affects the mechanical property measurement. This effect was studied at a 200 µN/s loading rate with dwell times of 1, 5, 10, and 20 s. In addition, the mechanical properties of the film were studied at a 1000 µN load with different loading/unloading rates (50, 100, 200, 500 µN/s) and a constant dwell time of 5 s.

(ii) Cyclic indentation

The seven-cycle indentation the test was carried out at 200, 400, 1000, 2000, 3500, 6000, and 10,000 µN loads, with the same experimental conditions as the conventional experiment.

Set 1 Results and discussion

The conventional indentation experiments on the pp-TVS film were performed at 200, 400, 1000, 2000, 3500, 6000, and 10,000 µN loads using loading/unloading and dwell times of 5 s as plotted in Fig 25. The load/unload vs. displacement curve (Fig. 26) was obtained by indentation experiment and the shape gave evidence of an elastic behavior of the plasma polymer. The Oliver-Pharr method [50] was used to calculate mechanical properties, such as the reduced modulus and hardness, using the upper portion of the unloading curve. The resulted mechanical parameters and the corresponding contact depth (vertical distance along which contact is made) are given in Table 4. A mean value of ten measurements and the standard deviation (SD) are used for the reduced modulus and hardness. The 10% rule means that the mechanical parameters evaluated from the unload-displacement curve are not influenced by the substrate significantly up to 10% of the film thickness [79]. The contact depth corresponding to a loading of 1000 µN was 102 nm, which is 11% of the film thickness. Hence, we can expect that the reduced modulus and hardness data up to the 1000 µN load characterize well the film properties. An increase of the reduced modulus and hardness with enhancing contact depth, due to the load increased from 1000 µN to 10,000 µN, can be explained by substrate influence of which elastic modulus and hardness is 150 GPa, 10 GPa, respectively.

An influence of both the dwell time and loading/unloading rate on evaluated mechanical parameters was observed using conventional indentation. Fig. 34 shows the relationships between the dwell time, which was varied from 1 to 20 s, and the reduced modulus, hardness, and contact depth at an applied load of 1000 µN with a 200 µN/s loading/unloading rate (loading/unloading time was 5 s). The mechanical parameters and the contact depth did not show noticeable changes when a shorter dwell time from 1 to 5 s was used. However, when the dwell time was increased above 5 sec to 20 s, mechanical parameters such as the reduced modulus and hardness decreased by 12% and 22%, respectively, while the contact depth increased by 14%. Creep or relaxation effects, which have the opposite trend, cannot explain a progressive increase of the contact depth with prolonged dwell time [80]. Besides, the plasma polymer is of elastic behavior at least up to an applied load of 1000 µN (Fig. 26) and thus the creep behavior cannot be expected. However, the progressive increase of the contact depth could result from time-variable system drift. The time-dependent displacement of the tip is not of linear behavior for longer times and thus the drift rate evaluated before the measuring cycle is not quite accurate to correct acquired data at prolonged measuring time. The reduction of mechanical parameters with prolonged dwell time is related with the enhanced contact depth that decreased the unloading slope (stiffness) and increased the contact area.

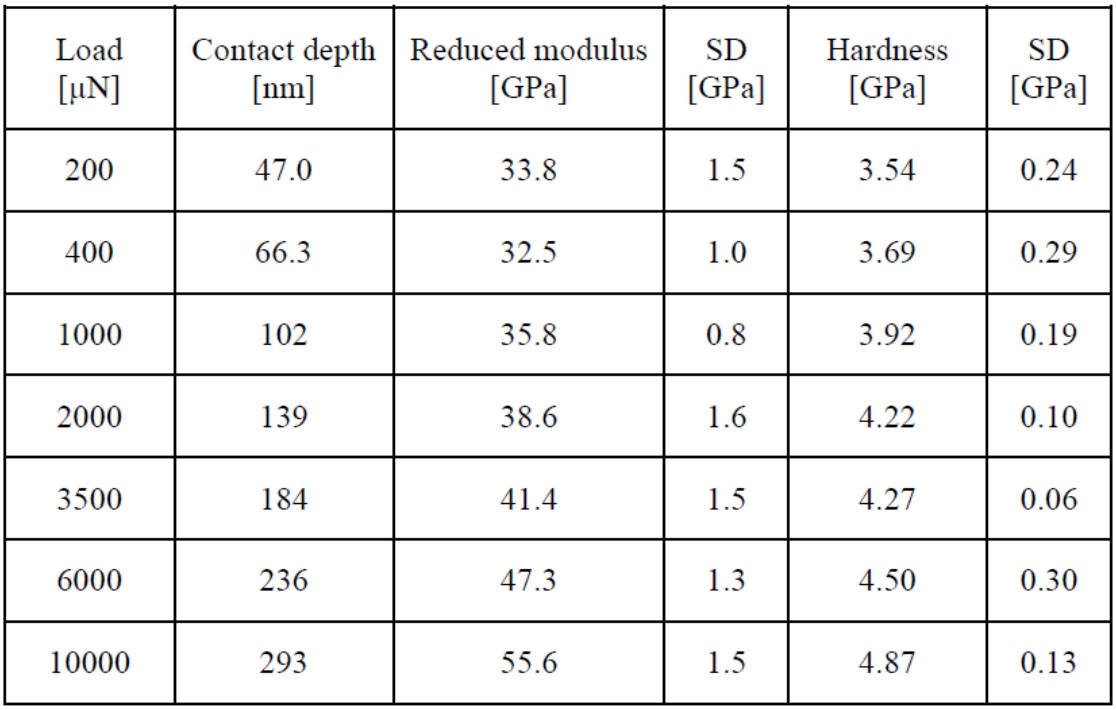

Load [μN]	Contact depth [nm]	Reduced modulus [GPa]	SD [GPa]	Hardness [GPa]	SD [GPa]
200	47.0	33.8	1.5	3.54	0.24
400	66.3	32.5	1.0	3.69	0.29
1000	102	35.8	0.8	3.92	0.19
2000	139	38.6	1.6	4.22	0.10
3500	184	41.4	1.5	4.27	0.06
6000	236	47.3	1.3	4.50	0.30
10000	293	55.6	1.5	4.87	0.13

Table 4 Mechanical properties of pp-TVS film evaluated by conventional nanoindentation.

The relationship between the loading/unloading rate and the reduced modulus, hardness, and contact depth at an applied load of 1000 uN with 5 s dwell time is plotted in Fig 35. The results show that the reduced modulus and hardness increased by 2% and 25%, respectively, when the contact depth increased by 11% as the loading rate increased from 50 uN/s (loading time 20 s) to 200 uN/s (loading time 5 s). However, the mechanical parameters and the contact depths did not change significantly if the loading rate enhanced from 200 to 500 uN/s (loading time 2 s). Therefore, the increase of the loading time from 5 to 20 s resulted in a progressive rise in the contact depth related with a descent of mechanical parameters. This trend is the same as in the case of prolonged dwell time over 5 s (Fig. 34). On a basis of the above results, we suggest the loading, unloading, and dwell time to be 3 – 5 s and thus one complete measuring cycle should not be longer than 15 s [80].

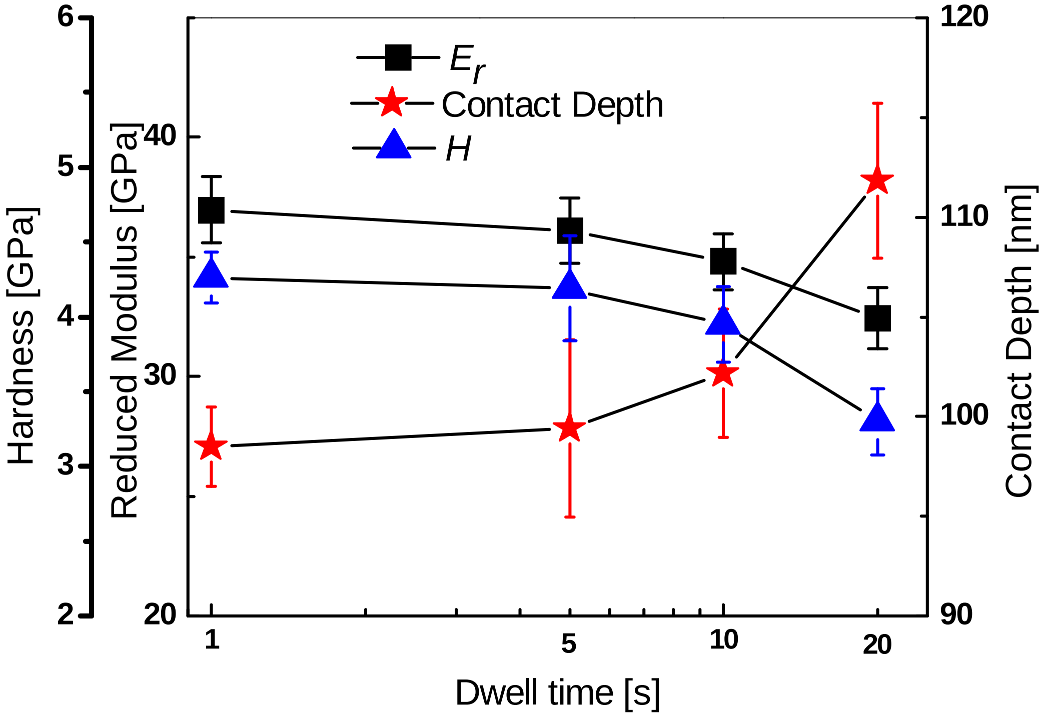

Fig. 34 Effect of variation of dwell time on hardness, reduced modulus, and contact depth.

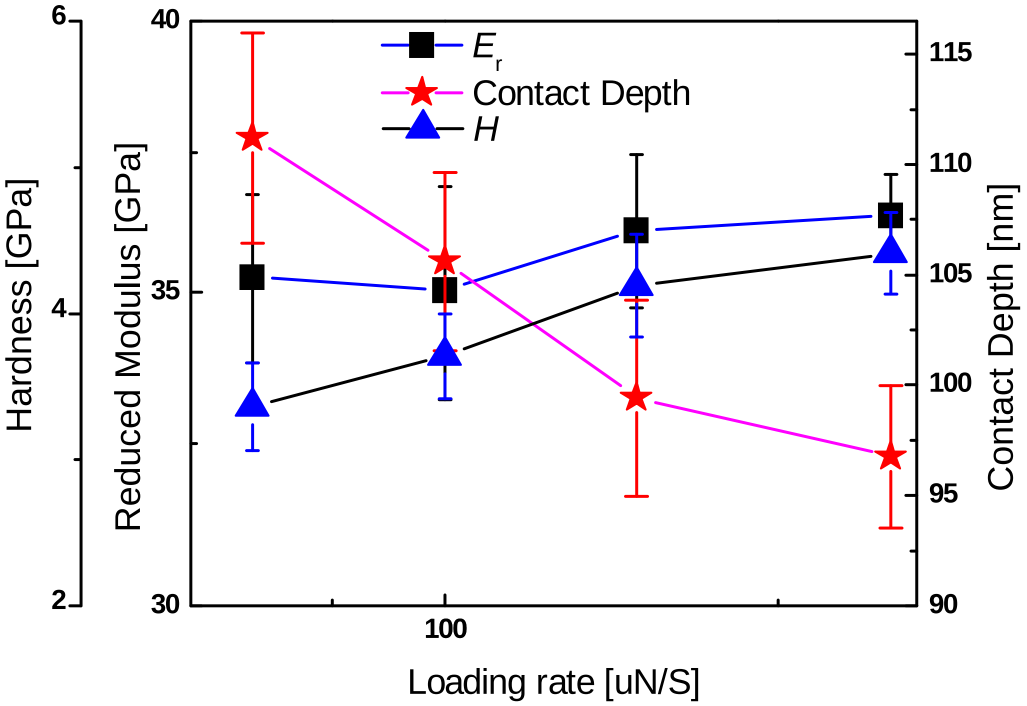

Fig. 35 Effect of variation of loading/unloading rate on hardness, reduced modulus, and contact depth.

The seven-cycle indentation was carried out to study the mechanical parameters of pp-TVS film with respect to the depth profile. The load vs. displacement curves obtained from the seven-cycle indentation (Fig 27(a)) is shown in Fig 27(b). There is only a small overlap between the reloading path and the unloading path of the new loading cycle, as evident from Fig. 27(b). The Oliver-Pharr method was used in a similar way to the conventional method to calculate the mechanical parameters from the load vs. the displacement curve. In the experiment, the contact depths 45, 69, 115, 164, 217, 280, and 351 nm were obtained for 200, 400, 1000, 2000, 3500, 6000, and 10,000 µN loads, respectively. The reduced modulus and hardness vs. contact depth, obtained from the seven-cycle experiment (square) and conventional nanoindentation (circle), are plotted in Figures 36 (a) and 36 (b). Both the sets of data follow the same increasing trend with enhanced contact depth showing the substrate effect for data over 10% of the film thickness. As evident from the figures, some shift of contact depth into a bulk of the film and reduced values of the mechanical parameters were observed for cyclic nanoindentation data compared to conventional nanoindentation. This might be due to the reloading followed by partial unloading in cyclic indentation, when only an incomplete recovery of the film was observed at higher loading values. An increasing difference in the reduced modulus up to 27% and hardness up to 34% at about 30% of the film thickness indicates an influence of prolonged measuring time and thus not properly corrected effect of the system drift [80].

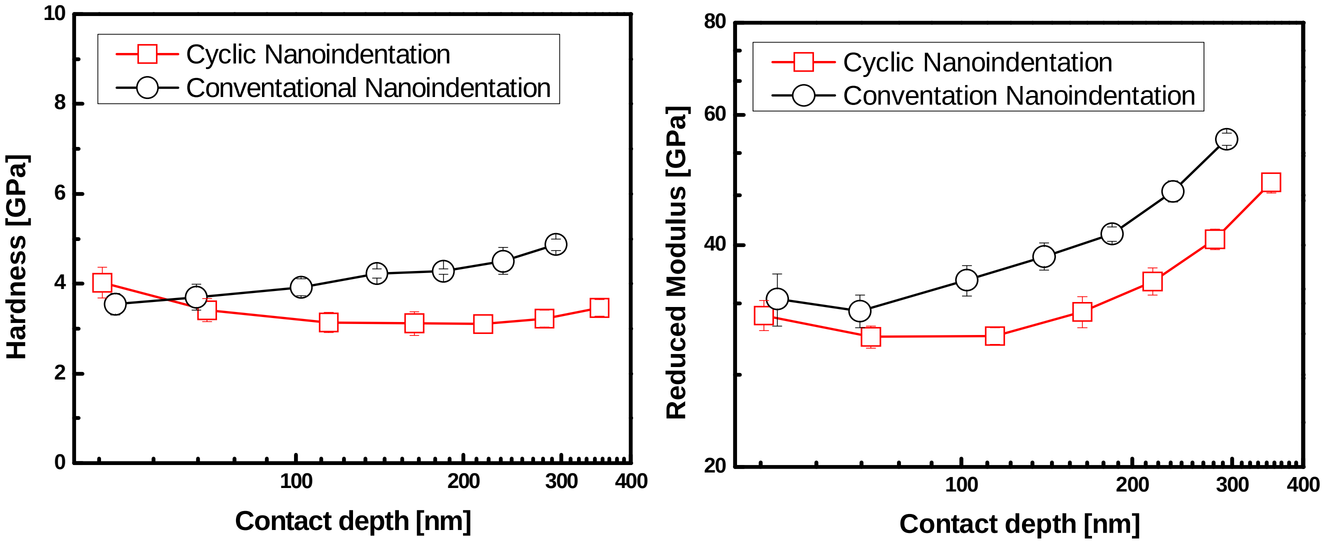

(a) (b)

Fig. 36 Comparison of mechanical properties between conventional indentation and seven-cycle indentation: (a) reduced modulus vs. Contact depth, (b) hardness vs. contact depth.

<u>Set 2 (drift rate ≤ 0.05 nm/s)</u>

Set 2 Experiment

In set 2, the mechanical properties of pp-TVS films deposited at 0.1, 2.5 and 10 W were evaluated. A Berkovich diamond indenter with a radius of curvature of 50 nm was used. The drift rate was measured for 120 s and evaluated from the last 100 s. Hence, the drift rate was ≤ 0.05 nm/s for all the measurements. Two types of nanoindentation test were done:
(i) Conventional indentation experiment was carried out for pp-TVS films to obtain the depth profile of mechanical constants such as Young's modulus and hardness until 15-20% of the film thickness. The depth profile was constructed using results of single indentations performed at increased loading (indenter displacement) changing indentation position. The loading, unloading, and dwell time was kept constant at 5 s for all the measurements.
(ii) Cyclic indentation experiment was also carried out to obtain the depth profile of mechanical constants until 15-20% of the film thickness but applying many loading cycles in one single indentation, while the unloading fraction was kept constant at 0.8. Further, the depth profile of mechanical properties of all the pp-TVS films was analyzed by cyclic indentation method at decreasing unloading fraction of 0.5 and 0.3.

Set 2 Results and discussion

In this study, we reduced the system drift significantly (≤0.05 nm/s) due to prolonged (3 min) contact of the indenter with the sample surface before nanoindentation measurement. The longer the probe is on the sample surface the lower the drift will be [81]. Typical values of drift rate were ranging from 0.01 to 0.05 nm/min for both the conventional depth-sensing and cyclic nanoindentation methods.

First, the pp-TVS films deposited at an RF power of 0.1, 2.5, and 10 W were analyzed by conventional depth sensing technique. The 20 single indentations were performed on all the films at different loads to study the depth profile of mechanical properties until 15-20% of the film thickness. The Oliver-Pharr method [50] was used to evaluate mechanical properties, such as the Young's modulus and hardness. The indentations into increasing indenter displacement enabled us to construct dependences of the Young's modulus and hardness on the contact depth (vertical distance along which contact is made).

Next, all the pp-TVS films were analyzed by cyclic nanoindentation method under similar experimental conditions like the conventional method, i.e., loading/unloading and dwell time of 5 s. The cyclic nanoindentation experiment consisted of 20 loading-partially unloading cycles with unloading fraction of 0.8 and the loading increased using displacement exponent of 2 (exponential function); an example is plotted in Fig. 37(a). The single indentation consisting of 20 cycles lasted for 300 s. The corresponding load/unload vs. displacement curve was obtained during nanoindentation measurements and is shown for the pp-TVS film deposited at a power of 10 W in Fig. 37(b). The shape of measured curves gave evidence about dominant elastic behavior of all the pp-TVS thin films. A detail is used to show that loading and unloading segments are slightly overlapped. The Oliver-Pharr method was used to evaluate the mechanical parameters from all the unloading segments at the corresponding contact depth. The Young's modulus and hardness as a function of the contact depth are compared in Fig. 38 for both the methods - conventional (full symbol) and cyclic (empty symbol) nanoindentation. Only two examples are presented corresponding to the pp-TVS film deposited at lower (0.1 W, Fig. 38 a) and higher (10 W, Fig. 38 b) power as character of plotted dependences is the same for the film deposited at 2.5 W. It can be seen that both the methods gave very similar results in case of a softer (0.1 W) and a stiffer (10 W) film as well except for region of small contact depth (5-30 nm); the discrepancy is discussed in later text. Thus, a reduced system drift enabled us to not only obtain more precise data and similar results for both the methods but also accelerate depth analysis of mechanical properties using cyclic nanoindentation.

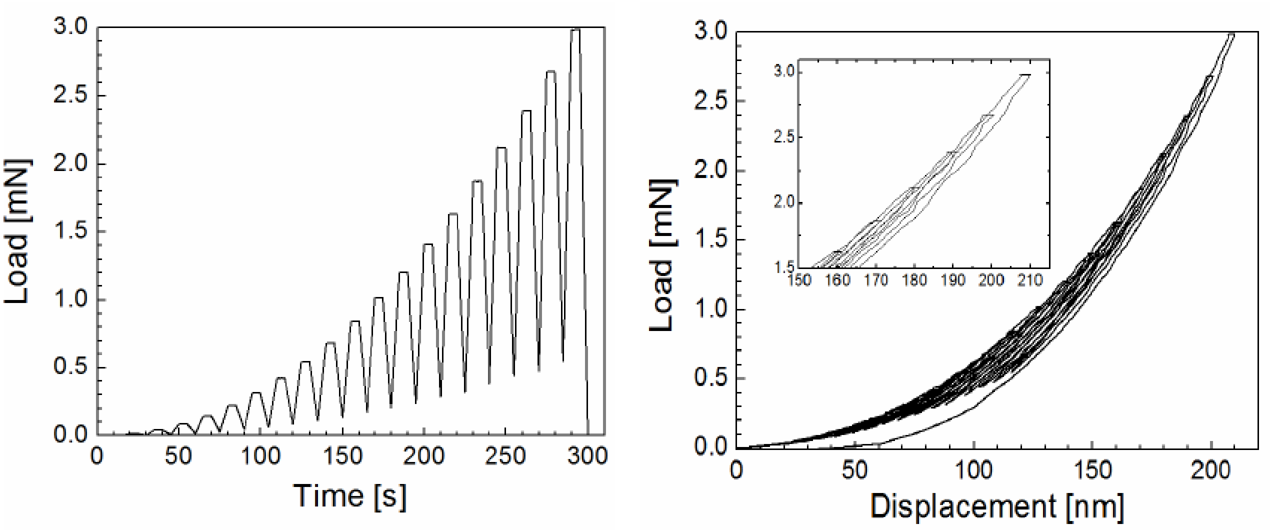

(a)

(b)

Fig. 37 Graphical presentation of cyclic nanoindentation method (20 Cycles), (a) load vs. time, (b) load/unload vs. displacement curves obtained by indentation.

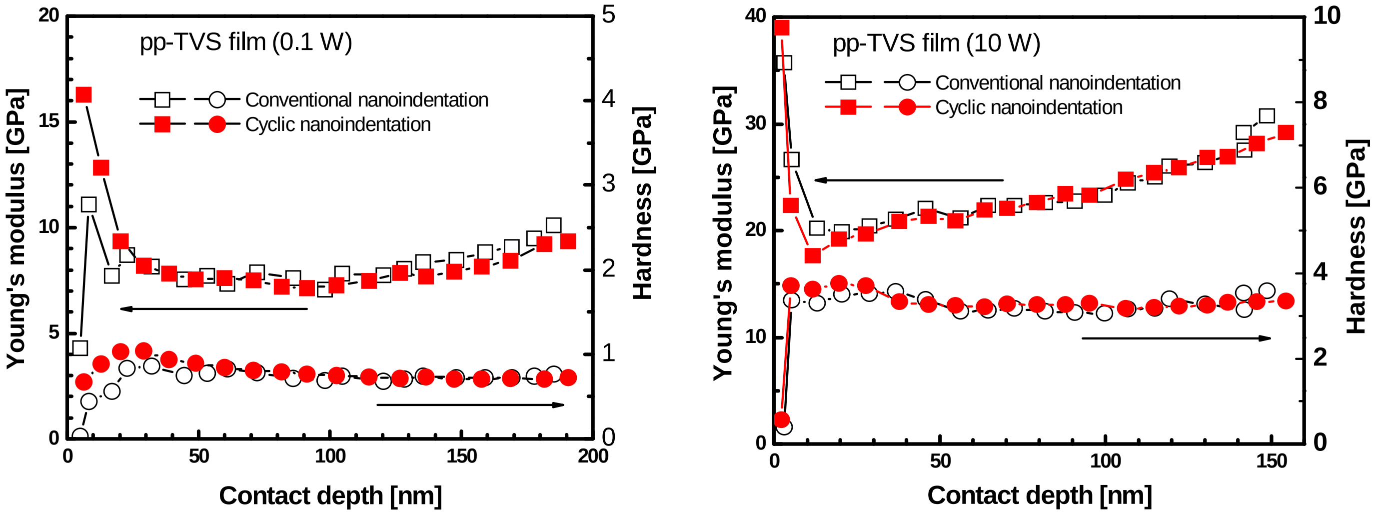

(a) (b)

Fig. 38 Comparison of Young's modulus and hardness vs. contact depth using conventional (empty symbol) and cyclic (full symbol) nanoindentation for pp-TVS films deposited at (a) 0.1 W, (b) 10 W.

Furthermore, the cyclic indentation method was used to study the depth profile of mechanical properties for pp-TVS films deposited at different powers in more details. Five cyclic nanoindentation experiments, each for 20 cycles, were used for each sample to estimate reproducibility of measurements. Therefore, the mean value and standard deviation were determined for the Young's modulus, E, and hardness, H, as given in Fig. 39 for all the films. The modulus increased abruptly accompanied by higher standard deviation decreasing the contact depth in range 5-30 nm from the film surface and this phenomenon will be discussed in next paragraph. The Young's modulus was reproducible and increased gradually for higher contact depth due to an influence of stiffer substrate (silicon wafer: E = 170 GPa, H = 11 GPa). Extrapolation (red dashed line) of the bottom portion of modulus curve (low standard deviation) to zero contact depth should result in a value of the Young's modulus for the pp-TVS film only (without substrate influence) [79]. The extrapolated values are given in Table 5. The trend of the hardness characteristics is similar for all the films and the hardness is approximately constant for higher contact depth used to evaluate (red dashed line) the mean value (Table 5). The contact depth (vertical blue dotted line) corresponding to the 10% rule is marked in Fig. 39 and the corresponding values of Young's modulus and hardness are given in Table 5. There is no difference in hardness data due to the horizontal character of hardness plot. However, an increasing difference between the extrapolated and 10%-rule values can be found for the Young's modulus with enhanced film stiffness and a difference of 29% due to the substrate influence was determined for the film deposited at a power of 10 W. It means that there is no so-called "flat region" for stiffer films, where the substrate influence is negligible, and an application of 10% rule results in wrong data. It is clearly seen from Table 5 that the enhanced power resulted in higher mechanical properties of deposited film. The increase of mechanical properties could be related to a higher cross-linking and/or an alteration of chemical structure with increasing organic character of plasma polymer, when the effective power was enhanced [82].

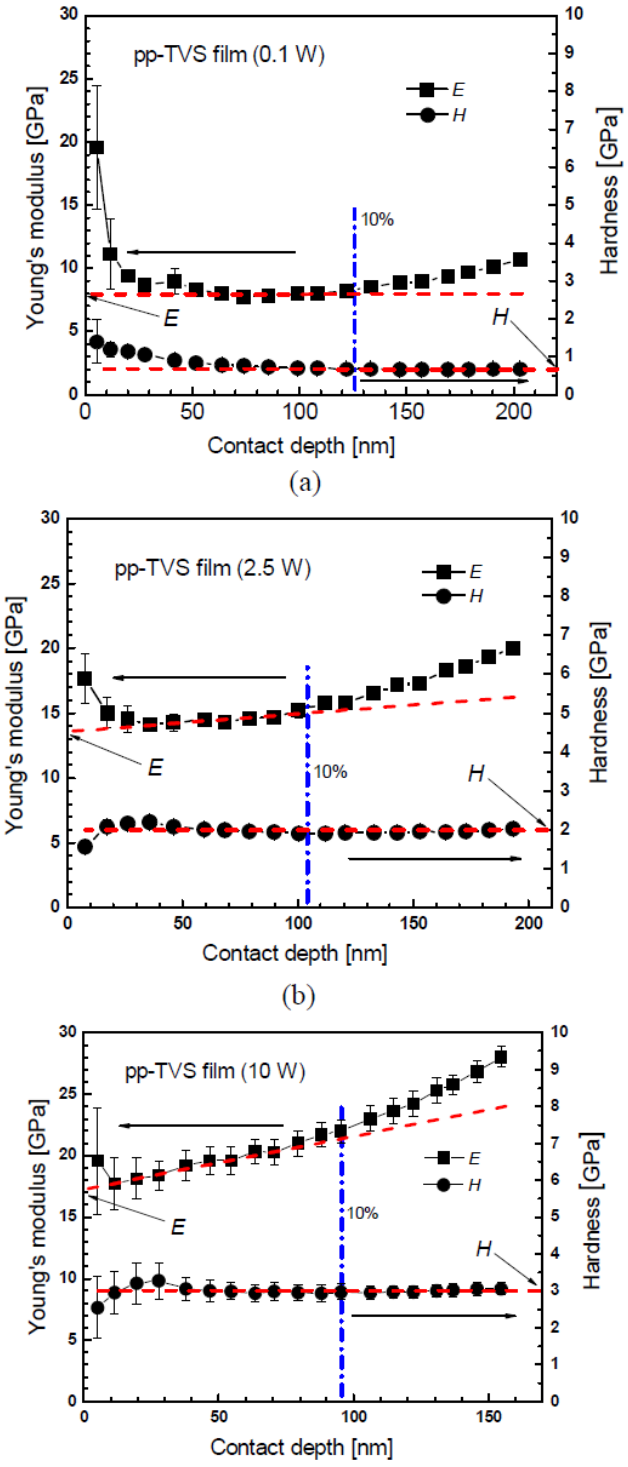

(a)

(b)

(c)

Fig. 39 Depth profile of mechanical properties for pp-TVS films deposited at, (a) 0.1 W, (b) 2.5 W, and (c) 10 W. Dotted lines indicate 10% of the film thickness

RF power [W]	Extrapolation		10% rule		Difference	
	E [GPa]	*H* [GPa]	*E* [GPa]	*H* [GPa]	*ΔE* [%]	*ΔH* [%]
0.1	7.9	0.69	8.2	0.69	4	0
2.5	14	2.0	15	2.0	7	0
10	17	3.0	22	3.0	29	0

Table 5 Mechanical properties of pp-TVS films determined by extrapolation to zero contact depth, using the 10% rule, and their differences.

The mechanical properties of thin films can be measured at a shallow depth, i.e., near to the thin film surface, if several conditions are fulfilled [83]: (i) sharp indenter, (ii) careful calibration of the indenter area function, (iii) minimal system drift and using drift correction, (iv) smooth sample [84]. Our measurements fulfil the conditions; the area function was calibrated for indenter displacement starting from 5 nm and the RMS roughness of films varied with power from 2.0 nm (0.1 W) to 5.8 nm (10 W) as measured in scanning area 5 μm × 5 μm by AFM. Moreover, the mechanical parameters could be influenced by the pile-up phenomenon, [85] i.e., where material is pushed upwards and piles up around the edges of the indentations. This would mean that more material is supporting the indenter load than is calculated for the area function. As a result, the film appears stiffer (higher modulus) and harder than it actually is. However, for pp-TVS films pile-up was not confirmed by AFM observations. Despite favorable condition for nanoindentation measurements, an increase of the Young's modulus with diminished contact depth in surface region 5-30 nm can be found in Fig. 39 accompanied by increased standard deviation marked by the error bar. Detailed analysis of unloading curves revealed increasing noise of measured data close to the film surface, especially for softer film due to a low contact stiffness at low indenter-film contact area resulting in non-reproducible modulus data and thus increasing standard deviation (error bar). Therefore, the modulus data are incorrect in surface region up to ~30 nm (0.1 W), 20 nm (2.5 W), and 10 nm (10 W) with respect to the stiffness of pp-TVS film. The hardness data seemed to be more reproducible in the surface region.

The important variable parameter in cyclic indentation test is the displacement exponent as the parameter could influence the dynamic behavior of tested material. For that reason, all the pp-TVS films were tested at different displacement exponent set as 0.3, 0.5, and 0.8 to estimate its influence on determined mechanical parameters. The Young's modulus and hardness as a function of the contact depth are plotted for selected values of displacement exponent in Fig. 40. No noticeable influence of displacement exponent on the Young's modulus and hardness was found for all the pp-TVS films due to elastic behavior of films.

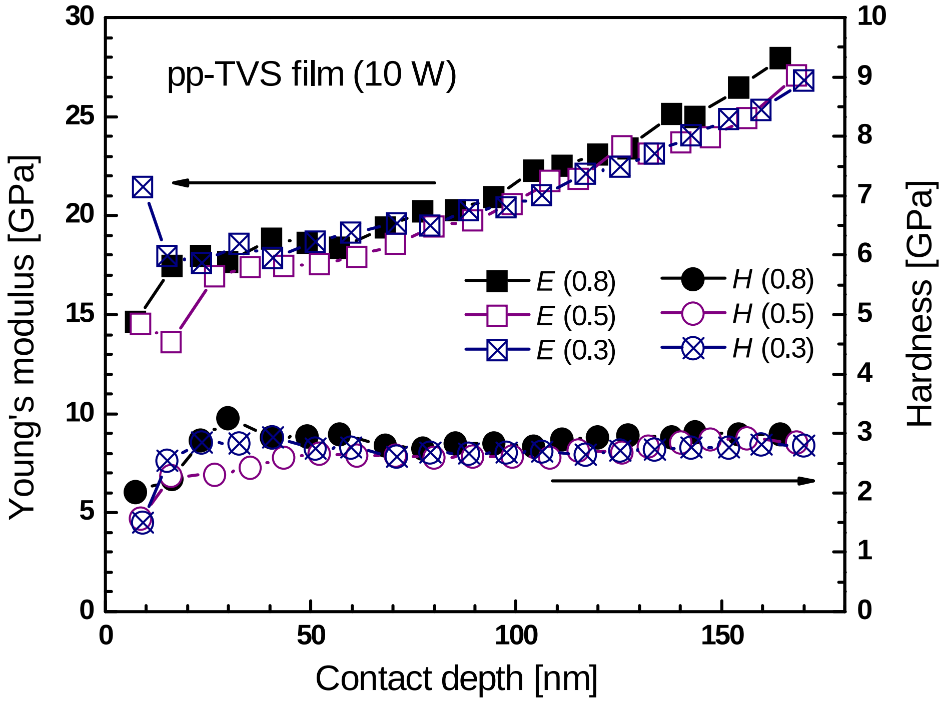

Fig. 40 Depth profile of mechanical properties for pp-TVS films deposited at 10 W analyzed at different unloading fraction (0.3, 0.5 and 0.8).

4.2 Hybrid film

Thin films in a form of hydrogenated amorphous carbon-silicon (a-SiC:H) alloy were deposited on polished silicon wafers (100) from tetravinylsilane monomer using PECVD (13.56 MHz). The surface morphology and mechanical properties of the films were analyzed by AFM, nanoindentation, finite element analysis (FEA) simulation and AFAM techniques. The current chapter of the thesis includes information about the thin film deposition, surface morphology and image analysis, mechanical properties analysis, simulation data, AFAM analysis and surface modification by UV irradiation.

4.2.1 Thin film preparation

Plasma polymer films of tetravinylsilane monomer (TVS) were deposited on polished silicon wafers by PECVD employing an RF (13.56 MHz) capacitive coupling system with plan-parallel electrodes [73]. The vacuum system was evacuated to a basic pressure of 1 x 10 $^{-5}$ Pa. The substrates were pretreated with argon plasma (10 sccm, 5 Pa, 5 W, continual mode) for 10 min to improve the film adhesion. The plasma polymerized tetravinylsilane (pp-TVS) films were deposited at a mass flow rate of 3.7 sccm and the effective power was in a range of 10 – 70 W. The deposition rate was ranging from 140-173 nm/min as a function of the deposition conditions.

Uniform plasma polymer films were deposited at a film thickness of about 1 µm. Deposition conditions (power and pressure) are given in Table 6.

P [W]	P_{dep} [Pa]	Film thickness [nm]
10	1.6	1004
20	1.4	1010
25	1.3	1124
50	1.2	1030
70	1.0	1010

Table 6 Deposition conditions for pp-TVS films.

The surface morphology of pp-TVS films were characterized in semi-contact mode by AFM technique using NTegra Prima Scanning Probe Microscope. The single crystal silicon probe of typical 10 nm tip radius of curvature was used for this purpose. The scan area was 5 x 5 µm^2. The mechanical properties of the pp-TVS films were characterized by nanoindentation technique by Hysitron Triboscope. The Berkovich diamond indenter with radius of curvature of 50 nm was used for it. Further, mechanical properties of the films were analyzed by finite elemental simulation and it was compared with nanoindentation data.

4.2.2 Surface morphology analysis by atomic force microscopy

The surface morphology of all pp-TVS films were studied by the help of height and magnitude imaging modes obtained simultaneously by semi-contact Atomic Force Microscopy (AFM). The height imaging mode gives the information about the z size distribution in nanometer (nm) scale. While, the magnitude mode imaging is an error signal but it helps to see the boundaries of grains or particles very clearly. RMS roughness value of pp-TVS films were obtained from the surface morphology analysis. The grain structure of all the films was extensively investigated by image analysis with the help of Nova software (NT-MDT, Russia). It helped to produce the histogram of grain size distribution for pp-TVS films. The mean grain size value for particular pp-TVS film was obtained from it. The detailed surface morphology of each pp-TVS samples are discussed in next paragraphs.

The surface morphology of pp-TVS film deposited at 10 W was observed from the height image and magnitude image mentioned in Fig. 41 (a) & (b). It is clearly seen that there are number of densely packed small grains. The grain's height from the surface profile mentioned in Fig. 41 (C) is in the range of 3 to 9 nm. The average RMS roughness that is the mean value of 5 different

RMS roughness measurements of the film was 3.4 nm. The average grain size for this film was 29 nm; this information was obtained from the histogram mentioned in Fig. 41 (d).

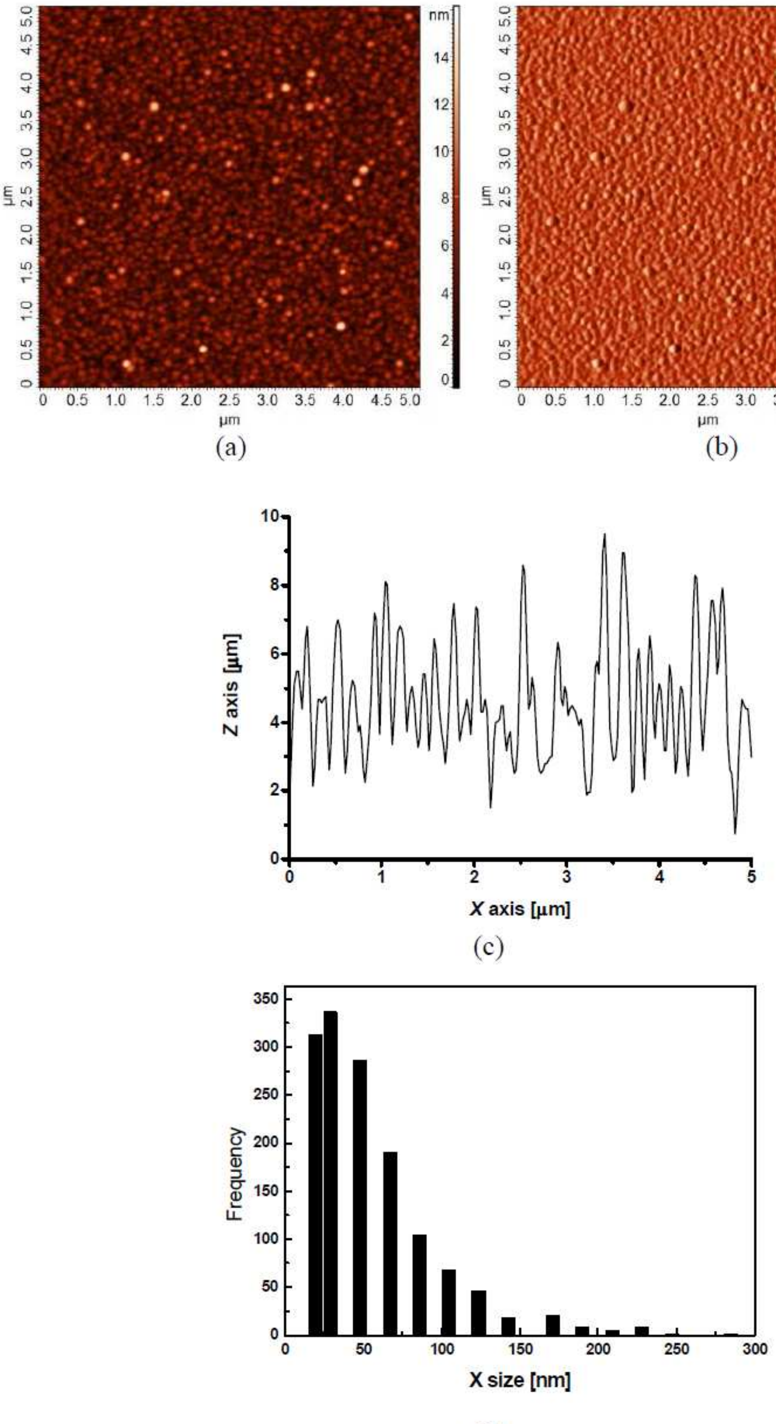

Fig. 41 Surface morphology of pp-TVS films deposited at 10 W: (a) height mode; (b) magnitude mode; (c) surface profile and (d) histogram

Similar way, the surface morphology of pp-TVS film (25 W) was observed in Fig. 42. The number of bigger grains was increased slightly for this film compared to the film deposited at 10 W. Hence, the average RMS roughness of this film was increased to 4.0 nm. The grain's height and average grain size was from 6-20 nm (Fig. 42 c) and 48 nm (Fig. 42 d), respectively. The film deposited at 20 W was having the similar kind of data hence they are not mentioned here.

The number of bigger grains was increased for pp-TVS film (50 W) which is clearly observed from the height and mag mode images mentioned in Fig. 43 (a) and (b). The height of grains was increased to 70 – 80 nm, which could be seen in Fig. 43 (c). The big grains were distributed through the film and hence the RMS roughness of the film was increased to 8.5 nm. When the surface morphology of plane area (area between the large grains) was characterized, the average RMS roughness of it was only 0.57 nm. The average grain size distribution for this film was increased to 500 nm because of large number of big grains.

In case of pp-TVS film (70 W), the big grains were found in huge numbers and they started to agglomerate i.e. fused in each other, mentioned in Fig. 44. The height distribution of big grains was from 40 nm to 120 nm, mentioned in Fig 44 (c). The average grain size and RMS roughness of this film was 241 nm and 21.7 nm, respectively. The average grain size for this film was lower than the film (50 W) because of application of higher threshold value for film analysis. The main reason behind higher threshold value was the agglomerates nature of big grains. The average RMS roughness of plane area (area between the big grains) was only 0.4 nm. The intensity of smaller grains was decreased ever further compare to pp-TVS film (50 W).

In simple words, the surface morphology i.e. surface roughness was increased from 3.4 nm to 21.7 nm for pp-TVS films as the deposition conditions changed from 10 to 70 W. The grains height and size distribution was also increased with RF-power. The surface morphology observed in AFM analysis for pp-TVS film (70 W) could be explained by Messier model [86] proposed for silicon film, mentioned in Fig. 45. According to it, the grains and the plane area were grown together as a crystal structure from the point of nucleation.

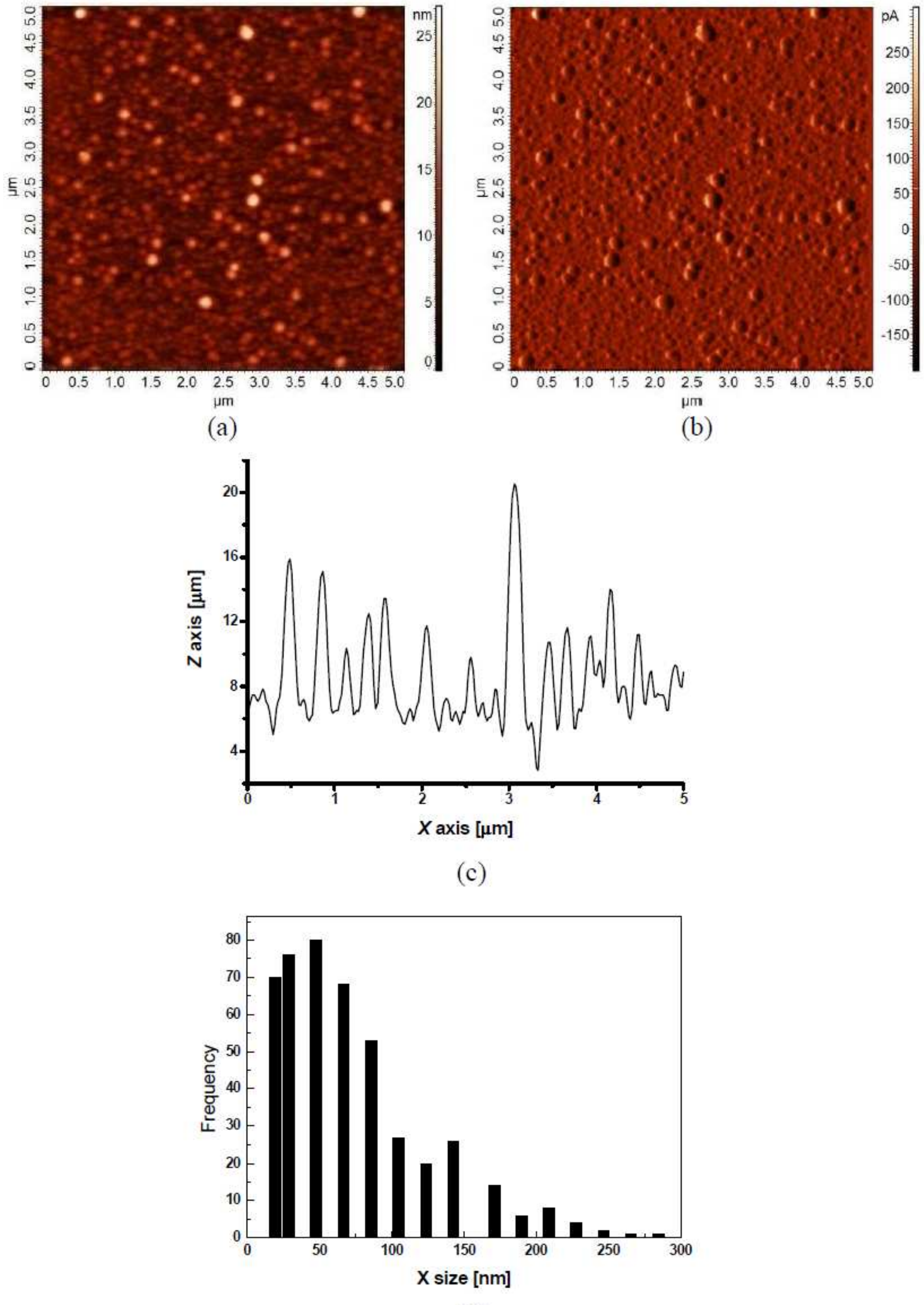

(a) (b)

(c)

(d)

Fig. 42 Surface morphology of pp-TVS films deposited at 25 W: (a) height mode; (b) magnitude mode; (c) surface profile and (d) histogram

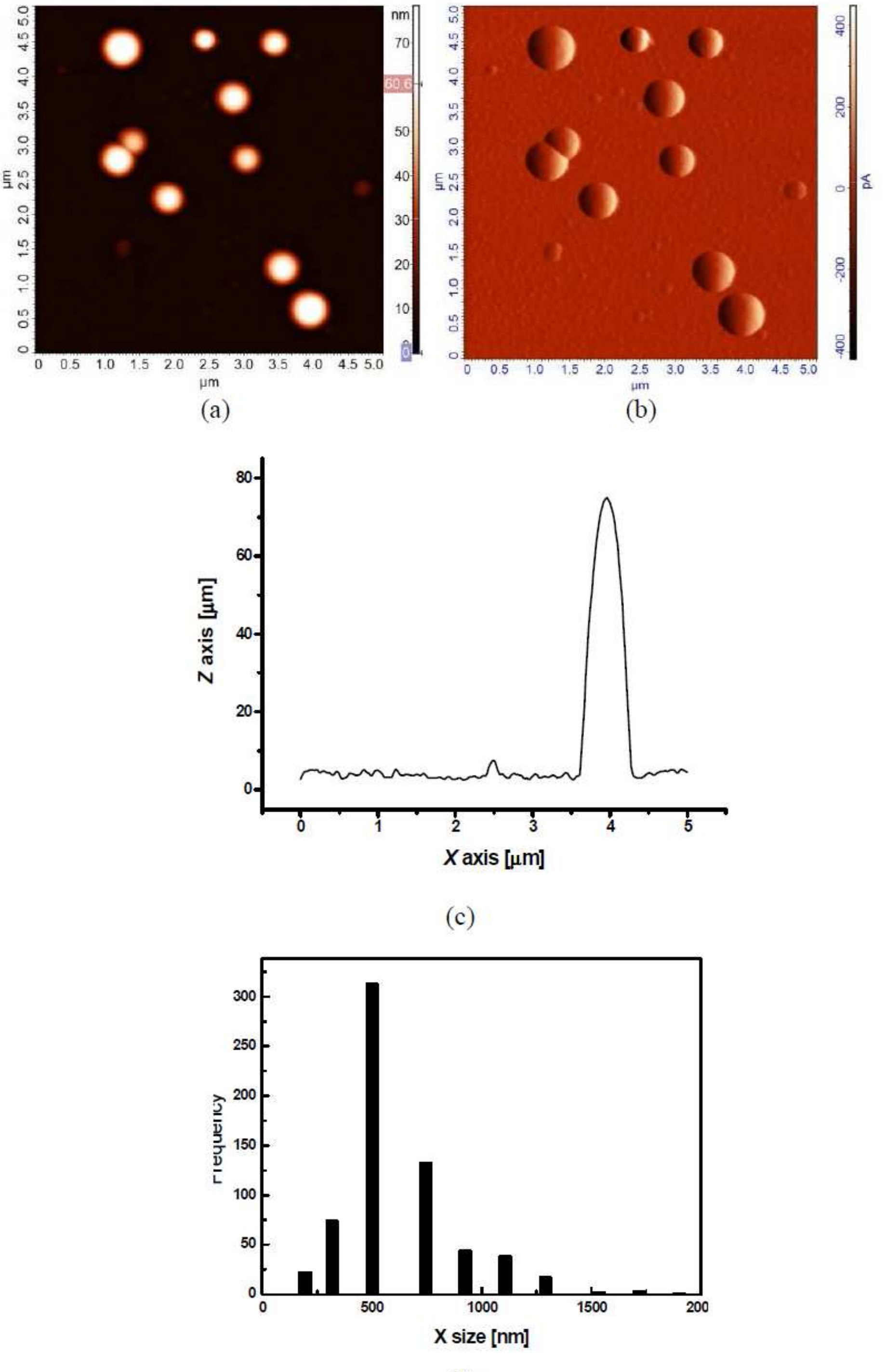

(a) (b)

(c)

(d)

Fig. 43 Surface morphology of pp-TVS films deposited at 50 W: (a) height mode; (b) magnitude mode; (c) surface profile and (d) histogram

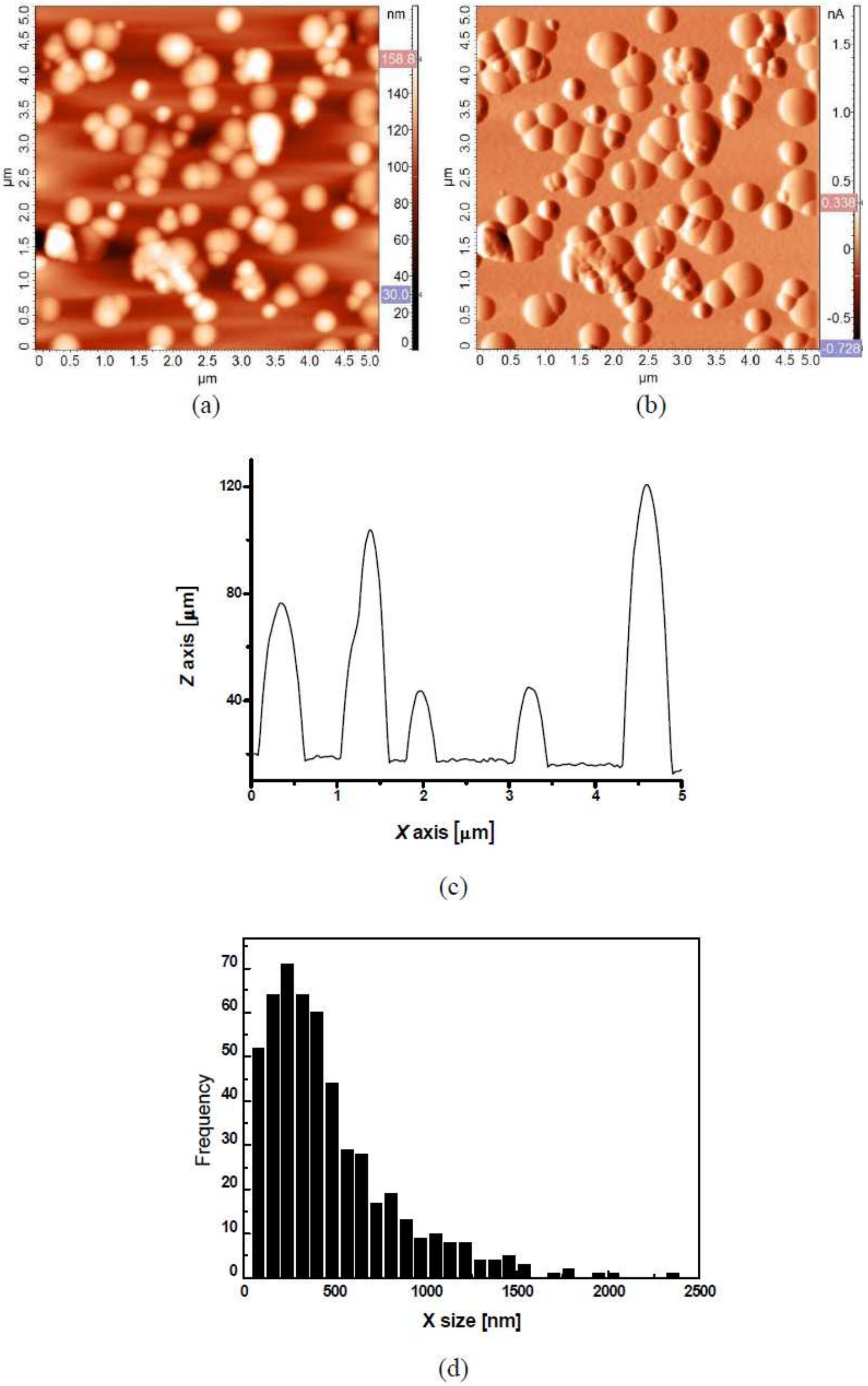

Fig. 44 Surface morphology of pp-TVS films deposited at 70 W: (a) height mode; (b) magnitude mode; (c) surface profile and (d) histogram

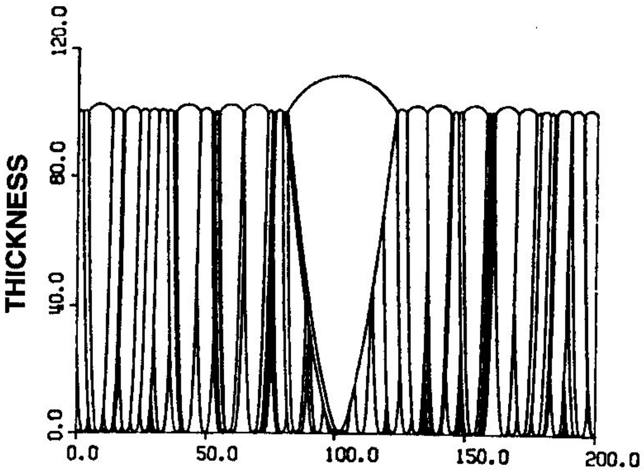

Fig. 45 The cone growth model by Messier [86]

4.2.3 Mechanical Properties

The mechanical properties such as the Young's modulus and hardness of pp-TVS films were characterized by nanoindentation method. The nanoindentation experiment was carried out in the plane area of the film, i.e., the area between the grains for comparison purpose. The mechanical properties were studied out at the 10 % of film thickness to avoid the substrate effect. The proper tip area calibration and control drift rate (≤ 0.05 nm/s) were used to obtain the correct data. At least five nanoindentation experiments were used for each sample to estimate the reproducibility of the measurements. Therefore, the mean value and standard deviation of the Young's modulus, *E*, and hardness, *H*, were given in the Table 7.

It is clearly seen from the Table 7 that the enhanced power resulted in higher mechanical properties. The increase of mechanical properties could be related to a higher cross-linking and/or alteration of chemical structure with increasing organic character of plasma polymer, when the effective power was enhanced [82].

Further, the detailed analysis of mechanical properties of plane area as well as big grains in all pp-TVS films were carried out. The analysis was carried out for the more than 5 different places to obtain the average value of the mechanical properties with control standard deviation. The obtained mechanical properties such as the Young's modulus, *E*, and hardness, *H*, for plane area as well as central area of grains for selected pp-TVS films (25, 50 and 70 W) are mentioned in Table 8. There is difference in mechanical constants for plane area and grains. It is observed from the Table 8 that the enhanced power resulted in higher differences in mechanical properties of plane and grain. For the pp-TVS film (70 W), the difference in mechanical properties is almost 50 %. This data leads to a possibility of hybrid nature of pp-TVS film being deposited at higher RF power.

RF power [W]	Contact depth [nm]	Young's modulus		Hardness	
		E [GPa]	Std. Dev.	*H* [GPa]	Std. Dev.
10	99.6	11.8	3.5	0.84	0.05
20	97.5	24.4	0.9	2.88	0.19
25	112.7	32.7	0.7	4.62	0.14
50	96.7	63.0	1.8	7.40	0.19
70	92.1	81.4	0.7	8.84	0.13

Table 7 Mechanical properties of pp-TVS films

RF power [W]	Position	Young's modulus		Hardness	
		E [GPa]	Std. Dev	*H* [GPa]	Std. Dev
25	Plane	32.7	0.7	4.62	0.14
	Grain	27.8	1.1	3.44	0.26
50	Plane	63.0	1.8	7.40	0.19
	Grain	35.7	3.1	3.21	0.23
70	Plane	81.4	0.7	8.84	0.13
	Grain	41.8	3.8	3.48	0.67

Table 8 Detailed mechanical properties of plane and grain of pp-TVS film deposited at 25, 50 and 70 W

As mentioned previously, the nanoindentation data indicates the possibility of two different kind of material with different mechanical properties to be present in pp-TVS film deposited at higher RF-power. The difference in measured data of plane area and grains can be explained by two possibilities:

(1) Effect of different geometry, i.e., different geometry of plane area and grains may lead to different deformations under indentation load,

(2) Difference in mechanical properties of plane area and grains.

To check the 1st possibility, the depth profile of mechanical properties was analyzed for pp-TVS film (70 W). The selected big grains were used whose height were around 120 nm. The obtained data such as the Young's modulus vs. contact depth and hardness vs. contact depth are mentioned in Fig. 46. It is clearly seen from Fig. 46 that there is a difference in mechanical properties of plane area and the grains. The linear extrapolation was used to obtain the true Young's modulus and hardness for plane area of pp-TVS (70 W) film, which were found out to be 73 GPa and 8.7 GPa respectively. The values of Young's modulus and hardness obtained by linear extrapolation were little higher than the value obtained by 10 % rule (mentioned in Table 8). The influence of hard silicon substrate (which is having the elastic modulus and hardness of 150 GPa and 10 GPa, respectively) on mechanical properties was clearly seen around 10 % of the film thickness i.e. around 100 nm of the film thickness.

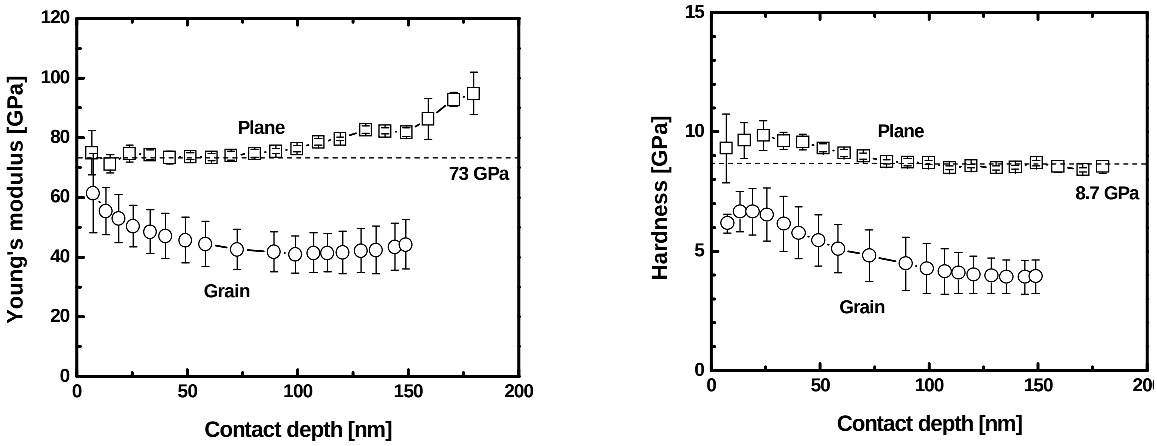

Fig. 46 Depth profile of mechanical properties of plane and grain area for pp-TVS film (70 W)

The data obtained from the depth profile study were sent for finite elemental analysis. The obtained simulated data can be seen in Fig. 47. The difference in mechanical properties for plane area and grain was also observed in simulated data.

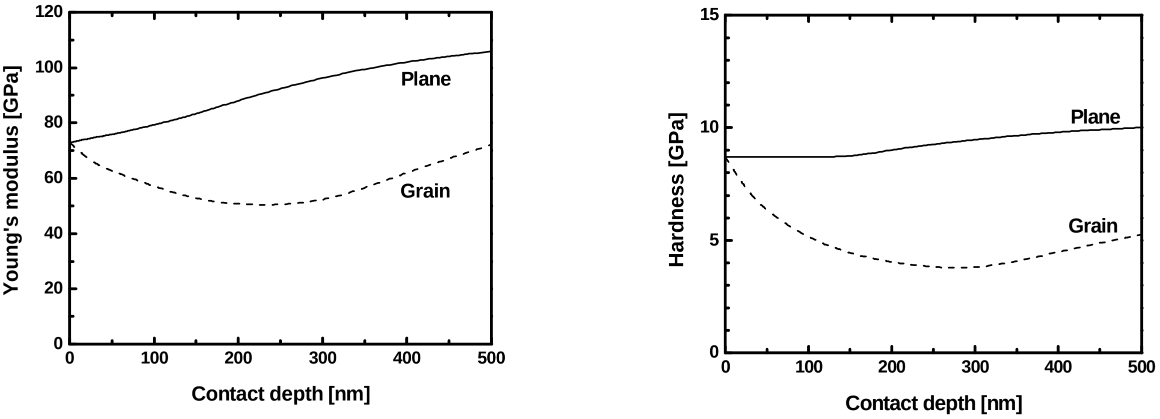

Fig. 47 Finite elemental analysis data

For better understanding, the simulated data (red line) were compared with depth profile data (black point) mentioned in Fig. 48. It is clearly seen that the mechanical properties (Young's modulus, hardness) obtained for the plane area from both methods (nanoindentation and simulation) were having the same trend and harmony.

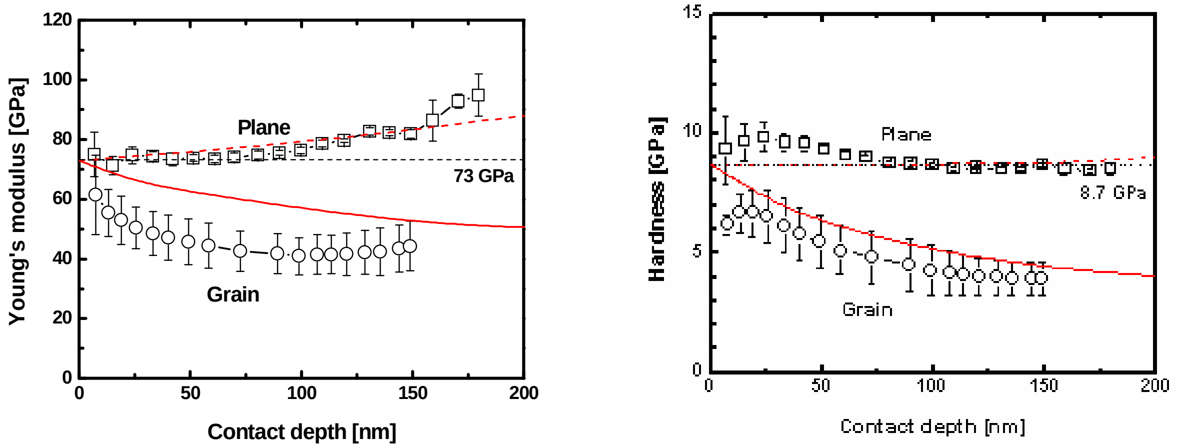

Fig. 48 Comparison of FEA simulated data with nanoindentation data for pp-TVS film [70 W]

In a similar fashion, the hardness data obtained from both methods for grains were having the same trend and within the error margin. However, the Young's modulus of grain was showing some difference. This difference helped to understand that at some extent there is a possibility of effect of different geometry of plane area and grain on nanoindentation data because of their different deformation under the loading conditions.

4.2.4 Surface analysis by Atomic Force Acoustic Microscopy

Atomic Force Acoustic Microscopy (AFAM) is a newly develop SPM method. It is a non destructive method and used for the mechanical properties analysis of surfaces of thin films or polymers. The AFAM experiment was carried out on pp-TVS film deposited at 70 W RF power. It was used to measure the magnitude change of cantilever vibrating near to its resonance frequency. The obtained data such as the (a) topography and (b) mag AFAM image were mentioned in Fig. 49. The topography is a contact mode topography produced simultaneously with mag AFAM image. In mag AFAM image, the dark part of the scale represents the material, which is softer in nature. On the contrast, the bright part of the scale represents the stiffer material. So it was concluded from the AFAM image that the grains were softer in nature compared to the plane area i.e. the grains were having the lower mechanical properties than the plane area. This result indicated the possibility of nanocomposite nature of this film.

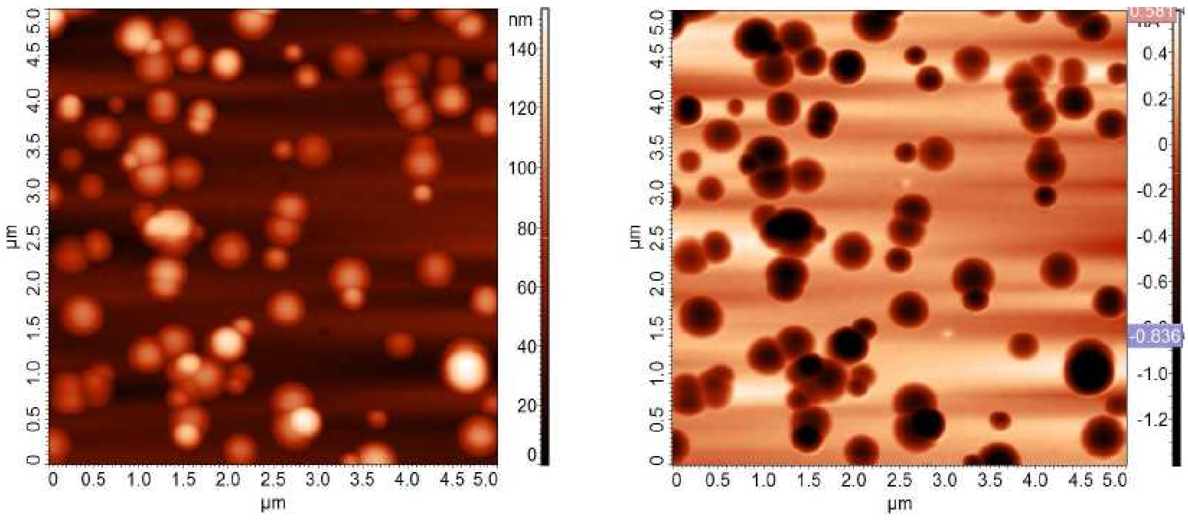

(a) (b)

Fig. 49 Images of the surface of pp-TVS film deposited at 70 [W]: (a) topography map; (b) AFAM mag contrast

4.2.5 Film modification by UV irradiation

Sample preparation

The pp-TVS films were prepared for this study was with a similar procedure like the hybrid films. Only some changes in film preparation steps are the Pp-TVS films were prepared at a mass flow rate of 3.8 sccm (3.0 Pa), a power of 10 W (self bias 100 V), and two deposition times in order to deposit two sets of six samples with film thickness of 0.1 and 0.5 µm, respectively. A batch of six samples was deposited simultaneously using a special bottom electrode enabling loading of up to six substrates under vacuum. When the deposition process was completed, the whole apparatus was flushed with argon gas (10 sccm, 5.0 Pa); after 60 min, the chamber was evacuated to a basic pressure of 1 x 10^{-5} Pa, and after a further 24 h, the prepared specimens were removed from the chamber and exposed to UV irradiation.

UV irradiation exposure

Five pp-TVS films from each set were irradiated by ultraviolet (UV) light at ambient conditions using a medium-pressure mercury UV lamp with a characteristic wavelength of 365 nm [87]. The time of UV exposition was set at 10 (sample A), 33 (B), 100 (C), 333 (D), and 1000 min (E). The sixth film (sample F) of each set was used as a reference sample and was not UV irradiated. All the samples were stored at room temperature (about 22 °C, 30% humidity) and observed over 134 days to investigate aging effects.

The near-surface mechanical properties of the pp-TVS films were investigated using a 2D Triboscope (Hysitron) attached to an NTegra Prima Scanning Probe Microscope (NT-MDT) enabling in situ topography analysis. A Berkovich tip with a radius of curvature of about 50 nm was used. The Young's modulus and hardness of films were determined using the Oliver–Pharr method [50]. Atomic Force Microscopy (AFM) images of the 5×5 μm^2 scanning area were used to determine the RMS roughness of the observed film surfaces.

Some researchers were able to analyze a decrease of the film thickness due to UV-induced chain scission and bond breakage producing volatile organics. The surface roughness of the polyethylene films increased as a result of the UV–ozone treatment because of the etching effect of the ozone. However, the RMS roughness of pp-TVS films decreased after 100 min of UV irradiation (Table 9), as no ozone was produced during our UV treatments (the wavelength threshold for ozone production is 181 nm). The surface morphology of sample E (UV exposed for 1000 min) and sample F (reference) were mentioned in Fig. 50 and Fig. 51 respectively.

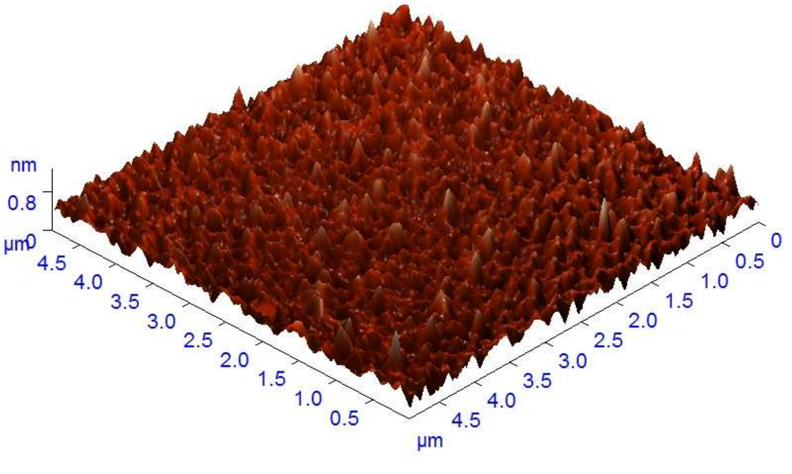

Fig. 50 AFM surface topography of sample E have exposed to UV for 1000 min

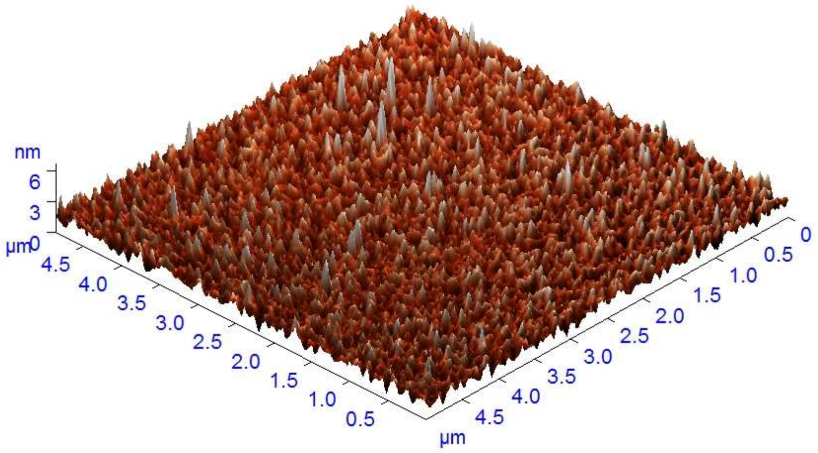

Fig. 51 AFM surface topography of sample F used as a reference one

UV-induced cross-linking of plasma polymer together with a stronger polymer network (Si–O–C) and the reduction of the film thickness could modify the mechanical properties and density of the material. For this reason, nanoindentation measurements were used to investigate selected mechanical properties (Young's modulus and hardness) of pp-TVS films after 134 days. An increase of the Young's modulus by 21% and hardness by 24% compared with the reference sample was found only for the film UV-irradiated for 1000 min (Table 9).

Sample	UV exposition [min]	Film thickness [nm]	RMS roughness [nm]	Young’s modulus [GPa]	Hardness [GPa]
F	0 (reference)	463 ± 46	0.41 ± 0.03	11.7 ± 0.5	0.82 ± 0.05
A	10	532 ± 53	0.41 ± 0.01	10.0 ± 0.5	0.80 ± 0.04
B	33	593 ± 59	0.41 ± 0.01	11.1 ± 0.6	0.91 ± 0.05
C	100	560 ± 56	0.38 ± 0.03	10.6 ± 0.8	0.75 ± 0.07
D	333	464 ±46	0.21 ± 0.04	10.2 ± 0.2	0.72 ± 0.02
E	1000	228 ± 23	0.12 ± 0.01	14.1 ± 0.4	1.02 ± 0.01

Table 9 Comparison of film thickness, surface and mechanical properties of films exposed to UV irradiation.

4.3 Adhesion test

The adhesion test for series of samples were carried out by nanoscratch test with the help of Hysitron triboscope instrument. The scratch testing was possible to perform in y direction only, because of 2 dimensional transducer of triboscope instrument. There were four experiments carried out to study the adhesion failurity of plasma-polymerised thin films on silicon substrate:

(1) Study of effect of different scratch speed (µN/s) on measured data

(2) Reproducibility of the adhesion data for thin films prepared under the same deposition conditions

(3) Effect of different film thickness on adhesion failures

(4) Effect of different mechanical properties of thin films on adhesion behaviour

4.3.1 Thin film deposition

Plasma-polymerised tetravinylsilane (pp-TVS) films were deposited on polished silicon wafers by PECVD empolying an RF (13.56 MHz) working in continuous plasma mode. The vaccum system was evacuated to a basic pressure of 1 x 10^{-5} Pa. The substrates were pretreated with argon plasma (10 sccm, 5.0 Pa, 5 W) for 10 min. The mass flow rate of TVS monomer is 3.8 sccm. Pp-TVS samples were prepared in 3 sets for adhesion failurity experiment:

(i) There are three samples A, B and C prepared at same deposition conditions of 10 W and similar in film thickness of 100 nm. These samples were used for checking the reproducibility of adhesion behaviour and for influence of sample aging. While, the sample A was used for scratch experiments with different scratch speed.

(ii) A set of samples was prepared at the same 10 W power but difference in film thickness by varying their deposition time. The films were prepared of different thickness of 25, 54, 99, 197, 334 and 468 nm. These samples were used to study the effect of different film thickness on adhesion failurity.

(iii) Another set of samples were prepared with the similar film thickness of about 100 nm but at different RF power of 10, 25, 50 and 70 W. Due to differece in deposition condition, these films were having different mechanical properties. Further, scratch tests were carried out to correlate the effect of different mechanical properties of thin films and their scratch behaviour.

Nano-scratch tests were performed with a Berkovich diamond indenter of 150 nm tip radius curvature. The outcome of the experiment were normal displacement, normal critical force, lateral critical force and coefficient of friction. This parameters helped to understand the adhesion failurity of pp-TVS films on silicon substrate. The data were normally ploted between lateral force (µN) vs. normal force (µN) and coefficient of friction vs. normal force (µN) as mentioned in Fig. 66 for pp-TVS film of 99 nm deposited at 10 W. It is clearly seen from the Fig. 66 that the normal force is increasing smoothly with lateral force till the tip is going through the film thickness. The disturbance (failure) was observed in normal force as well as in lateral force when delamination of film was started. The same behaviour was also observed in coefficient of friction vs. normal force plot. Similar kind of adhesion failurity behavior were observed for all the pp-TVS films except the pp-TVS film, which was having the thickness of 25 nm. The adhesion failurity for pp-TVS film of 25 nm will be discussed in chapter 3.3.3. The selected scratches of pp-TVS films were further analysed with non-contact mode AFM to understand the delamination behaviour as well as to corelate it with scratch data.

4.3.2 Study of effect of different scratch speed on measured data

This experiment was carried out on sample deposited at 10 W and having the thickness of 99 nm. The mechanical constant such as the Young’s modulus and hardness of this film was 12 GPa and 0.8 GPa, respectively. By varying the scratch time from 120 to 7 s, the loading rate was also changed from 16.7 µN/s to 285.7 µN/s. Hence, the scratch speed was also changing from slowest to fastest. The data were summarized in Fig 52.

It was observed from the Fig. 52 that the critical normal force was slightly higher for increased scratch speed due to stress. The fracture occurs at higher or lower of the scratch speed of about 100 (µN/s) were considered consistent and it was overlapping in the range of measurement error (see in Fig. 52).

The increase in strength at the higher speed could be explained by the reason that the material would have got less time to response or deform, hence the measured critical power was higher than that would have been at a lower speed. This feature is characteristic of polymeric materials and it was observed for the organosilicon film, which is also polymeric in nature.

The present experiment indicated that the changing in scratch speed has a little effect on obtained adhesion failure data. Hence, now on words the selected scratch time used for further experiments was 30 seconds with a length of 10 µm Corresponding to a scratch speed of 66.7 µN/s.

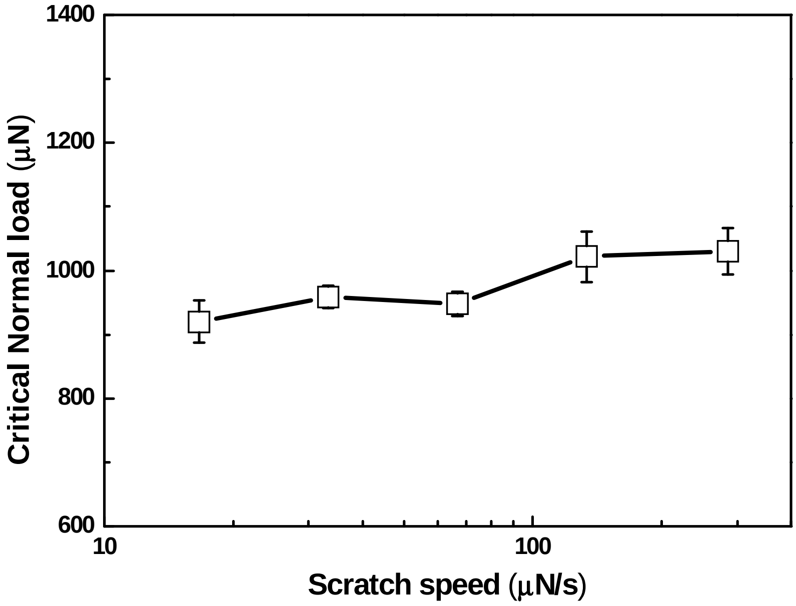

Fig. 52 Critical normal load (µN) vs. scratch speed (µN/s) for pp-TVS film deposited at 10 W

4.3.3 Reproducibility of the adhesion data

The samples used for this experiment were prepared at 10 W, having the same mechanical properties (Young's modulus of 12 GPa, Hardness of 0.8 GPa) and about 100 nm in thickness. The samples A, B and C were prepared at different time interval of 06/2008, 10/2009 and 11/2009, respectively. The aim of the expeiment was to evaluate the reliability of the plasma deposition of reproducible thin layers and to reveal a possible aging effect. 10 sets of exepriments were carried out for each sample to produce the average value of critical normal force with std. dev, mentioned in Table 10.

Samples	Average Critical Normal Force (µN)	Std. Dev. (µN)
A	811	44
B	948	19
C	893	41

Table 10 Scratch data of sample A, B and C prepared at different time interval

The mean critical normal force of these three samples is approximately 884. The mean value obtained from the experiments do not exceed the acceptable range of measurement errors of 10

%. The obtained data indicate that the plasma deposition equipment is capable to reproduce the organosilicon thin films with similar adhesion characteristics.

4.3.4 Effect of different film thickness on adhesion failures

As mentioned previously in film preparation, a series of pp-TVS films deposited at 10 W rf-power discharge with variable film thickness of 25, 54, 99, 197, 334 and 468 nm were used for this experiment. Ten scratch experiments were used for each sample to estimate reproducibility of measurements. The scratch behaviour of each sample were scanned in height mode and mag mode image by the help of AFM. The selected AFM data were explained in next paragraphs.

The scratch experimental data such as the critical normal load and critical lateral load with std. dev. mentioned in Table 11 for different film thickness. It is clearly seen from Table 11 that enhanced film thickness from 25 nm to 468 nm resulted in higher critical normal load from 212 µN to 8864 µN and higher critical lateral load from 29 µN to 2049 µN for adhesion failurity. The obtained critical normal load plotted against film thickness, metnioned in Fig. 53.

The results show (Fig 53) that the critical normal load increases approximately linearly with film thickness upto a thickness of 334 nm. In general, if we assume that the adhesion is the same and critical load is determined by the extent of the deformation, an increased film thickness requires an increased indenting load to obtain the same deformation so that the critical normal load increases with the film thickness [88].

Film thickness (nm)	Critical Normal load (µN)	Std. Dev.	Critical Lateral load (µN)	Std. Dev.
25	212	17	29	3
54	414	25	71	3
99	893	41	206	10
197	2181	122	455	24
334	3936	117	849	49
468	8864	650	2049	184

Table 11 Influence of different film thickness of pp-TVS films on scratch data

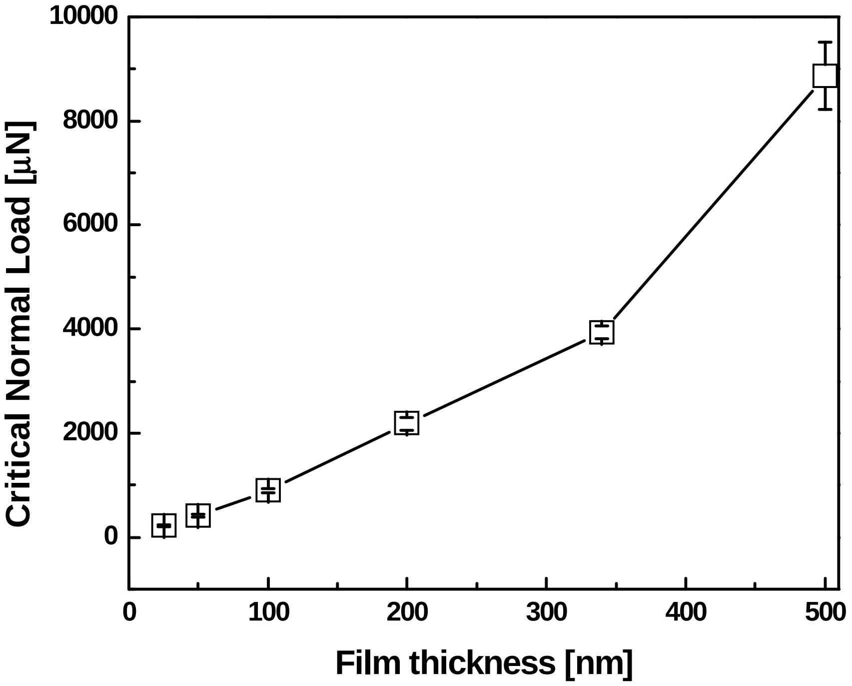

Fig. 53 Critical normal load vs. film thickness plot for pp-TVS film

The correalation of scanned AFM images with scratch measurement data was really helpful to understand the mechanism of adhesion failurity of pp-TVS films as thickness increased from 25 nm to 468 nm. The pp-TVS film of 25 nm was deformed under the normal critical load of 212 µN and normal lateral load of 29 µN, mentioned in Table 11. Scanned height mode and magnitude mode images for this film are mentioned in Fig. 54. It was clearly observed that it is really difficult to see the delamination point for this film becuae of elastic recovery. Only a small amout of deformation was observed. Simlar kind of problem was observed for the scratch data of this film mentioned in Fig. 55. For this film, there was no disturbance in normal force vs. lateral force plot observed. But a small transition repetative in normal force and lateral force was seen. As the film thickness was increased from 54 nm to 468 nm, the delamination point of each film was clearly observed from normal force vs. lateral force plots mentioned in Fig. 55 and Fig. 57.

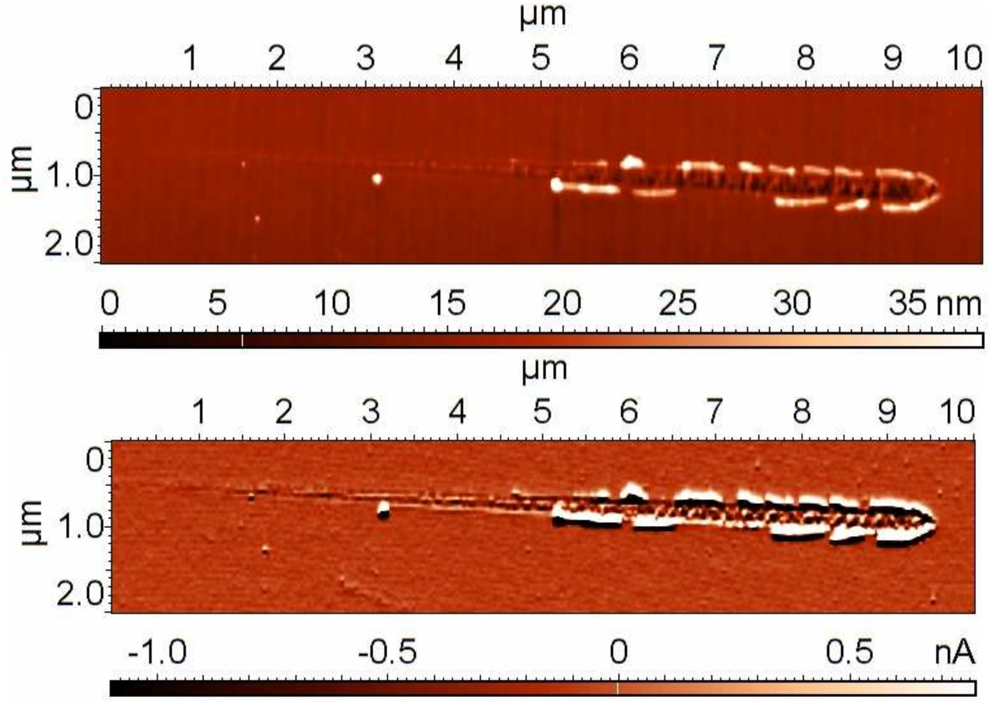

Fig. 54 AFM images of the scratch of pp-TVS film of 25 nm. top: height mode; bottom: magnitude mode

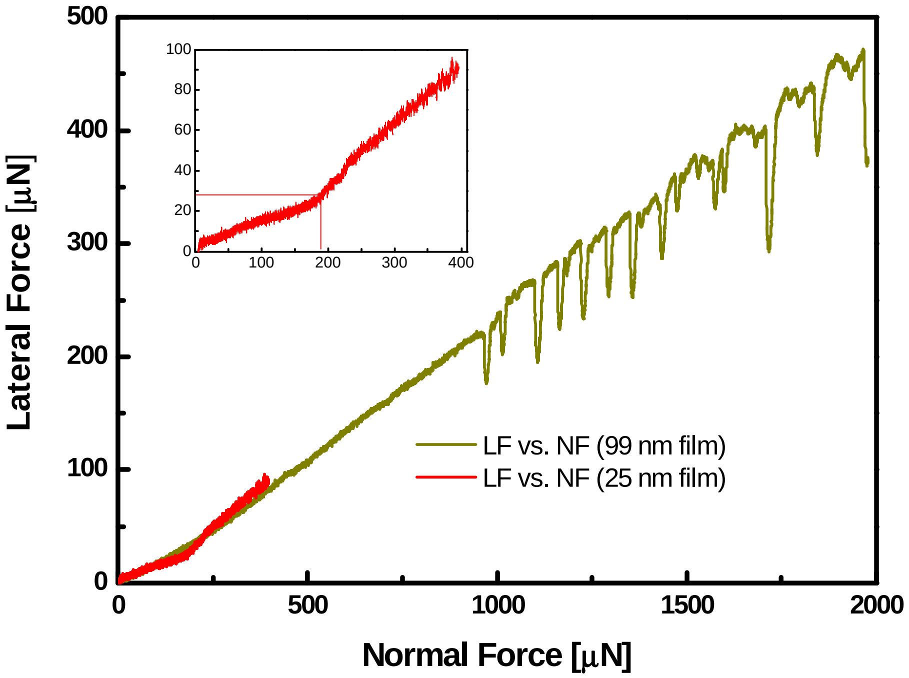

Fig. 55 Comparison of Lateal force (µN) vs. normal force (µN) data of pp-TVS films having thickness of 25 nm and 100 nm

The height mode and magnitude mode scan images of thick pp-TVS film of 468 nm are mentioned in Fig. 56. The critical normal load and critical lateral load for this film was 8864 µN and 2049 µN, respectively. In comparison with the film of 25 nm (Fig. 54), this film showed a clear delamination point on scratch track. It showed a large area of the film around the second half of the scratches were completely delaminated. The delaminated and removed large part of the film was also clearly observed by a huge decline in lateral force vs. normal froce curve as mentioned in Fig. 57. Similar kind of behaviour was also observed in scratch data and in AFM images for pp-TVS film deposited at 50 W and 70 W rf power discharge mentioned in next part of the chapter. Pp-TVS film of 468 nm, the large part of the film was delaminated and removed it might be due to the higher internal stress in the film caused by higher normal force. Thus, one can conclude that the thicker film has better adhesion to the substrate.

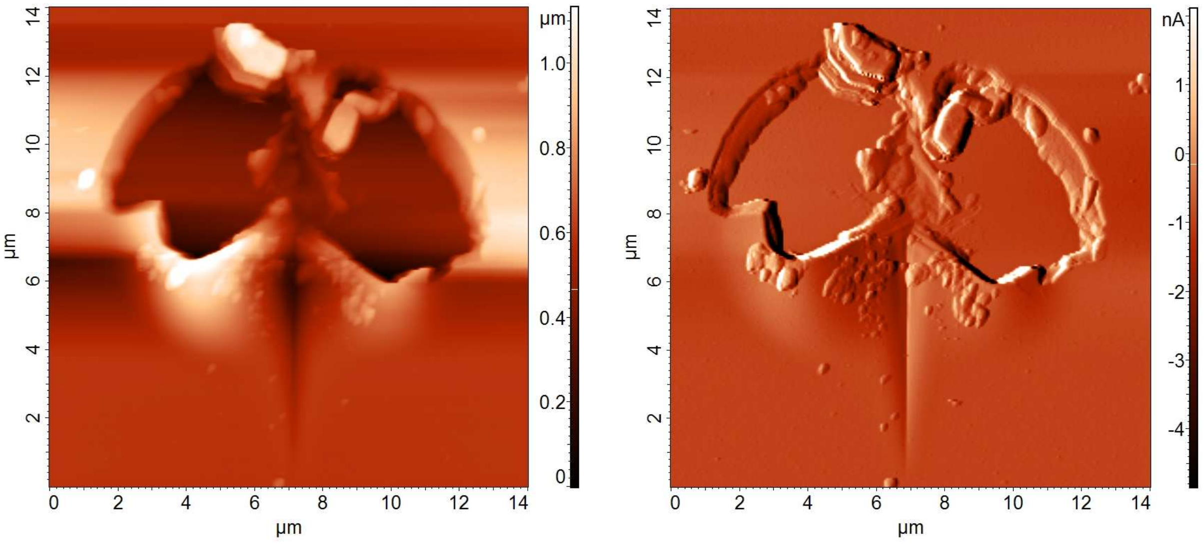

Fig. 56 Images of the scratch of pp-TVS film of 468 nm. left: height mode; right: magnitude mode

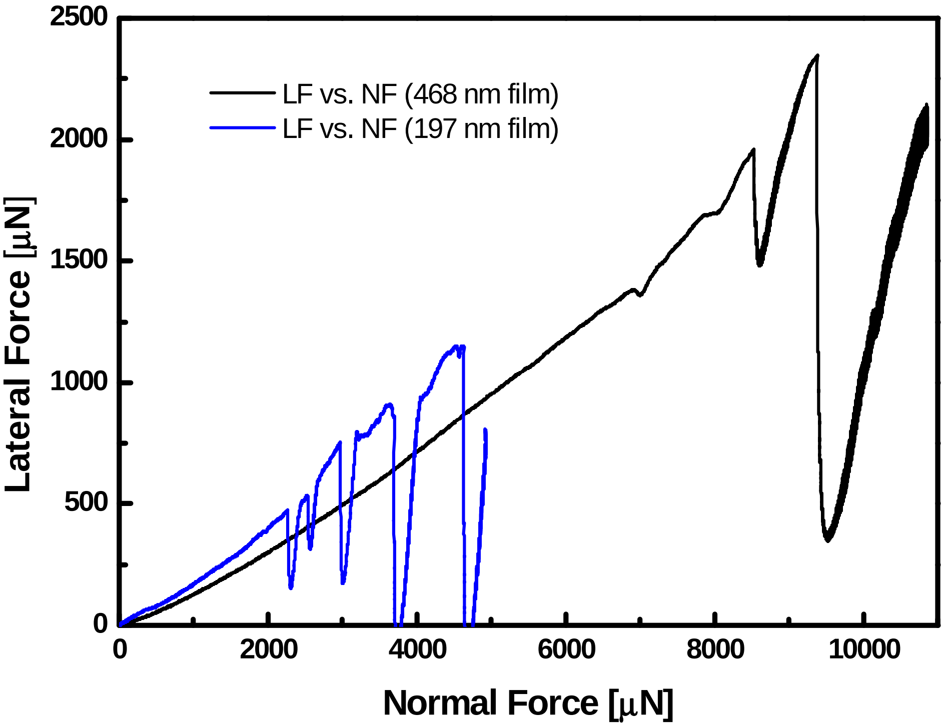

Fig. 57 Comparison of Lateal force vs. normal force data of pp-TVS films having thickness of 197 nm and 468 nm

The critical normal force and critical lateral force was clearly observed for all the pp-TVS films of thickness 25, 99 and 197 nm as mentioned in Fig. 55 and Fig. 57. One interesting point came in focus when the lateral foce vs. normal force plot was observed carefully for the pp-TVS film of thickness 468 nm, stated as Fig. 58. It is seen from Fig. 58 that there is a possibility of two normal critical force (N_{C1}, N_{C2}) and two lateral critcal force (L_{C1}, L_{C2}) for this film. The 1st point (N_{C1}, L_{C1}) was observed with a very small changes on scratch track and plot. While, the 2nd point was clearly visible and hence it was used as the data in current study. Similar kind of behavior also observed for the pp-TVS film of 334 nm thickness. On the basis of the scratch test and the scanned AFM images conclude that the film thickness has a significant impact on the adhesion failurity data.

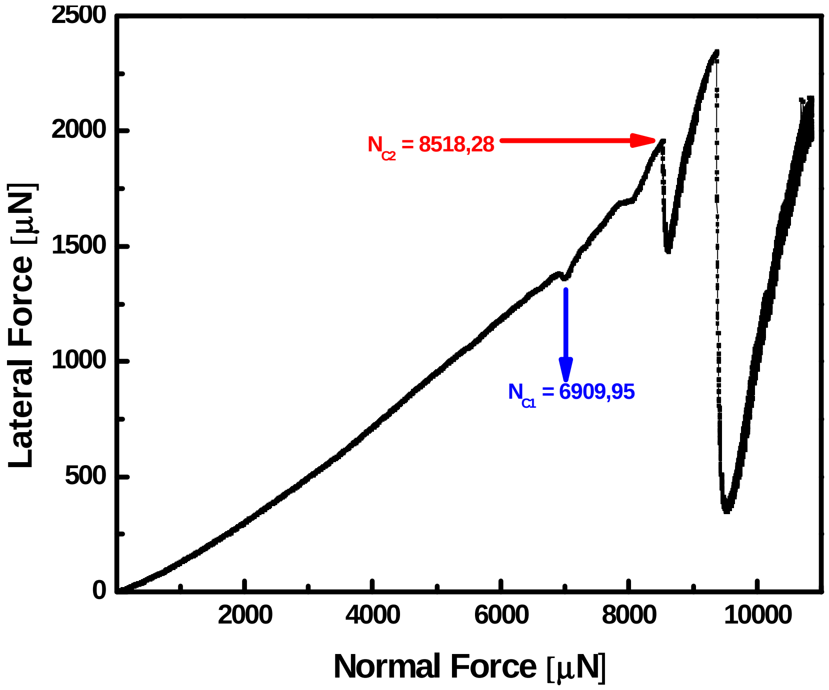

Fig. 58 Lateal force vs. normal force plot for pp-TVS film of 468 nm

4.3.5 Effect of different mechanical properties of thin films on adhesion behavior

A series of films were prapared at different rf power of 10, 25, 50 and 70 W with similar film thickness of about 100 nm for comparing the scratch adhesion data. The enhanced RF power resulted in higher mechancial properties of deposited film i.e. the pp-TVS films of 10, 25, 50 and 70 W were having the Young's modulus of 12, 33, 63 and 81 GPa, respectively and hardness of 0.8, 4.6, 7.4 and 8.8 GPa, respectively. The increase of mechanical properties could be related to higher cross-linking of plasma polymer, when the effecitve power was enahnced [82].

The scratch experiment were performed on each sample for 10 times to obtain the mean value and standard deviation of critical normal load and critical lateral load, as given in Table 12 for all the films. The obtained critical normal load was ploted against the RF-power, which is mentioned in Fig. 68. The atomic force microscopy (AFM) was used in semi-contact mode to study the scratch behavior of pp-TVS films in height mode (topography) and magnitude mode (error signal) imaging, which are mentioned in Fig. 59 – 62.

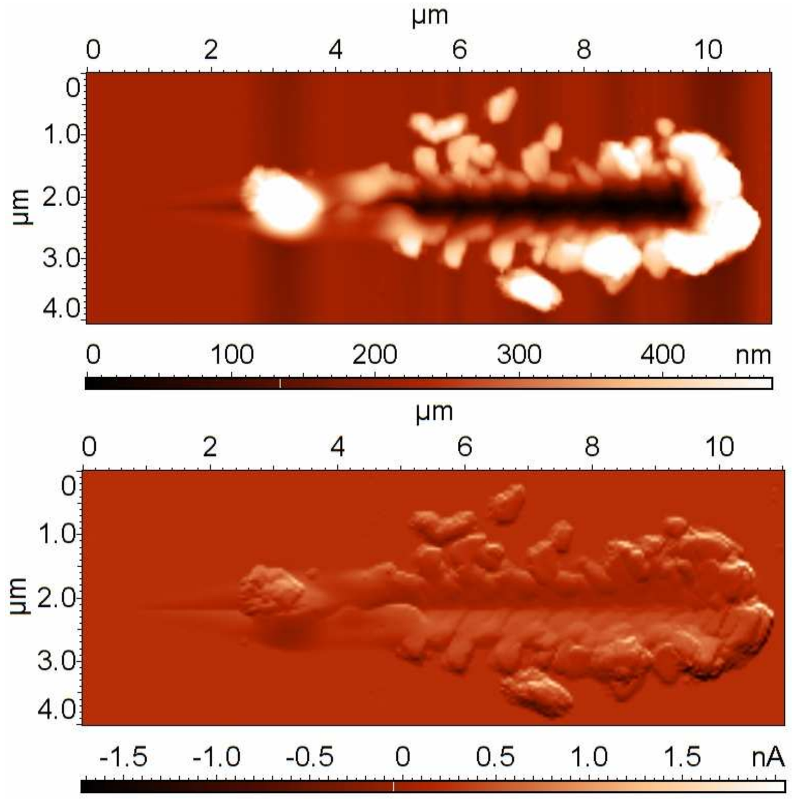

Fig. 59 AFM scratch image of pp-TVS film (10 W), top: height mode; bottom: magnitude mode.

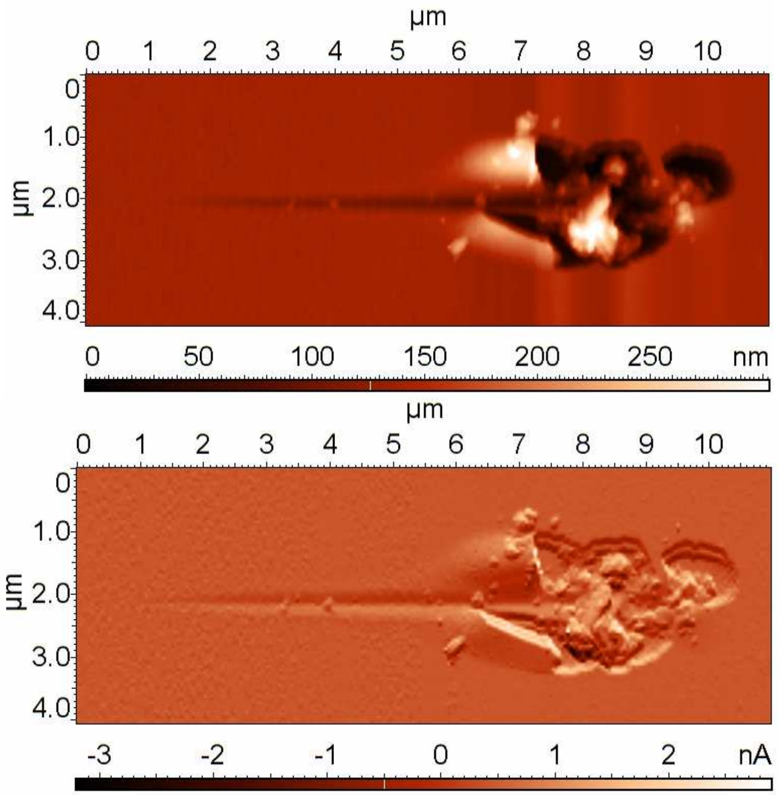

Fig. 60 AFM scratch image of pp-TVS film (25 W), top: height mode; bottom: magnitude mode.

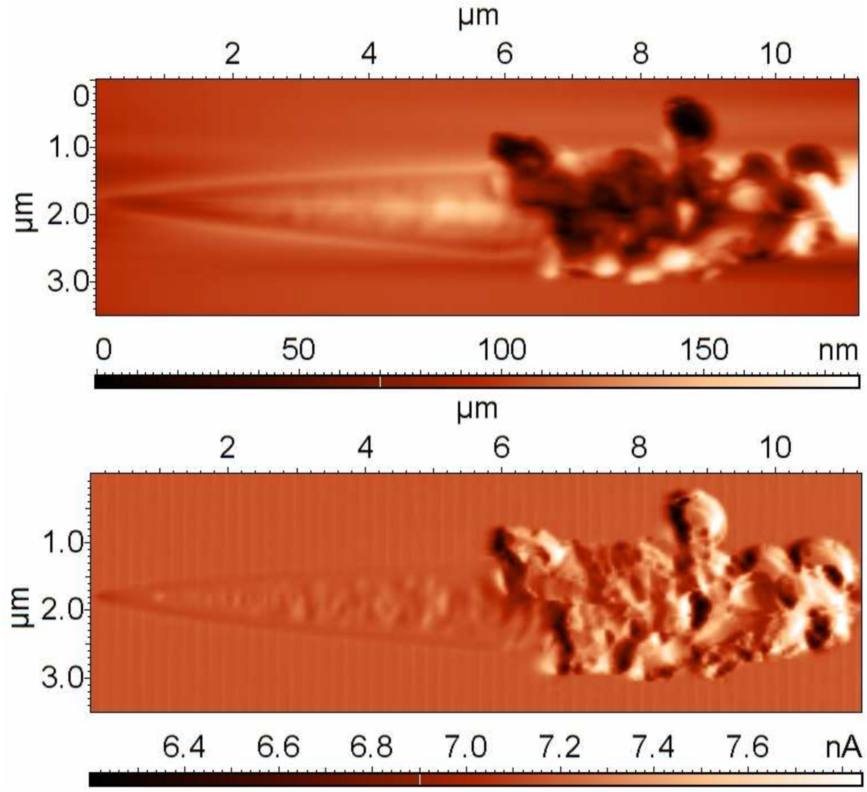

Fig. 61 AFM scratch image of pp-TVS film (50 W), top: height mode; bottom: magnitude mode

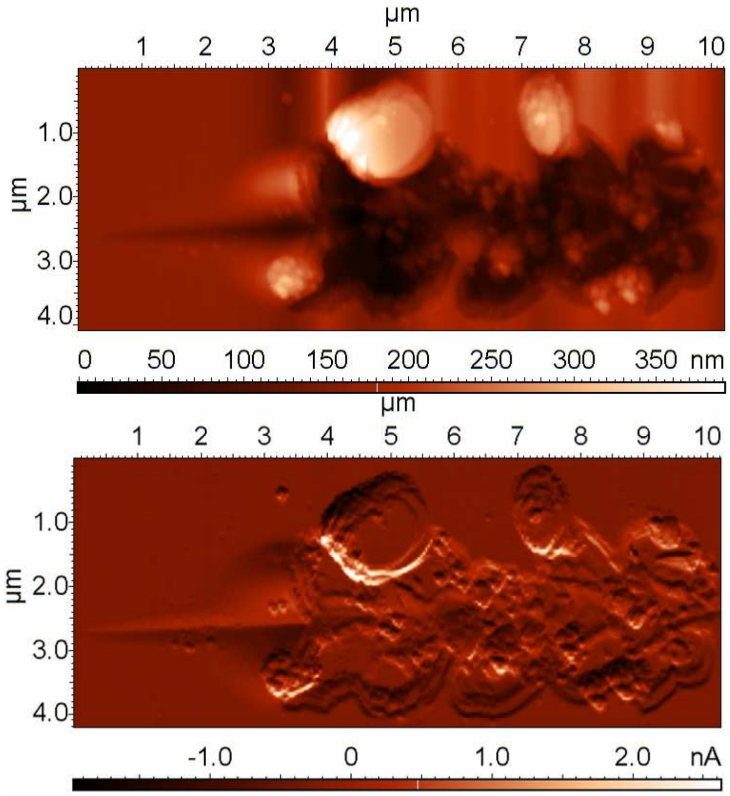

Fig. 62 AFM scratch image of pp-TVS film (70 W), top: height mode; bottom: magnitude mode

Deposition conditions (W)	Critical normal load (μN)	Std. Dev.	Critical Lateral Load (μN)	Std. Dev.
10	893	41	206	10
25	1473	129	280	35
50	7456	1147	1649	257
70	2396	235	527	57

Table 12 Scratch data such as the critical normal force and critical lateral force of pp-TVS films deposited at different RF-power

The AFM scratch images (Fig. 59 – 62) helped to study the visible point of adhesion failure on thin films i.e. the place where the tip broke the path of the scratch in the thin films to touch the substrate. The initial phase of scratches, as mentioned in Fig. 59 – 62, was not seen clearly due to a very small amount of force and elastic recovery of the film at low amount of deformation. Further, the middle section of scratches was clearly visible due to higher amount of deformation taking place at high forces. It could be seen that the scratch track of pp-TVS film deposited at 10 W and having the modulus of 12 GPa was distinct from the rest of the samples, which were having higher modulus. This information leads to a conclusion that the scratches were more clearly visible in softer films compared to the stiffer films.

Furthermore, the image analysis was used to study the depth profile of scratches on pp-TVS films of 10 and 50 W. Three horizontal depth profiles were created for each of them to understand the progress of the scratches, mentioned in Fig. 63 and 64. The depth profile for pp-TVS film deposited at 10 W (fig 63 A) at the beginning part of the scratch was only 20 nm and it was not clearly visible also. Further, the 1st point of delamination was mentioned at point B in Fig 63, where the depth profile reached almost to 100 nm (which is film thickness). From point B to C, completely delaminated film was observed. There was huge pile-up behavior as well as debris of broken film was observed surrounding the scratch track.

In case of pp-TVS film deposited at 50 W, the depth profiles were completely different as mentioned in Fig 64. Due to high modulus and hardness, this film has higher resistance to scratch deformation and delamination compare to the film of lower mechanical properties. The highest depth profile was measured for this film was 65 nm at point B and C, seen in Fig 64.

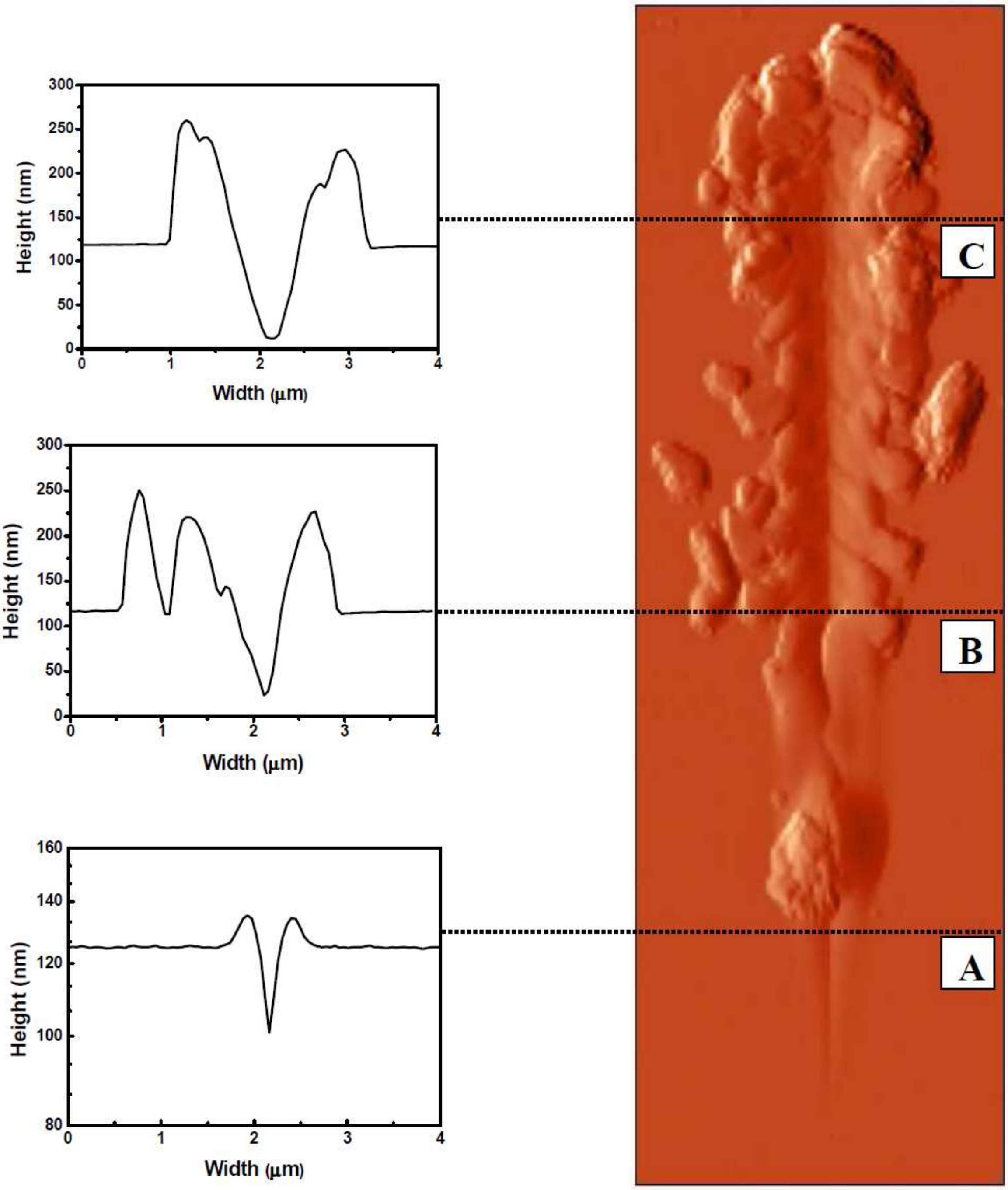

Fig. 63 Study of horizontal depth profiles of scratch for pp-TVS film deposited at 10 W at 3 different places: (A) starting of scratch track; (B) adhesion failure point; and (C) ending of the scratch

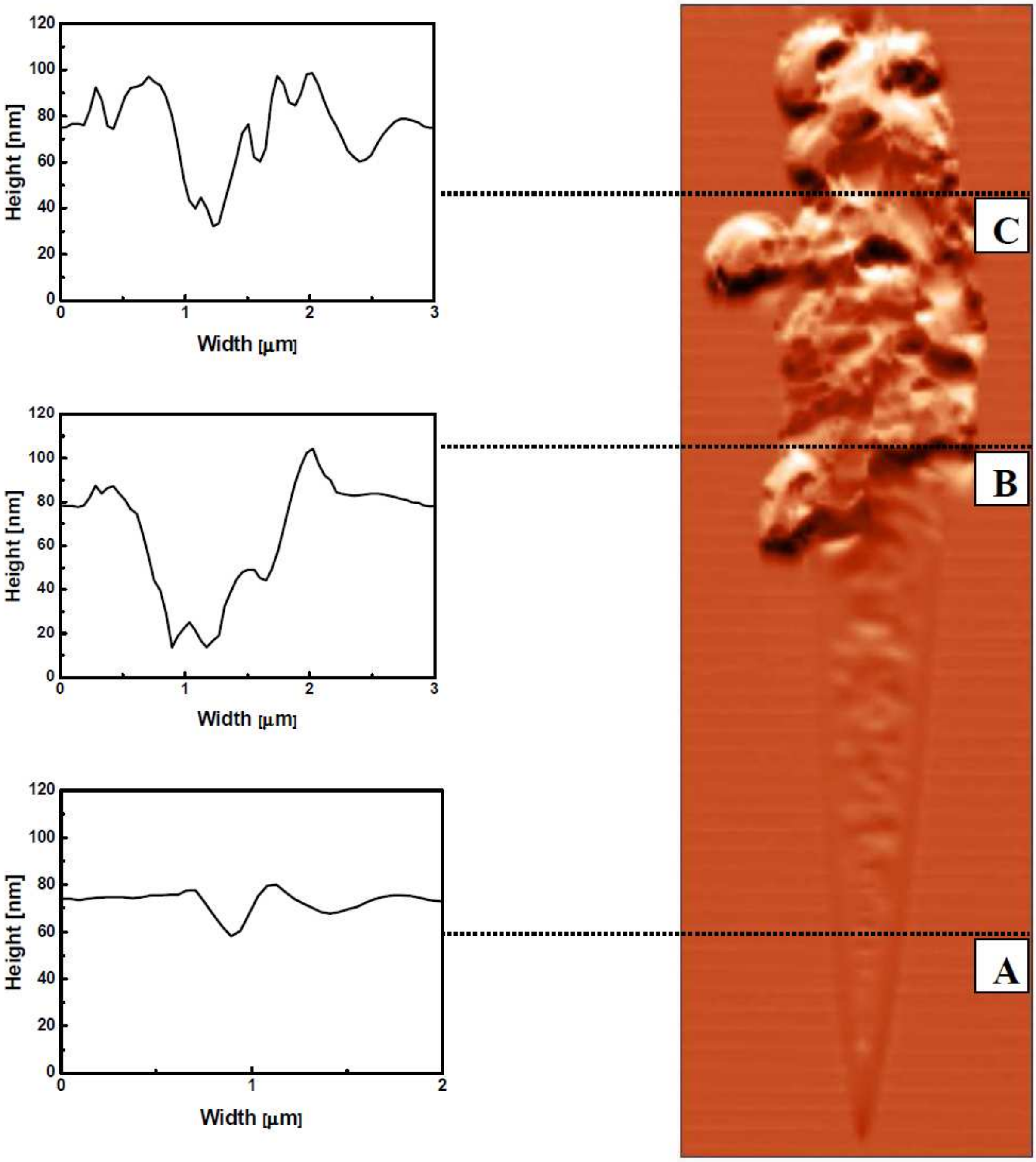

Fig. 64 Study of horizontal depth profiles of scratch for pp-TVS film deposited at 50 W at 3 different places: (A) starting of scratch track; (B) adhesion failure point; and (C) ending of the scratch

For comparison purpose, the lateral forces were plotted against normal forces for all the films as seen in Fig. 65. It was seen that as the RF power increases from 10 to 70 W, the lateral force value (friction coefficient) decreases for the same normal force due to increased stiffness.

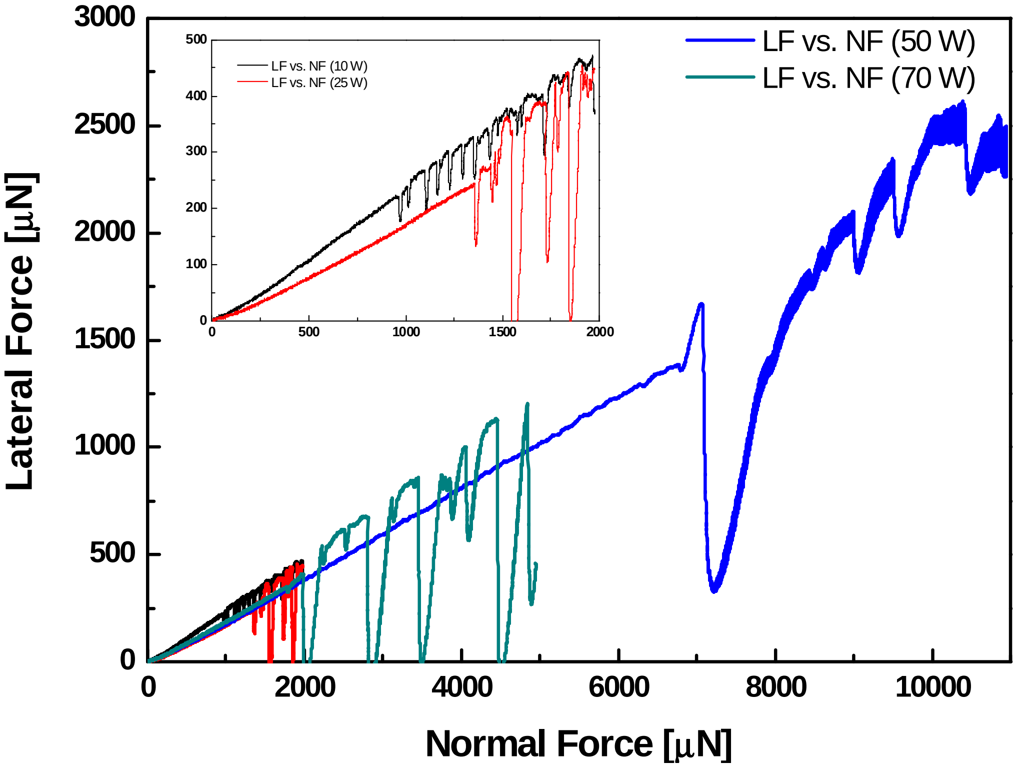

Fig. 65 Lateral force vs. normal force data of pp-TVS films deposited at 10, 25, 50 and 70 W

Further, the scratch data such as the lateral force vs. normal force and coefficient of friction vs. normal force were correlated to scratch track for pp-TVS film deposited at 10 W and 50 W, as mentioned in Fig. 66 and 67. Only two examples are presented corresponding to the pp-TVS film deposited at 10 W (Fig. 66) and 50 W (Fig 67) as character of plotted dependences is the same for the film deposited at 25 W and 70 W. The scratch data were in harmony with scanned scratch track as mentioned in fig. 66 and 67. There is a huge disturbance in lateral force vs. normal force (µN) as well as in coefficient of friction vs. normal force plot was observed for the pp-TVS film deposited at 50 W compare to the pp-TVS film deposited at 10 W. It was due to the delaminating of huge part of films around that disturbance point.

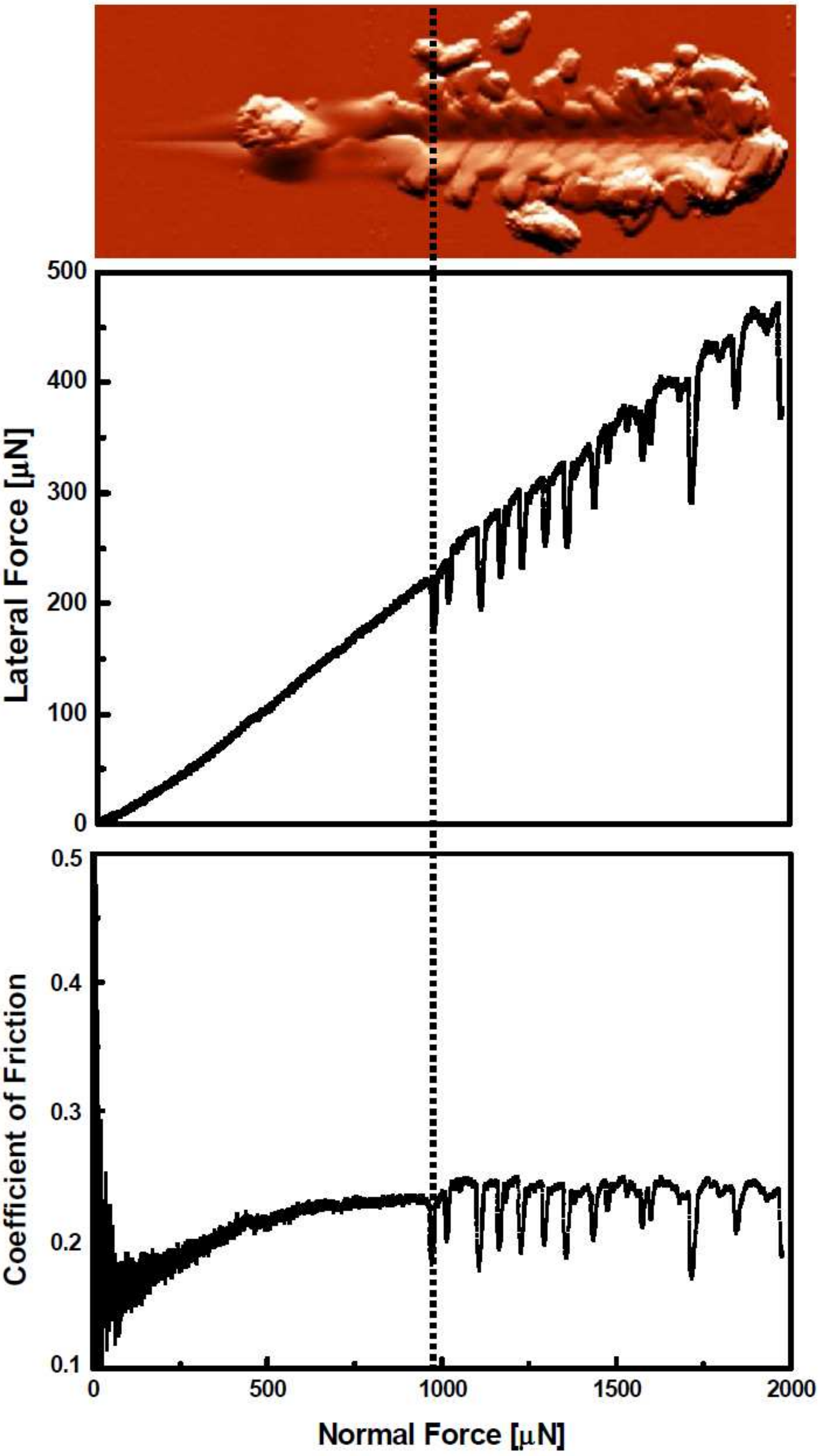

Fig. 66 Approximate highlight the point of adhesion failure of the film with an indication of the critical points on the curve of the lateral force vs. normal force and coefficient of friction vs. normal force for pp-TVS film (10 W, 12 GPa)

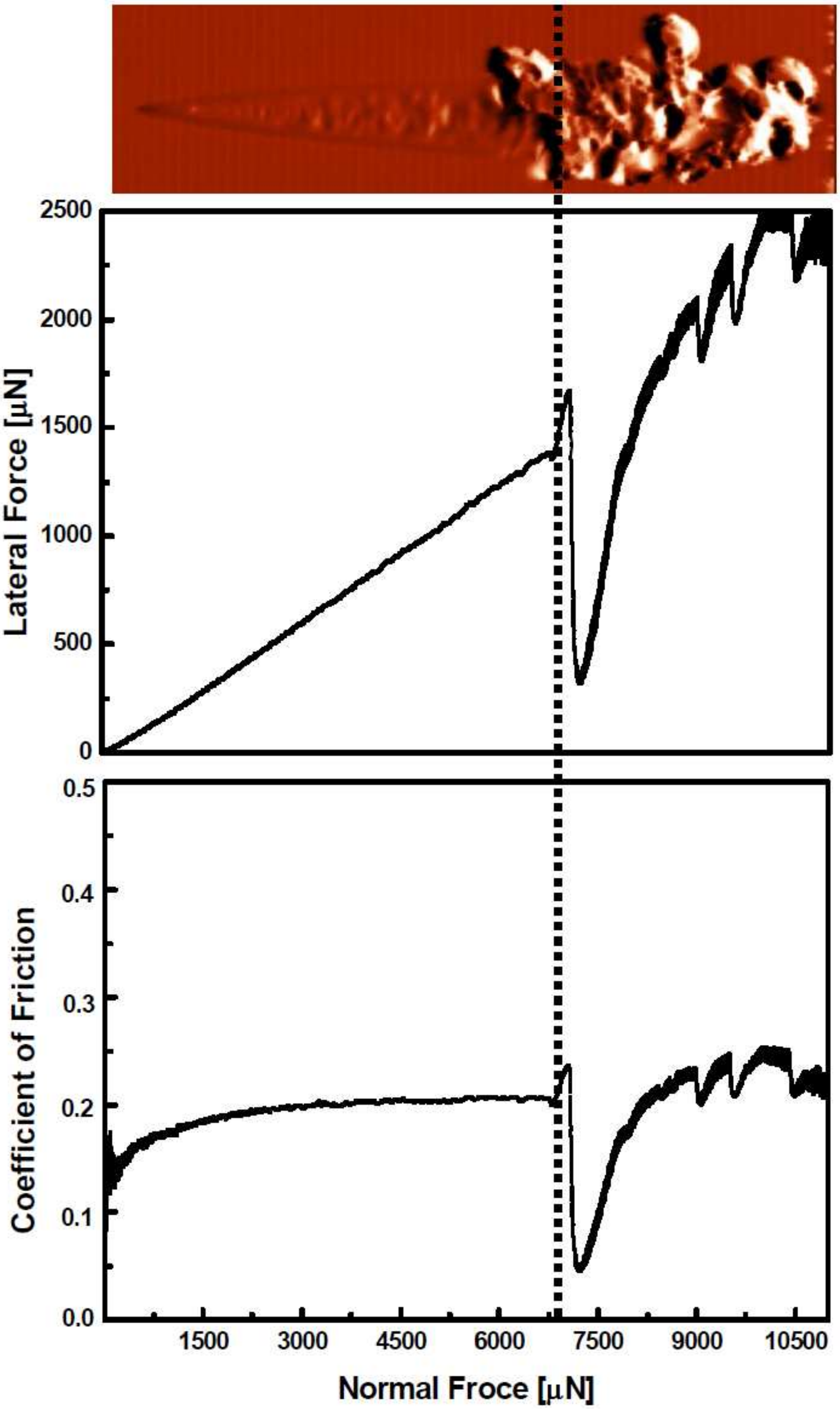

Fig. 67 Approximate highlight the point of adhesion failure of the film with an indication of the critical points on the curve of the lateral force vs. normal force and coefficient of friction vs. normal force for pp-TVS film (50 W, 63 GPa)

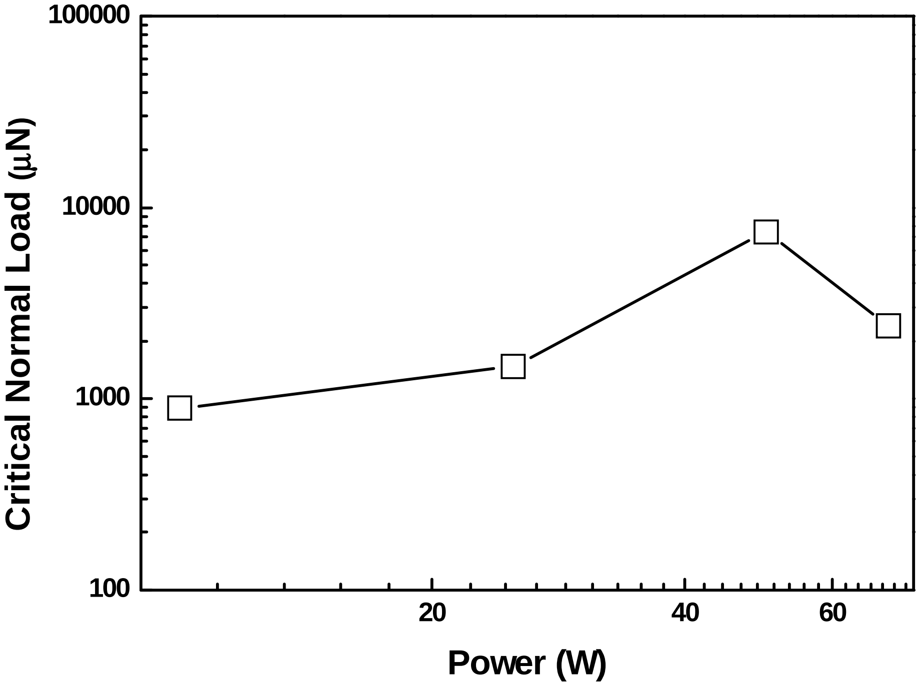

Fig. 68 Behavior of Critical normal load vs. RF-power for pp-TVS films

It is clearly visible from Table 12 and Fig. 68 that the increased RF power from 10 to 50 W resulted in higher critical normal force and higher critical lateral force. Hence, the better adhesion at higher RF power can be explained by the enhancement of cross-linking nature of the films. The pp-TVS film deposited at 70 W was having the lower scratch data compared to the film deposited at 50 W, despite this film has better mechanical constants than 50 W film. This behavior lead to an explanation that this film was having the strong network in the film but week linkage between the film and the silicon substrate. This behavior could be explained by more internal stress in the film.

4.4 Multilayer film

This part of the chapter deals with characterization of the well-defined single layer and multilayer film. A novel way was used to intensively characterize the multilayer structure of the film by scanning probe microscopy and nanoindentation method. The objective of this study is to evaluate the surface morphology and the mechanical properties of individual layers in multilayer film system.

4.4.1 Thin film deposition

Plasma-polymerized tetravinylsilane films were deposited on single-side polished silicon wafers using PECVD (13.56 MHz) working in a pulsed regime. The effective power of the pulsed plasma was controlled by changing the ratio of the time when the plasma was switched on (1 ms) to the time when it was switched off (4 – 499 ms) at a total power of 50 W and therefore, the effective power was varied from 0.1 to 10 W. The silicon wafer was pretreated by O_2 plasma (5 sccm, 4 Pa, 25 W) for 10 min. Single layers and multilayer of a-SiC:H were deposited at a flow rate of 0.50 sccm and a corresponding pressure of 1.3 Pa using TVS plasma. The multilayer was hidden in the load lock, while the different power was set up to deposit the subsequent individual layer. Deposited films were held for 1 hour in argon gas (10sccm, 10 Pa) and then moved to the load lock and flushed with air to atmospheric pressure. During deposition process, the evaluation of single layer or multilayered film was employed by in-situ spectroscopic ellipsometry. The technique allows investigation of thickness of individual layers and their optical parameters, such as refractive index and extinction coefficient.

The single layer tetravinylsilane film (A) of thickness 1217 nm was prepared at an RF-power of 10 W. The film (B) of thickness 748 nm was deposited at an RF-power of 0.1 W. The multilayered a-SiC:H film consisted of 10 individual layers of film – A and film – B type with a buffer layer in the bottom. The total thickness of multilayer film was around 2 µm. In which, the buffer layer was having thickness of 1 µm and the thickness of individual layers of multilayer film was around 100 nm, which was measured by using spectroscopic ellipsometry (SE).

Atomic Force Microscopy (AFM) (NT-MDT, Russia) was used to study the surface morphology of the single layer and multilayered films. AFM images were performed in tapping mode, under ambient conditions using triangular Si_3N_4 cantilevers (NT-MDT) with a nominal sprint constant of 3 N m^{-1}. The mechanical properties such as the young’s modulus and the hardness of single layer and multilayer films were measured using Triboscope (Hysitron Inc., Minneapolis, MN). Several indents were performed to obtain the mean value and standard deviation of mechanical properties. The Berkovich diamond tip with 50 nm nominal radius was used as the indenter.

4.4.2 Surface analysis of thin films in normal direction

The surface morphology of single layers (A & B) and the multilayer film had studied out by the help of semi-contact mode AFM technique. The root mean square (RMS) roughness was calculated from the surface morphology. The RMS roughness of individual films A and B was 2.4 nm and 1.4 nm, respectively. While, the RMS roughness of multilayer a-SiC:H film was 4.0 nm. The multilayer film was having such a high roughness because of the contribution of roughness of individual layers in it.

The mechanical properties such as the hardness and the Young's modulus of single layer film A and film B have been studied out by nanoindentation technique are mentioned in Table 13. The mechanical properties were measured until 10 % of the film thickness to avoid the influence of substrate in measurement. The standard deviation values were within the error bar (10 %); hence, they were not mentioned here.

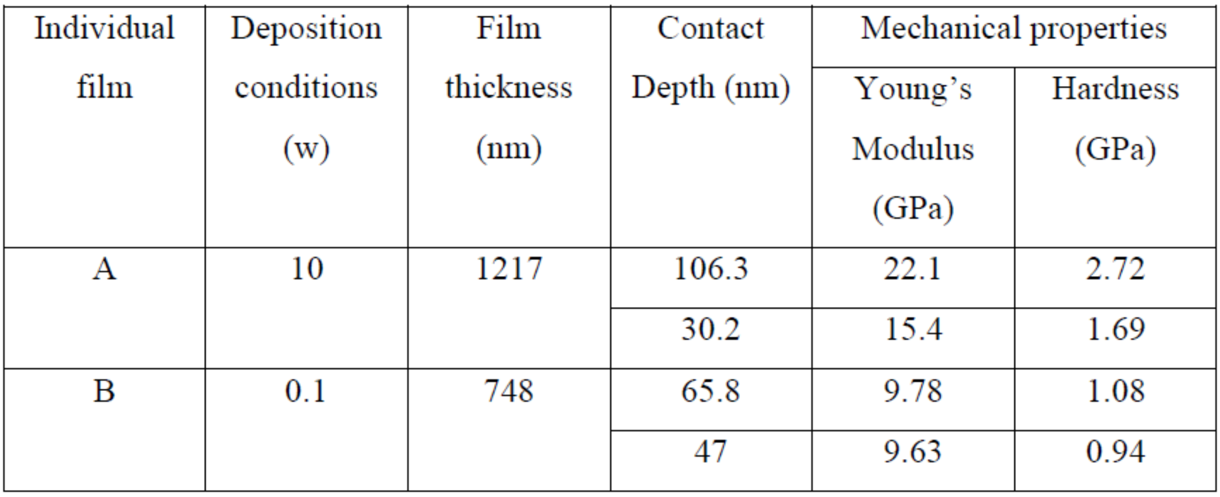

Individual film	Deposition conditions (w)	Film thickness (nm)	Contact Depth (nm)	Mechanical properties	
				Young's Modulus (GPa)	Hardness (GPa)
A	10	1217	106.3	22.1	2.72
			30.2	15.4	1.69
B	0.1	748	65.8	9.78	1.08
			47	9.63	0.94

Table 13 Mechanical properties of Single layer films

Further, the nanoindentation method was used to study the depth profile of mechanical properties for multilayer a-SiC:H film in normal direction (i.e. direction perpendicular to the surface). The Young's modulus and hardness as a function of the contact depth are mentioned in Fig 69. Here, the influence of bottom layers and the substrate in measurement of mechanical properties can be observed from the progressive increased of the curves. Hence, the mechanical constant of the individual layers cannot be determined by nanoindentation measurements in normal direction to the surface of multilayered film.

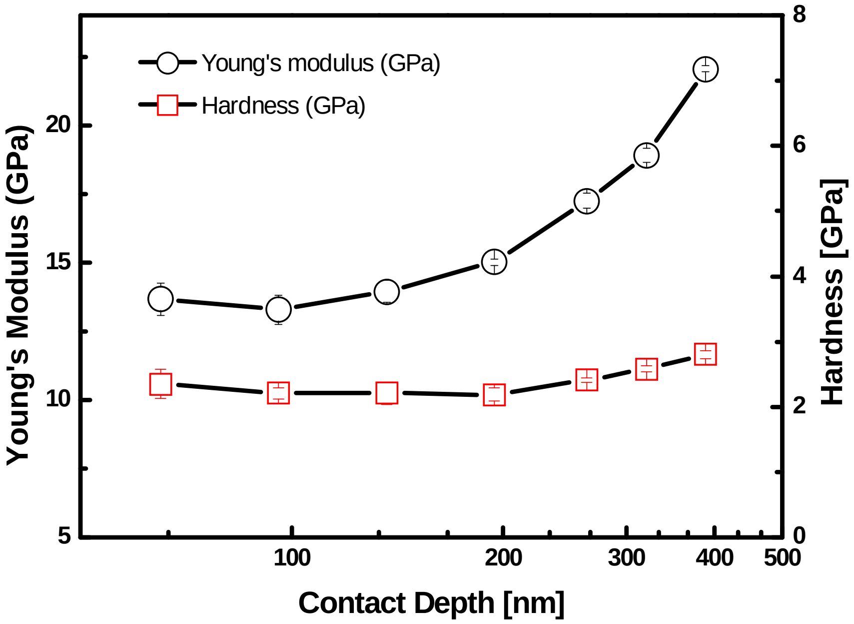

Fig. 69 Young's modulus and Hardness vs. Contact Depth for a-SiC:H multilayer film in normal direction.

4.4.3 Multilayer film analysis by Atomic Force Microscopy and nanoindentation

Normally, the multilayer structure of thin films was observed with the help of transmission electron microscopy (TEM) or high-resolution transition electron microscopy (HRTEM) after making the cross section of that particular film by the help of ultramicrotomy or ion beam thinning method [89]. As well as, the mechanical properties of multilayer films were evaluated by many researchers in normal direction only as it was mentioned in Fig 69. However, in our present study, a novel approach was used to characterize the structure, morphology and mechanical properties of individual layers in the multilayer a-SiC:H system by sectioning method. The 10-layered a-SiC:H film was sectioned at a small angle of 4° by a Leica EM UC6 ultramicrotome as mentioned in Fig 70. The 1-µm-thick buffer layer was used to protect the diamond knife from damage during sectioning process.

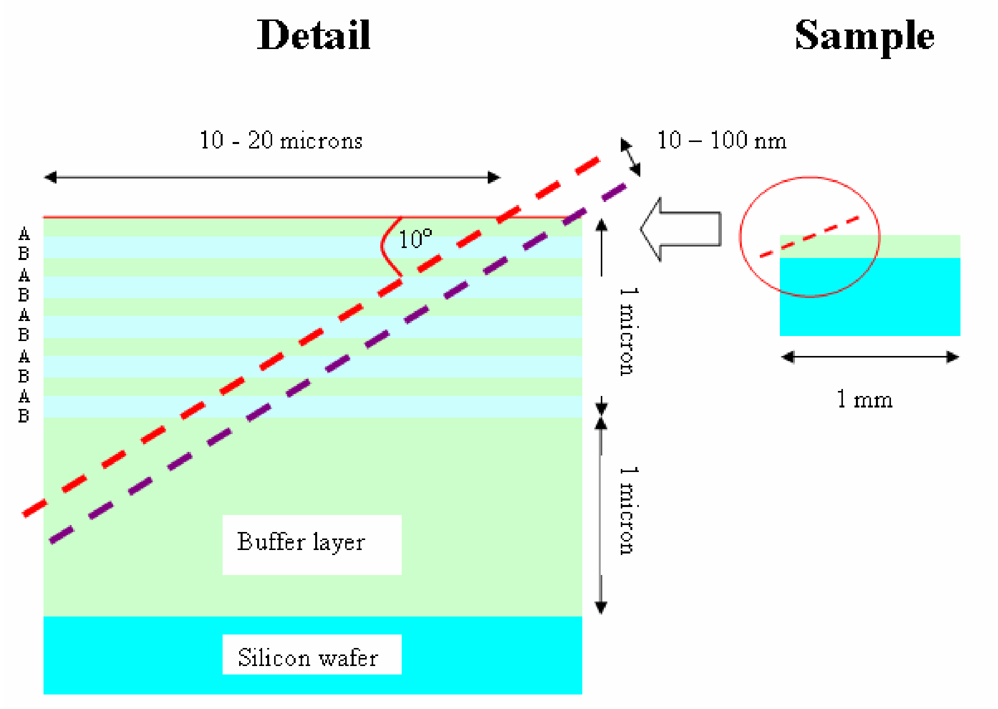

Fig. 70 Schematic diagram of sectioning of multilayer film.

After sectioning, the individual layers of multilayer film were analyzed in details by Atomic Force Microscopy (AFM), nanoindentation, Lateral Force Microscopy (LF) and Atomic Force Acoustic Microscopy (AFAM). The AFAM and LF measurement were conducted by using a gold-coated silicon cantilever with a spring constant of 1.8 N/m and a resonance frequency of 23-25 kHz.

First, the surface morphology of uncovered multilayered a-SiC:H film was examined by non-contact mode AFM. This enabled us to recognize the individual layers as mentioned in Fig 71. It can be seen from Fig. 71 (a) that the non-contact mode topography of eight individual layers, which mentioned from right to the left with the topmost layer at the extreme right side corner. The magnitude mode image (Fig 71 b) helped to study the sharp boundaries between the layers as well as some particles. The 3D view of individual layers shown in Fig. 72 gives the clear idea about the multilayer structure. The alternative layers 1, 3, 5, 7, 9 and the buffer layer were prepared at higher RF-power (10 W) and having the higher mechanical properties, were squeezed up. The layers of lower mechanical properties such as 2, 4, 6, 8, and 10 were, squeezed down.

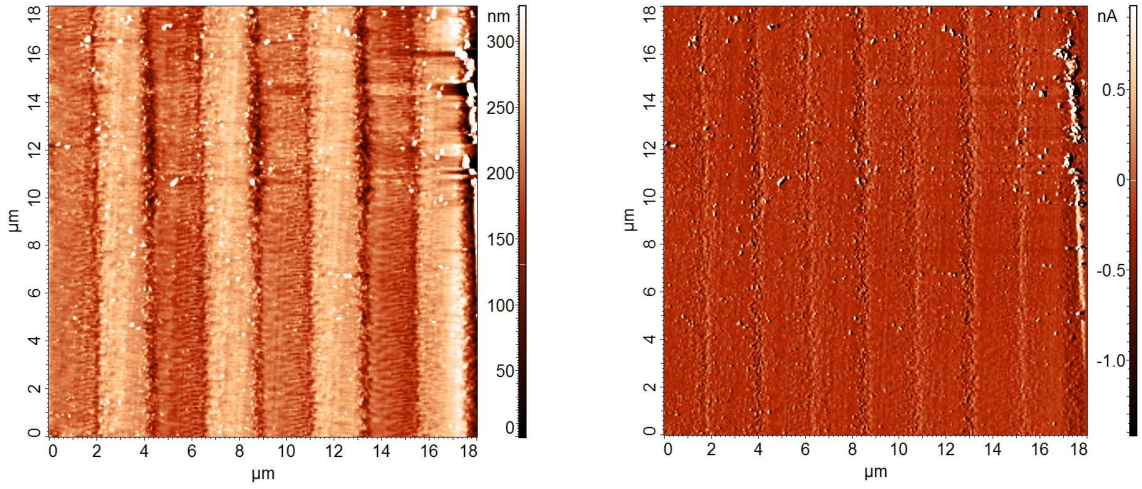

(a) (b)

Fig. 71 Non-contact mode AFM surface morphology of sectioned 10-layered a-SiC:H film (a) Topography height image, (b) Magnitude image.

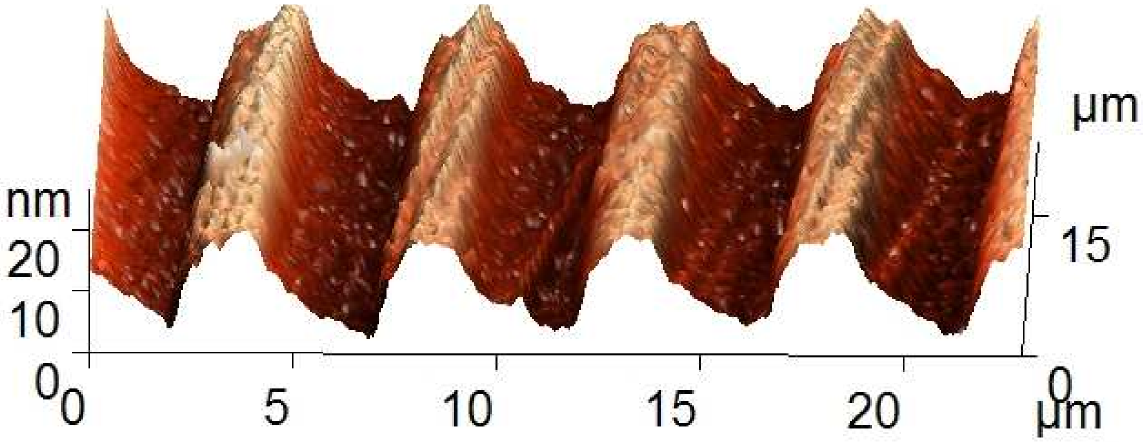

Fig. 72 3-Dimension view of Multilayer film structure

The dispersion of the refractive index of each individual layers in multilayer (a-SiC:H) films was well corresponds to particular single layer film and thus, It was expected that the mechanical constants of individual layer were similar to particular single layer films.

The mechanical properties of each individual layers were characterized by nanoindentation method. The mean value of Young’s modulus and hardness of individual layers are mentioned in Table 14. As mentioned previously, the individual layers in multilayered film were deposited of thickness of 100 nm and, hence the mechanical properties of them were measured until the contact depth of 30 to 40 nm, only. The obtained data were found to be similar to particular single layer films (A & B) as mentioned in Table 13.

The 1st individual layer was not possible to characterized by nanoindentation technique due to the sharp cut was produced by sectioning method. The influence of substrate was observed on mechanical properties measurement, as the nanoindentation experiment was carried out from layer -2 to towards buffer layer.

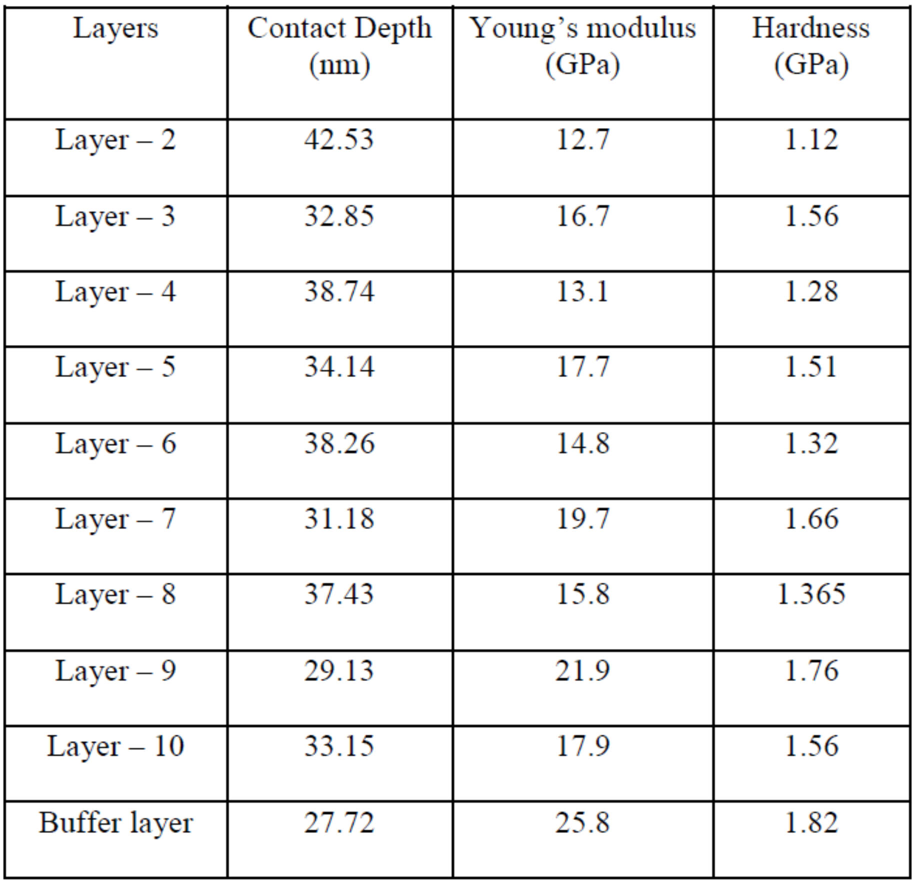

Layers	Contact Depth (nm)	Young's modulus (GPa)	Hardness (GPa)
Layer – 2	42.53	12.7	1.12
Layer – 3	32.85	16.7	1.56
Layer – 4	38.74	13.1	1.28
Layer – 5	34.14	17.7	1.51
Layer – 6	38.26	14.8	1.32
Layer – 7	31.18	19.7	1.66
Layer – 8	37.43	15.8	1.365
Layer – 9	29.13	21.9	1.76
Layer – 10	33.15	17.9	1.56
Buffer layer	27.72	25.8	1.82

Table 14 Mechanical properties of individual layers of a-SiC:H multilayer film

4.4.4 Multilayer film analysis by Lateral Force Microscopy (LFM)

The friction characteristic of uncovered layers of the multilayer a-SiC:H film was analyzed by the help of the Lateral Force (LF) Microscopy. The Fig. 73 (a) depicts the topographic image in contact mode and 73 (b) shows the LF image. There is a strong correlation between the surface slopes and frictional forces [21] that could be observed from the LF image (Fig 73 b). It was seen that the frictional force is high, locally at the edges of the grids and pits with a positive slope and is low at the edges with a negative slope. It was also observed from the LF image (Fig 73 b) that there is no friction coefficient difference between the layers, in spite of having different mechanical properties. This is due to the multilayer a-SiC:H film was deposited from the same monomer composition with only the changes of RF-power. Hence, the layers were having same friction coefficient.

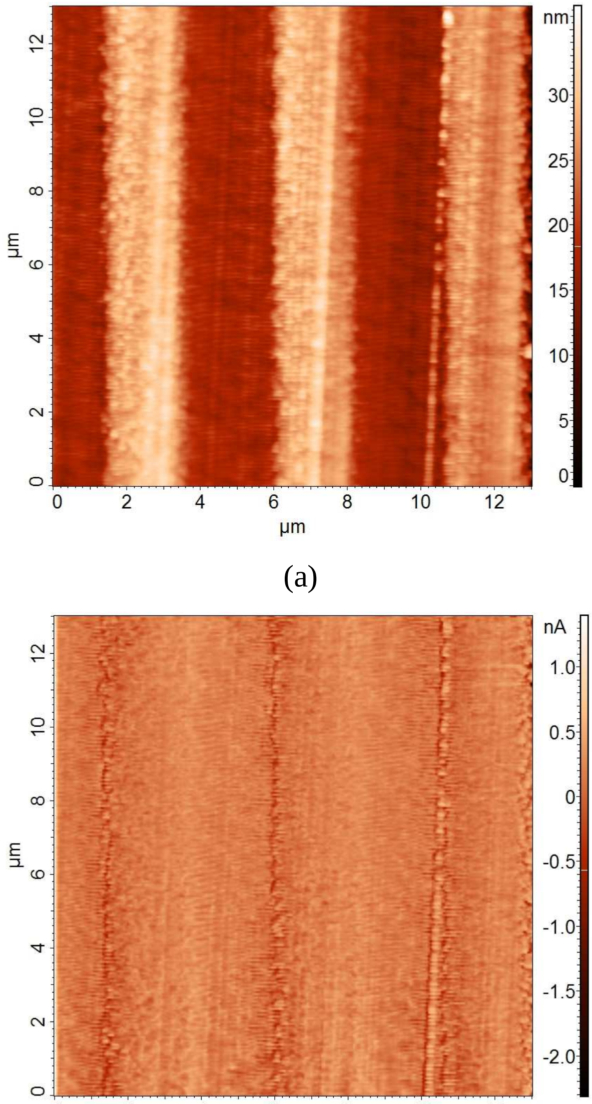

(a)

(b)

Fig. 73 Lateral Force Microscopy images of the sectioned a-SiC:H multilayer film (a) topography (height) image and (b) lateral force map.

4.4.5 Multilayer film analysis by Atomic Force Acoustic Microscopy (AFAM)

Further, the modulus mapping of multilayer a-SiC:H film was carried out by AFAM method. The AFAM is a newly developed non-destructive technique, used for the modulus mapping of thin films or polymers. The topographic image of multilayer structure in contact mode is mentioned in Fig 74 (a), while the AFAM image was produced at constant resonant phase (90.4^0 for the a-SiC:H multilayer film) is mentioned in Fig 74 (b). The frequency variation of the vibrated surface was scanned via phase modulation. In the AFAM image, the regions of the sample with lower stiffness are darker [35]. We observed that the spatial variation in the AFAM and conventional

AFM images are identical, hence surface morphology of layer structure has no influence on mechanical property mapping.

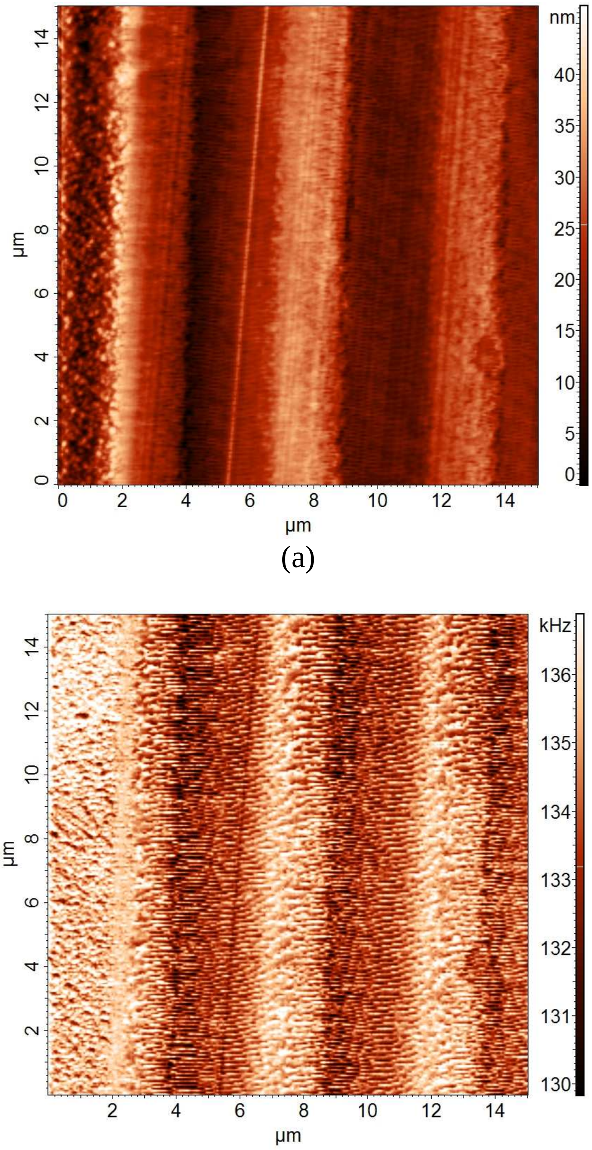

(a)

(b)

Fig. 74 AFAM images of the sectioned a-SiC:H multilayer film. (a) topography, (b) AFAM frequency contrast.

5 CONCLUSION

Plasma-polymerized single and multilayer organosilicon films were deposited on silicon wafers using plasma-enhanced chemical vapor deposition. The study of surface properties and adhesion characteristics of these films were analyzed successfully by scanning probe microscopy, nanoindentation and nanoscratch tests.

The surface morphology and RMS roughness of single layer pp-VTES and pp-TVS films were successfully characterized by atomic force microscopy. The single layer pp-VTES films with thickness ranging from 15 nm to 8.6 µm were deposited at an effective power of 5 W. The RMS roughness was increased from 0.04 to 15.5 nm as a function of film thickness for pp-VTES films. In another experiment, single layer pp-TVS films were deposited at different RF-power of 10, 25, 50 and 70 W with the similar film thickness of about 1 µm. The RMS roughness was also increased from 1.90 to 4.0 nm for pp-TVS films as a function of different deposition power.

Mechanical properties of single layer pp-TVS films were measured using nanoindentation technique in 2 experimental set-ups. The 1st experimental set up was carried out at drift rate of ≤ 0.5 nm/s, while the 2nd set was carried out at a lower drift rate of ≤ 0.05 nm/s.

In the 1st experimental set up, the mechanical properties of the single layer pp-TVS film deposited at 10 W was used for analysis. We pointed out an influence of the dwell time and loading/unloading time >5 s that produced a progressive increase of the tip displacement due to the system drift not correctly subtracted at prolonged measuring time. The experiment was carried out using an open-loop load function as mentioned above. The open-loop load function means that the measurement is performed without any feedback control and the drift rate is determined before the measuring cycle. The increased tip displacement at prolonged measuring time resulted in underestimated reduced modulus and hardness. Further, the mechanical properties of pp-TVS film was studied using both the conventional indentation method and cyclic indentation method accelerating depth-profile analysis. The mechanical parameters obtained from both the methods were similar and followed the same trend. However, prolonged time used at the cyclic indentation method resulted in diminished values of the reduced modulus by 27% and hardness by 34%. The close-loop load function or drift rate < 0.05 nm/s could reduce the differences.

The 2nd experimental set up was carried out for pp-TVS films deposited on silicon wafers by PECVD at three different powers (0.1, 2.5, and 10 W) using pulsed plasma for the purpose to prepare films of different mechanical properties. All the films were characterized by conventional and cyclic nanoindentation methods under the drift rate ≤0.05 nm/s to construct the depth profile of mechanical properties. We found out that both the methods gave similar results but the cyclic nanoindentation accelerates depth analysis of mechanical properties significantly from hours using conventional method to minutes. The films of thickness about 1 µm were characterized for contact depth ranging from 5 to almost 200 nm. The Young’s modulus and hardness data were reproducible, except for surface region up to 30 nm from the film surface, depending on film stiffness. Bulk reproducible data enabled to evaluate the Young's modulus and hardness of pp-TVS film deposited at different power: *E*=7.9 GPa, *H*=0.69 GPa (0.1 W), *E*=14 GPa, *H*=2.0 GPa (2.5 W), and *E*=17 GPa, *H*=3.0 GPa (10 W). The depth profiles of mechanical properties for films of different stiffness revealed that the 10% rule can be applied reliably to evaluate the hardness of film, but in case of Young's modulus, the rule cannot be used for stiffer film (*E*>14 GPa) deposited on silicon wafer. Based on this study, we can complete conditions necessary for successful analysis of mechanical properties at a shallow depth: (i) sharp indenter, (ii) careful calibration of the indenter area function, (iii) minimal system drift and using drift correction, (iv) smooth sample, (v) no pile-up, and (vi) stiffer sample.

Further, hybrid nature of single layer pp-TVS films was investigated. The pp-TVS films deposited by PECVD with film thickness of 1 μm at different effective power, ranging from 10 – 70 W. Surface analysis (AFM) revealed grain structure of pp-TVS films deposited at different RF power. The RMS roughness and average grain size were increased from 3.4 nm to 21 nm and 29 nm to 241 nm, respectively with enhanced power. Nanoindentation measurements into the plane area and grains resulted in different depth profile of mechanical parameters. The difference was explained by influence of grain geometry and by lower mechanical parameters of grains with respect to the smooth area as confirmed by FEA simulation and AFAM measurements.

The UV irradiation can modify the surface of single layer film (pp-TVS). For that purpose, two batches (each of six pp-TVS) with a film thickness of 0.1 and 0.5 μm, respectively, were deposited using the same deposition conditions. The as-deposited films were subjected to UV irradiation at ambient conditions for different times ranging from 10 to 100 min. The modification of the surface morphology (RMS roughness) and mechanical properties of the irradiated films were successfully investigated by atomic force microscopy and nanoindentation. The RMS roughness of the irradiated films decreased from 0.41 to 0.12 nm with prolonged UV exposed time and the mechanical constants (Young's modulus, hardness) increased for prolonged UV exposed time due to the UV-induced-cross linking.

The adhesion behavior of single layer pp-TVS films on silicon substrates were tested by nanoscratch test and the surface morphology of scratches was examined by AFM. The correlation of both methods was informative. The different scratch speed experiment indicated that critical normal load was almost remained constant at different speed. The PECVD apparatus can reproducibly prepare the thin films with same adhesion characteristic. The different film thickness (thickness varying from 25 to 468 nm) has a great impact on adhesion behavior of the films. For thinner film like 25 nm, it was very difficult to see the adhesion failure point on critical normal load data as well as in AFM images. While, the thicker film of 468 nm has shown an extensive damage in scratch data as well in AFM images. Similar way, the film of different mechanical properties (deposited from 10 – 70 W) had different adhesion behavior. The critical normal load and lateral normal load was increased with increased RF power from 10 to 50 W. However, the subsequent decline in scratch data (critical normal load, critical lateral load) was observed for film deposited at 70 W, probably due to the high internal stress and fragility. One can successfully use the nanoscratch test with the combination of atomic force microscopy in the evaluation of adhesion behavior of organosilicon thin films on silicon substrate.

Furthermore, a novel approached was discussed for the surface analysis of multilayer film. For that purpose, single layer and multilayered a-SiC:H films were deposited on silicon substrate from tetravinylsilane using PECVD. The 10-layered multilayer film was constructed as a, Si-SiO_2/BABABABABA, where Si-SiO_2 means a substrate of the silicon together with a silicon oxide layer. Layer A was deposited at an effective power of 10 W and layer B at 0.1 W. The multilayer film was sectioned using ultramicrotomy at an angle of 4° to reveal the individual layers. The individual layers were observed by atomic force microscopy and the surface morphology influenced by layer structure was noticed. There was no difference in friction characteristic of individual layers observed by lateral force microscopy. The mechanical properties of distinguished individual layers were successfully investigated by nanoindentation and atomic force acoustic microscopy. The analysis indicated that mechanical properties of individual layers A and B were the same in single layer and multilayer films. The results enable us construction of functional multilayered films of controlled mechanical properties applicable in polymer composites with controlled interphases.

REFERENCES

[1] R. Hippler, S. Pfau, M. Schmidt, K.H. Schoenbach, “Low Temperature Plasma Physics”, Wiley-VCH-Verlag Berlin (2001).
[2] N. Inagaki, “Plasma Surface Modification and Plasma Polymerisation”, Technomic Publications Inc, Lancaster, USA (1996).
[3] H. Yasuda, J. Polym. Sci., Macromol. Rev. 16 (1981) 199.
[4] T. Steiner, “Semiconductor Nanostructures for Optoelectronic Applications”, Arctech house, NorWood, MA (2004).
[5] V. Cech, J. Studynka, F. Janos, V. Perina, Plasma Proc. Polym. 4 (2007) 776.
[6] S. Gaur, G. Vegason, Proc. 43rd Annual Tech. Conf. Proc., Denver (2000) 267.
[7] P. Favia, R. D’agostino, F. Fracassi, J. Pure & Appl. Chem. 66 (1994) 1373.
[8] V. Cech, N. Inagaki, J. Vanek, R. Prikryl, A. Grycova, J. Zemek, Thin Solid Films 502 (2006) 181.
[9] V. Cech, J. Vanek, A.A. Goruppa, F.R. Jones, J. Mater. Sci. Lett. 40 (2005) 5099.
[10] P. Yashar, W. Sproul, Vacuum 55 (1999) 179.
[11] J. Musil, Surf. Coat. Technol. 125 (2000) 322.
[12] H. Holleck, J. Vac. Sci. Technol. A 4 (1986) 2661.
[13] G. L. Chen, C. C. Chang, S. C. Chien, T. S. Tung, H. H. Lee, W. C. Ling, H. L. Lee, Conf. Proc. 35th International MATADOR 2 (2007) 17.
[14] J. Ubrig, S. Martin, S. Cros, J.-E. Bouree, J. Phys. Conference Series 100 (2008) 082030.
[15] V. Cech, IEEE Trans. Plasma Sci. 34 (2006) 1148.
[16] Joinet M., Pouliquen S., Thomas L., Teyssandier F., Aliaga D., Surf. Coat. Technol. 202 (2008) 2252.
[17] Logothetidis S., Kassavetis S., Charitidis C., Panayiotatos Y., Laskarakis A., J. Carbon 42 (2004) 1133.
[18] R. Wilber, M. Falz, B. Bucken, H.U. Poll, J. Soc. Vac. Coat. 314 (1997) 56.
[19] N. Dutta, N. Tran, N. Choudhury, J. Polym. Sci. 43 (2005) 1392.
[20] G. Binning, H. Rohrer, Ch. Gerber, E. Weibel, Phys. Rev. Lett. 49 (1982) 57.
[21] B. Bhushan, “Handbook of Nanotechnology”, Springer, Heidelberg (2004).
[22] B. Bhushan, “Handbook of Micro/Nanotribology”, CRC Press, Boca Raton, Florida (1999).
[23] N.A. Burnham, D.D.Domiguez, R. J. Colton, R. L. Mowery, Phys. Rev. Lett. 64 (1990) 1931.
[24] M. Reinstaedtler, U. Rabe, V. Scherer, U. Hartmann, A. Goldade, B. Bhushan, W. Arnold, Appl. Phys. Lett. 82 (2003) 2604.
[25] B. Bhushan, J.N. Israelachvili, U. Landman, Nature 374 (1995) 607.
[26] N.A. Burnham, R.J. Colton, J. Vac. Sci. Technol. A7 (1989) 2906.
[27] B. Bhushan, V. N. Koinkar, Appl. Phys. Lett. 75 (1994) 5741.
[28] O. Marti, B. Drake, P.K. Hansma, Appl. Phys. Lett. 51 (1987) 484.
[29] B. Drake, C. B. Prater, A. L. Weisenhorn, S.A.C. Gould, T.R. Albrecht, C.F. Qutate, D.S. Canell, H.G. Hansma, P.K. Hansma, Science 243 (1989) 1586.
[30] G. Meyer, N.M. Amer, Appl. Phys. Lett. 53 (1988) 1045.
[31] F. J. Giessibl, Ch. Gerber, G. Binning, J. Vac. Sci. Technol. B9 (1991) 984.

[32] C. Basire, D. A. Ivanov, Phys. Rev. Lett. 85 (2000) 5587.
[33] H. Liu, B. Bhushan, Ultramicroscopy 91 (2002) 185.
[34] C.T. Gibson, G.S. Watson, S. Myhra, Wear 213 (1997) 72.
[35] U. Rabe, S. Amelio, E. Kester, V. Scherer, S. Hirsekorn, W. Arnold, J. Ultrasonics 38 (2000) 430.
[36] D. Rugar, H.J. Mamin, P. Guethner, S.E. Lamber, J.E.Stern, I.McFadyen, T.Yogi, J. Appl. Phys. 63 (1990) 1169.
[37] E. Betzig, P.L. Finn, J.S.Weiner, Appl. Phys. Lett. 60 (1992) 2484.
[38] A. Majumdar, Annual Rev. Mater. Sci. 29 (1999) 505.
[39] B. Bhushan, A. V. Goldade, Wear 244 (2000) 104.
[40] V.L. Mironov, “Fundamental of Scanning Probe Microscopy”, Russian Academy of Sciences, Nizhniy Novgorod (2004).
[41] D. Sarid, V. Elings, J. Vac. Sci. Technol. B 9 (1991) 431.
[42] E. Meyer, Surf. Sci. 41 (1992) 3.
[43] R. Coratger, V. Sivel, F. Ajustron, J. Beauvillain, Micron 25 (1994) 371.
[44] U. Rabe, S. Amelio, M. Kopycinska, S. Hirsenkorn, M. Kempf, M.Goeken, W. Arnold, Surf. Interface Anal. 33 (2002) 65.
[45] J.N. Barisci, R. stella, G. M. Spinks, G.G.Wallace, Synthetic Metals 124 (2001) 407.
[46] O. Vatel, M. Tanimoto, J. Appl. Phys. 85 (1999) 2358.
[47] Q. Xu, J.W.P. Hsu, J. Appl. Phys. 85 (1999) 2465.
[48] Y. Martin, C. C. Williams, H. K. Wickramasinghe, J. Appl. Phys. 61(1987) 4723.
[49] F. Helvaci, J. Cho, MRS Symp. Proc. 841 (2005) 375.
[50] W.C. Oliver, G.M. Pharr, J. Mater. Res. 7 (1992) 1564.
[51] J.B. Pethica, Proc. 3rd International Conference on Modification of Surface Properties of Metals by Ion-Implantation, Manchester, England (1981) 23.
[52] B.N. Lucas, W. C. Oliver, J.E. Swindeman, MRS Symp. Proc. 522 (1998) 3.
[53] W.C. Oliver, J.B. Pethica, United States Patent, 4848141 (1989).
[54] W.A.Bonin, United State Patent, 5576483 (1996).
[55] W.A.Bonin, United State Patent, 5661235 (1997).
[56] M.F. Doerner, W.D. Nix, J. Mater. Res. 1 (1986) 601.
[57] R. Saha, W.D. Nix, Acta Mater. 50 (2002) 23.
[58] T.Y. Tsui, G.M. Pharr, J. Mater. Res. 14 (1999) 292.
[59] J.S. Field, M.V. Swain, J. Mater. Res. 8 (1993) 297.
[60] B. Zhou, B.C. Prorok, MRS Symp. Proc. 1086 (2008).
[61] A.C. Fischer-Cripps, “Nanoindentation”, Springer, New York (2002).
[62] C.C. Broomell, M.A. Mattoni, F.W. Zok, J.H. Waite, J. Exp Biol 209 (2006) 3129.
[63] L. Lu, M.L. Sui, K. Lu, Scr. Mater. 287 (2001) 1463.
[64] F.D. Torre, S.H. Van, M. Victoria, Acta Mater. 50 (2002) 3957.
[65] F.X. Liu, Y. F. Gao, P. K. Liaw, Metal. Mater. Trans. A 39 (2008) 1862.
[66] B.-G. Yoo, K.-W. Lee, J.-I. Jang, J. Alloys Comp. 483 (2009) 136.
[67] F. Wang, K. Xu, Mater. Lett. 58 (2004) 2345.
[68] T.-H. Fang, W.-J. Chang, Microelectron. J. 35 (2004) 595.
[69] X. Li, B. Bhushan, Scripta Mater. 42 (2000) 929.

[70] X. Li, B. Bhushan, J. Mater. Char. 48 (2002) 11.
[71] T.W. Wu, J. Mater. Res. 6 (1991) 407.
[72] C. Charitidis, S. Logothetidis, M. Goiti, Surf. Coat. Technol. 125 (2000) 201.
[73] R. Prikryl, V. Cech, P. Hedbavny, N. Inagaki, *Proc. 17th Int. Symp,* Plasma Chemistry, Toronto (2005) 1.
[74] R. Prikryl, O. Salyk, J. Vanek, V. Cech, Czech. J. Phys. 52 (2002) D816.
[75] V. Cech, L. Xu, J. Vanek, L.T. Drzal, Japanese J. of Appl. Phys. 45 (2006) 8440.
[76] Hysitron Triboscope user Manual (software version 8.0).
[77] R. Trivedi, V. Cech, *Proc. 5th Int. Symp. Juniormat*, Brno (2007) 121.
[78] V. Cech, in: S. Zhang (Ed.), Nanostructured Thin Films and Coatings, Volume 1, CRC Press, New York, 2010, pp. 481.
[79] A.C. Fischer-Cripss, The IBIS handbook of nanoindentation, Fischer-Cripps Laboratories, Forestville, 2005, p. 42.
[80] R. Trivedi, V. Cech, Surf. Coat. Technol. (2010), doi:10.1016/j.surfcoat.2010.08.002.
[81] R. Cooper, Hysitron Inc. (private communication).
[82] V. Cech, J. Studynka, N. Conte, V. Perina, Surf. Coat. Technol. 201 (2007) 5512.
[83] K.W. Lee, Y.-W. Chung, C.Y. Chan, I. Bello, S.T. Lee, A. Karimi, J. Patscheider, M.P. Delplancke-Ogletree, D. Yang, B. Boyce, T. Buchheit, Surf. Coat. Technol. 168 (2003) 57.
[84] P.S. Baker, Thin Solid Films 308-309 (1997) 289.
[85] K.W. Elhaney, J.J. Vlassak, W.D. Nix, J. Mater. Res. 13 (1998) 1300.
[86] R. Messier, J. Vac. Sci. Technol. A4 (1986) 490.
[87] V. Cech, S. Lichovnikova, R. Trivedi, V. Perina, J. Zemek, P. Mikulik, O. Caha, J. Surf. Coat. Technol. (2010), doi: 10.1016/j.surfcoat.2010.07.046.
[88] W. Tang, K. Xu, J. Mater. Sci. Technol. 20 (2004) 78.
[89] Li R., Wadsworth I., Young J., Acheson R., J. Microscopy 184 (1996) 62.

LIST OF USED SYMBOLS

A = Projected contact area
C_k, K = 0, 1, 2, 3, 4, 5 are the constants of the empirical fit.
E = Young´s modulus
E_r = Reduced modulus
F = Flow rate
F_L = Lateral force
F_N = Normal force
F_T = Tangential force
H = Hardness
h_c = Contact depth
h_{max} = Maximum indentation depth
M = Molecular weight
P = Indentation load
P_{max} = Peak load or maximum load
RMS = Root mean square
S = Contact stiffness
T = Temperature
T_e = Electron temperature
T_i = Ion temperature
W = tungston
W_{eff} = Effective power
μ = friction coefficient
υ_s = Poisson's ratio of the substrate
υ_i = Poisson's ratio of the indenter

LIST OF USED ABBREVIATIONS

AFM = Atomic force microscopy
AFAM (or SFAM) = Atomic force acoustic microscopy (or scanning force acoustic microscopy)
CCP = Capacitive coupling plasma
Co = Cobalt
CSM = Continuous stiffness measurement
CVD = Chemical vapor deposition
EFM = Electric force microscopy
FIB = focused ion beam
FRP = Fiber-reinforced plastics
HMDSO = Hexamethyldisiloxane
ICP = Inductivly coupled plasma
LFM (or FFM) = Lateral froce microscopy (or Friction force microscpy)
Mag = Magnitude
MFM (or SMM) = Magnetic force microscopy (or scanning magnetic force microscopy)
NI = nanoindentation
PECVD = Plasma-enhanced chemical vapor deposition
Pt = Platinum
PZT = Piezo electric tube
RBS = Rutherford backscattering spectroscopy
RF = Radio Frequency
sccm = Standard Cubic Centimeters per Minute
SEM = Scanning electron microscopy
SKPM (or KPM) = Scanning Kelvin probe microscopy (or Kevlin probe microscopy)
SNOM = Scanning near field optical microscopy
STM = Scanning tunneling microscopy
SThM = Scanning thermal microscopy
TVS = Tetravinylsilane
VTES = Vinyltriethoxysilane
W2C = Tungsten Carbide
XPS = X-ray photoelectron spectroscpy